ELECTROCHEMICAL SYNTHESIS OF METAL AND INTERMETALLIC COMPOSITES

Electrochemical Synthesis of Metal and Intermetallic Composites

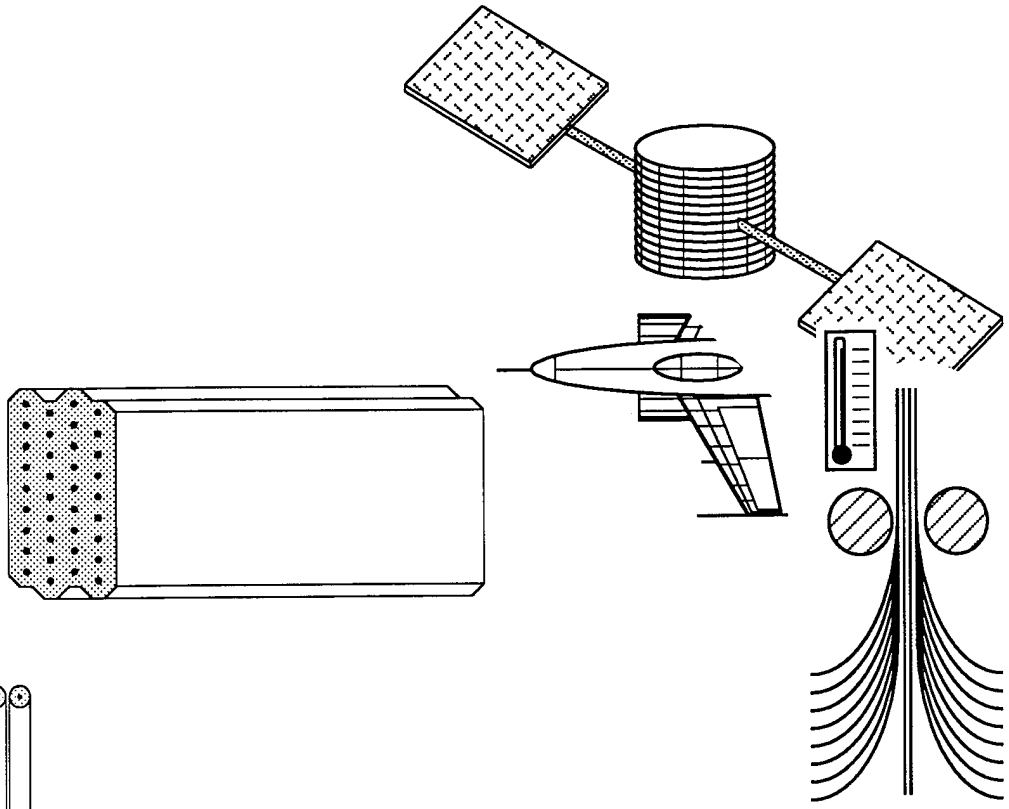

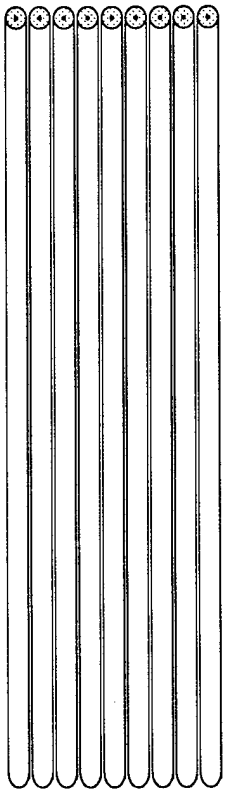

Principle Investigators:

D. S. Lashmore
C. R. Beauchamp
C. E. Johnson
T. Moffat
J. L. Mullen
G. R. Stafford

Building 224, Room B164
Gaithersburg, Maryland 20899
(301) 975-6405

Acknowledgements:

NIST Competence Building Program
Office of Naval Research: Dr. S. Fishman
DARPA: Dr. W. Barker

UNITED STATES DEPARTMENT OF COMMERCE
National Institute of Standards and Technology
Gaithersburg, Maryland 20899

February 24, 1994

Thank you for your inquiry regarding our Metal Matrix Composites Program. We have enclosed a number of appropriate published papers and patents along with a more complete list of all we have published and patented. Several of the patents are still pending. These patents are available for licensing. If you would like further information please contact:

Mr. Michael Blaney
NIST
Technology Transfer Office
Physics Building, Room B254
Gaithersburg, MD 20899
(301) 975-2870

Also enclosed with this package is a description of the NIST Cooperative research and Development Program. We have focused much of our attention on deposition of high strength intermetallics particularly titanium aluminides, but are capable of producing a range of compositions of aluminum as well as most alloys which can be deposited from aqueous solutions.

If you would like further information please call me at (301) 975-6405.

Sincerely,

David Lashmore

Dr. David S. Lashmore

OUTPUTS

Outputs Resulting From the MMC Competence Initiative

Presentations

1. N. S. Wheeler, D. S. Lashmore, A. J. Shapiro, and C. A. Handwerker, "Structural Characterization of the Nickel - Graphite Interface," to be presented, Fall Meeting of the Electrochemical Society, Phoenix, AZ, October 13-18, 1991

2. N. S. Wheeler, "Formation of Diamond Structures in Metal-Coated Carbon Fibers," American Cyanamid Co., Stamford, CT, March 8, 1990 (Invited).

3. N. S. Wheeler, D. S. Lashmore, A. J. Shapiro, C. A. Handwerker, and F. W. Gayle, "High - Temperature Characterization of Alloy Coatings on Graphite Fibers," Department of Defense seminar, American Ceramics Society, Coco Beach, January, 1990 (Invited).

4. D. S. Lashmore, "Metal Matrix Composites Produced by Electrodeposition", NBS Composites Seminar Series, 18 June, 1987

5. D. S. Lashmore, " Electrodeposited Metal Matrix Composites", Case Western Reserve University, March 3, 1988 (invited)

6. D. S. Lashmore, "Electrodeposition of Metal Matrix Composities", Electrochemical Society Symposia on Electrochemical Processing, Detroit Mich., April 7, 1988 (invited)

7. D. S. Lashmore,"Electrodepostiion of Titanium Aluminides from Molten Salts", 14th Annual Conferenc on Composites, Materials and Structures, January 17-19, 1990, Cocoa Beach, Florida

8. D. S. Lashmore, "The Electrodeposition of Metal Matrix Composites", 177th Electrochemical Society Meeting, Montreal, Canada, May 1990, Abstract #539

9. D.S. Lashmore, "Electroformed Metal Matrix Composites", DARPA-3M Workshop on Metal Matrix Composites, Morgantown, West Virginia, July 10, 1990. (invited)

10. D. S. Lashmore, "High Speed Fabrication of Composites using Electrodeposition", Wright Patterson AFB, Materials Laboratory, Wright Patterson Airforce Base, August 8, 1990.(invited)

11. D S. Lashmore, "High Speed Deposition on Moving Fibers", SDI symposia, Woods Hole Mass. June10,12, 1991

12. D. S. Lashmore, "Electroformed Intermetallic Composites", Johns Hopkins Univrsity, Invited Speaker, Oct. 2, 1991(invited)

13. G.R. Stafford, "Electrochemical Materials Processing - Aluminum Alloy Deposition from Chloroaluminate Melts", Seventh Penn State Read Conference on Electrodeposition, June 20-24, 1988.(invited)

14. G.R. Stafford, "Properties of Electrocomposites", Eighth Penn State Read Conference on Electrodeposition, July 8-11, 1991.(invited)

15. G.R. Stafford, "Electrochemically Derived Composites", Capital Section of The Electrochemical Society, Nov. 7, 1991. (invited)

16. G.R. Stafford and C. Turner, "The Electrodeposition of Aluminum Alloys from Molten Salts", AESF 73rd Annual Technical Conference, July 1987, Chicago, Paper E-4.

17. G.R. Stafford, "The Electrodeposition of an Aluminum/Manganese Metallic Glass from Molten Salts", 172nd Meeting of the Electrochemical Society, Oct 1987, Abstract #227.

18. D.E. Hall and G.R. Stafford, "The Corrosion Behavior of Electrodeposited Aluminum-Manganese Alloys", 173rd Meeting of the Electrochemical Society, Atlanta, Georgia, May 1988, Abstract #37.

19. B. Grushko and G.R. Stafford, "The Effect of Mn Content on the Microstructure of Al-Mn Alloys Electrodeposited at 150 °C", 4th Israel Materials Engineering Conference- I.M.E.C. IV, Beer-Sheva, Israel 7-8 December, 1988.

20. G.R. Stafford and B. Grushko, "The Electrodeposition of Metastable Structures from Molten Salt Electrolytes", Proceedings of the Third International Conference on Quasicrystals and Incommensurate

Structures, Vista Hermosa, Mexico, May 27-June 2, 1989.

21. G.R. Stafford and B. Grushko, "The Electrodeposition of Al-Mn Quasicrystals and Intermetallics from Molten Salt Electrolytes", 176th Electrochemical Society Meeting, Hollywood, Florida, Oct. 1989, Abstract #255.

22. G. Stafford and D. Lashmore, Electrodeposition of Titanium Aluminides from Molten Salts", 14th Annual Conference on Composites, Materials and Structures, January 17-19, 1990, Cocoa Beach, Florida.

23. B. Grushko and G.R. Stafford, "A Comparison of Icosahedral Grain Size in Electrodeposited and Transformed Amorphous Al-Mn Alloys", Colloque 90 sur les Quasi-Cristaux, Orsay, France, 29-30 March, 1990.

24. C. R. Beauchamp, C.E. Johnson, D.S. Lashmore, E. Rosset, G.R. Stafford and N.S. Wheeler, "The Electrodeposition of Metal Matrix Composites", 177th Electrochemical Society Meeting, Montreal, Canada, May, 1990, Abstract #539.

25. C. E. Johnson, D.S. Lashmore, J.P. Moran, G.R. Stafford and G.M. Janowski, "The Electrodeposition of Metal Matrix Composites", IST-SDIO/ONR Woods Hole IV Research on Advanced Materials Review, Woods Hole, MA, June, 1990.

26. G.M. Janowski and G.R. Stafford and J.P. Moran, "The Fabrication and Microstructure of Electrodeposited Titanium Aluminides", The Materials Society Meeting, Detroit, Michigan, Oct. 1990.

27. G.R. Stafford, G.M. Janowski and J.P Moran, "The Electrodeposition of Aluminum-Titanium Intermetallics from Molten Salts", 178th Electrochemical Society Meeting, Seattle, Washington, Oct. 1990, Abstract #357.

28. D.S. Lashmore, P.N. Sharpless, G.R. Stafford and G.M. Janowski, "The Electrodeposition of Metal Matrix Composites", IST-SDIO/ONR Woods Hole VI Research on Advanced Materials Review, Woods Hole, MA, June, 1991.

29. G.R. Stafford and B. Grushko, "The Electrodeposition of

Aluminum-Based Intermetallics from Molten Salt Electrolytes", 180th Electrochemical Society Meeting, Phoenix, Arizona, Oct. 1990, Abstract #357.

Publications on Composites

1. N. S. Wheeler, D. S. Lashmore, and A. J. Shapiro, "Electrodeposited Cobalt-Tungsten, as a Diffusion Barrier for Nickel and Graphite at High Temperatures," (in progress).

2. N. S. Wheeler, D. S. Lashmore, A. J. Shapiro, and C. A. Handwerker, "Structural Characterization of the Nickel-Graphite Interface," (in WERB review).

3. N. S. Wheeler, "Review of the Nickel-Graphite Interface," *J. of Composites Technology and Research*, **12** (3), 1990, pp. 177-183.
G.R. Stafford, "The Electrodeposition of an Aluminum-Manganese Metallic Glass from Molten Salts", J. Electrochem. Soc. 136, 635-639 (1989).

4. B. Grushko and G.R. Stafford, "A Structural Study of Electrodeposited Aluminum-Manganese Alloys", Met. Trans. 20A, 1351-1359 (1989).

5. B. Grushko and G.R. Stafford, "A Structural Study of a Metastable BCC Phase in Al-Mn Alloys Electrodeposited from Molten Salts", Scripta Met. 23, 557-562 (1989).

6. B. Grushko and G.R. Stafford, "Formation of the Al-Mn Icosahedral Phase by Electrodeposition", Scripta Met. 23, 1043-1048 (1989).

7. B. Grushko and G.R. Stafford, "Phase Formation in Electrodeposited and Thermally Annealed Al-Mn Alloys", Met. Trans. 21A, 2869-2879 (1990).

8. G.R. Stafford, G.L. Cahen, Jr., and G.E. Stoner "Graphite Fiber-Polymer Matrix Composites as Electrolysis Electrodes", J. Electrochem. Soc. 138, 425-430 (1991).

9. G.M. Janowski and G.R. Stafford, "The Microstructure of Electrodeposited Titanium-Aluminum Alloys", MET. TRANS. 23A, 2715-2723 (1992).

10. G.R. Stafford, "The Electrodeposition of Aluminum-Titanium Alloys From Chloroaluminate Electrolytes", J. Electrochem. Soc., In Press. (Proceedings)

11. G.R Stafford and C. Turner, "The Electrodeposition of Aluminum from Molten Salts", Proc. AESF, Chicago, 1987.

12. G.R. Stafford, "The Electrodeposition of an Aluminum-Manganese Metallic Glass from Molten Salts", Proc. Corr., Electrochem. and Cat. of Metallic Glasses, Vol. 88-1, 172 Meet. Electrochem. Soc., Honolulu, Hawaii (1987).

13. B. Grushko and G.R. Stafford, "The Effect of Mn Content on the Microstructure of Al-Mn Alloys Electrodeposited at 150 °C", 4th Israel Materials Engineering Conference- I.M.E.C. IV, Beer-Sheva, Israel 7-8 December, 1988.

14. G.R. Stafford and B. Grushko, "The Electrodeposition of Metastable Structures from Molten Salt Electrolytes", Proceedings of the Third International Conference on Quasicrystals and Incommensurate Structures, Vista Hermosa, Mexico, May 27-June 2, 1989, Published by World Scientific, Singapore.

15. B. Grushko and G.R. Stafford, "A Comparison of Icosahedral Grain Size in Electrodeposited and Transformed Amorphous Al-Mn Alloys", Colloque 90 sur les Quasi-Cristaux, Orsay, France, 29-30 March, 1990.

Patents

1. N. S. Wheeler and D. S. Lashmore, "Metal-coated Fiber Compositions Containing Alloy Barrier", U. S. Patent Application #31,109, Pending.

2. N. S. Wheeler, D. S. Lashmore, and A. J. Shapiro, "A Process For Producing Diamond", U. S. Patent #31,282, Pending.

3. D. S. Lashmore and M. P. Dariel, "Predetermined Concentration Graded Alloys and Method for Production Thereof", Application 07/219,531 (Due to be issued shortly)

PUBLICATIONS

Scripta METALLURGICA Vol. 23, pp. 1043-1048, 1989
Printed in the U.S.A.

FORMATION OF THE Al-Mn ICOSAHEDRAL PHASE BY ELECTRODEPOSITION

Benjamin Grushko
Department of Materials Engineering
Technion-Israel Institute of Technology
Haifa, Israel

Gery R. Stafford
Metallurgy Division
National Institute of Standards and Technology
Gaithersburg, Maryland

(Received April 13, 1989)

Introduction

Alloys which are formed under conditions far from equilibria generally contain metastable phases which can be crystalline, amorphous or quasicrystalline. Stable crystalline phases can be formed fairly easily as a result of slow cooling during conventional casting or prolonged heat treatment. Metastable amorphous phases have also been formed quite easily by low temperature processing such as ion-beam irradiation (1-3), sputtering deposition (4), and electrodeposition (5). The direct formation of completely quasicrystalline single-phase material, having a level of free energy between that of an amorphous and a stable crystalline phase (6), requires rigorous control of several processing variables.

In the Al-Mn system, icosahedral grains of about 20 μm have been observed in specimens prepared by electron beam surface melting (7). These grains however, often coexist with additional phases and the primary forces influencing phase growth cannot be rigorously controlled. Vacuum processing which affords one somewhat greater control over the solidification process, allows one to achieve a fine, somewhat more homogeneous structure (1-3).

It has been reported previously (5,8) that Al-Mn alloys electrodeposited at 150 °C from a molten salt electrolyte comprised of $AlCl_3$, NaCl and $MnCl_2$, contain amorphous and crystalline metastable phases. The amorphous phase has a lower Mn composition limit of 26 wt.%, quite close to that of Al_6Mn (5). The higher composition limit for Mn in the amorphous phase has not been determined precisely; however at compositions exceeding 39 wt.% Mn, the amorphous phase is gradually replaced by a crystalline bcc phase, believed to be high temperature Al_8Mn_5 with the Cu_5Zn_8 (γ-brass) structure (8).

The study of sputter deposition of an Al-Mn alloy containing 30 wt.% Mn (4) revealed that at deposition temperatures of -98 and 52 °C, only an amorphous phase was observed. At temperatures between 225 and 375 °C, the icosahedral phase was formed (4). Consequently, one might expect that an increase in electrolyte temperature would favor the direct electrodeposition of the quasicrystalline phases in a manner somewhat analogous to that reported for sputter deposition.

We report below on the formation of the icosahedral and decagonal phases by electrodeposition of Al-Mn alloys from a molten salt electrolyte.

Experimental Procedure

The Al-Mn alloys were electrodeposited galvanostatically onto planer copper substrates from a chloroaluminate electrolyte comprised of a 2:1 mole ratio of $AlCl_3$:NaCl with controlled additions of $MnCl_2$. The electrochemical cell, heated by a muffle furnace, was made of quartz and held approximately 125 ml of electrolyte. The cell was

0036-9748/89 $3.00 + .00

covered by a teflon cap through which the electrodes were tightly fit. The counter electrode was an aluminum wafer (99.999%) measuring 2.5cm x 2.5cm and placed parallel to and 2 cm from the copper substrate (working electrode) which measured 1cm x 2.5cm x .05cm. The reference electrode was an aluminum wire (99.999%) placed in the same electrolyte and positioned between the working and counter electrodes. An argon purge was maintained over the melt at all times. Methods for electrolyte handling and preparation are given elsewhere (9,10). Alloys were electrodeposited at temperatures ranging from 150 to 325 °C. The pertinent electrolyte compositions and deposition parameters for selected specimens are shown in Table I.

The electrodeposits were studied by transmission electron microscopy (TEM), scanning electron microscopy (SEM), energy dispersive spectroscopy (EDS), and x-ray diffraction. Alloy composition of all specimens (Table I) was determined by performing EDS (quantitative analysis) on polished cross-sections using pure aluminum and manganese standards. The reported values are an average of at least four measurements.

The portion of the deposit facing the counter electrode was removed from the substrate by dissolving the copper in concentrated HNO_3. The short exposure times required for copper dissolution has little effect on the electrodeposited alloy. TEM of the bulk electrodeposit was performed on specimens electropolished by a twin jet technique using 20% perchloric acid in methanol at -20 °C. Selected specimens were prepared so that the electrodeposit in contact with the copper substrate could be examined. These samples were prepared by tapered grinding on metallographic paper, followed by copper dissolution in concentrated HNO_3.

Results

The study of electrodeposited specimens by x-ray diffractometry reveals that the deposits obtained at electrolyte temperatures from 150 up to 250 °C are entirely amorphous in the compositional range of 26-39 wt.%Mn (fig 1a,b). TEM observations of the bulk electrodeposit confirm the complete amorphous structure of these alloys. No contrast is visible in the TEM image and typical electron diffraction patterns for these specimens consist of one strong and two to three weaker rings.

As opposed to the bulk structure, the initial layers of material electrodeposited at 225 and 250 °C consist of fine, bright amorphous grains divided by a darker network (fig 2). Contrast fluctuations which do not correlate to the above grains are visible in the dark field image of specimens deposited at 250 °C.

Different electron diffraction patterns were observed in these interfacial regions of specimens deposited at different temperatures. Normalized line scan plots of ring selected area diffraction (SAD) patterns are shown in fig 3. An increase in the deposition temperature from 150 to 225 °C results in the appearance of additional reflections which correspond to d-spacings of 0.385 nm and 0.146 nm (fig 3b). A sharpening of these reflections is observed in the specimen deposited at 250 °C, while additional reflections corresponding to d-spacings of 0.338 nm and 0.249 nm are resolved (fig 3c). In addition, a shift of d-spacings with respect to the main reflection is observed. The diffraction pattern in fig 3c is consistent with that of the fine-grain icosahedral phase. A similar electron diffraction pattern, observed in certain areas of a 25 wt.% Mn alloy deposited at 150 °C (5), is shown in fig 3e. Such diffraction patterns were not observed in other regions of the specimen however.

A further increase in the deposition temperature to 275-300 °C under otherwise identical conditions to those which produced the 33-35 wt.% Mn amorphous phase at 250 °C, results in a dramatic increase in Mn content (to approximately 45 wt.%) and a crystalline deposit. The x-ray diffraction pattern (fig 1c) obtained from this specimen is consistent with that seen for stable triclinic $Al_{11}Mn_4$.

In order to maintain an alloy composition within the limits which allow for the formation of the amorphous phase, the $MnCl_2$ content of the electrolyte was reduced to 0.2 wt.% for the deposition at elevated temperatures. Deposition from this electrolyte at 300 °C produced an alloy containing 16 wt% Mn. X- ray diffraction indicates the appearance of fcc-Al reflections (fig 1d) in agreement with previous studies which reveal a mixture of fcc-Al and an amorphous phase in Al-Mn alloys electrodeposited at 150 °C for compositions ranging from 10 to 26 wt.% Mn (5). Additional reflections appear with the broad, amorphous peak and are resolved further when the deposition temperature is increased to 325 °C (fig 1e). TEM examination of the last specimen reveals areas which are completely icosahedral. Additional areas of this specimen (No.7, Table I) are composed of fcc-Al plus the icosahedral phase. The amorphous and decagonal phases were also observed in this specimen.

TABLE I

Deposition Parameters and Electrolyte Compositions for Selected Specimens.

Specimen	1	2	3	4	5	6	7
$MnCl_2$ Wt.%	0.7	2.4	1.2	1.6	1.3	0.2	0.2
Cur. Den. mA/cm^2	22	50	50	50	50	20	12
Potential Volts/Al	*	-0.45	-0.29	-0.24	-0.19	-0.10	-0.11
Temp. °C	150	150	225	250	300	300	325
Charge Den. $Coul/cm^2$	100	30	32	30	30	30	30
Alloy Comp. Wt.% Mn (EDS)	25.0	39.0	28.1	33.4	45.8	16.4	16.2

* not measured

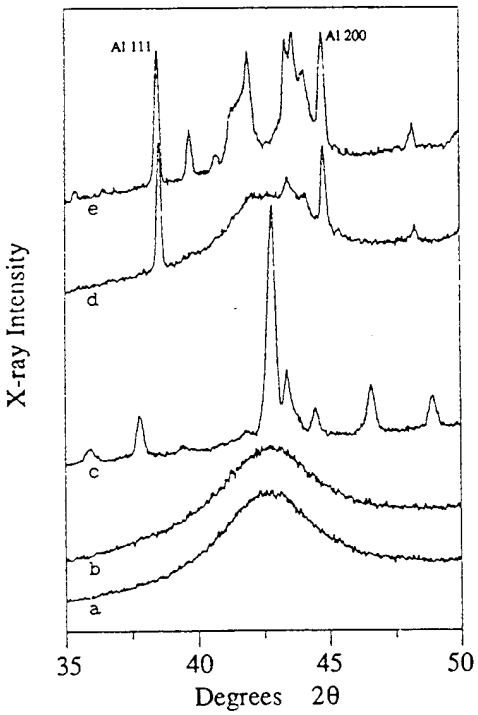

FIG. 1. X-ray diffraction patterns of electro-deposited specimens: (a) specimen 2, Table I; (b) specimen 4; (c) specimen 5; (d) specimen 6; (e) specimen 7.

FIG. 2. Transmission electron micrograph of the interfacial area of the as-deposited 28 wt.% Mn alloy; specimen 3, Table I.

Under the conditions used for depositing this specimen, the icosahedral regions are seen to grow as nodular, partially disconnected grains (fig 4a,b). The line scan plot of the selected area diffraction of these regions is shown in figure 3d and reveals that the two strongest reflections at 0.217 nm and 0.207 nm for the icosahedral phase are resolved. The individual grains are relatively large (fig 4c) and allow one to perform spot selected area diffraction, thereby confirming the icosahedral symmetry (fig 4d).

Discussion

A fine-grained icosahedral phase has been observed at the deposit-substrate interface at temperatures as low as 225 °C while the bulk alloy has an amorphous structure. This region in the vicinity of the interface is the first deposited and is essentially subject to an isothermal anneal for the duration of the deposition process, 10 minutes. One could argue that the presence of the icosahedral phase at the interface is the result of short term heat-treatment at 225-250 °C. In principle, these deposition temperatures are high enough for transformation of the amorphous to quasicrystalline phase to occur (1,5), but generally longer times are required to affect this transformation than those incurred during the deposition process. Controlled heat treatment of the bulk alloy at 250 °C for 10 min does not show the above effect. One can then conclude that the icosahedral phase found at the interface is directly formed in these experiments.

Similarly, the formation of relatively coarse icosahedral grains at 325 °C is evidently direct. Coarsening of this magnitude has not been observed during heat treatment of the amorphous phase; transformation into the stable crystalline phases is favored over coarsening of the icosahedral grains (5).

The degree of ordering during growth is defined by the processes of new layers formation and surface diffusion, the latter being temperature dependent. Deposition at the higher temperature results in a greater diffusion path on the surface, and consequently, larger areas of coherency. This is reflected in the evolution of the electron diffraction patterns of electrodeposited alloys with increasing deposition temperature (fig 3a-d). Similar changes

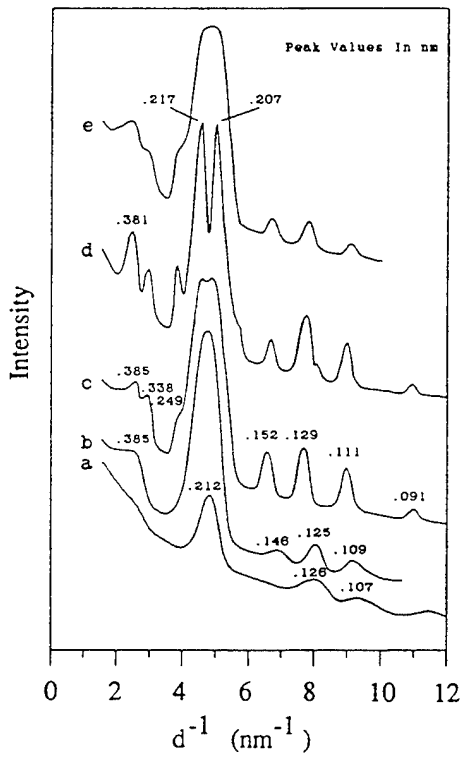

FIG. 3. Line scan plots of ring electron diffraction obtained from the following specimens: (a) specimen 2, Table I; (b) specimen 3; (c) specimen 4; (d) specimen 7; (e) specimen 1.

have been observed for the isothermally heat-treated amorphous phase with increasing time (3). Observation of the icosahedral phase in an alloy electrodeposited at 150 °C supports the opinion that icosahedral ordering can be achieved at a lower temperature if the deposition rate is reduced. Subsequently, the time at which a reduced species is allowed to move on the surface is increased. Of course dramatic reductions in deposition rate (probably orders of magnitude) need to be made to compensate for the reduced surface diffusion because of its exponential dependence on temperature. The current densities reported in Table I are average values and though the electrode configuration used in these experiments should provide a uniform current distribution, localized fluctuations in the deposition rate frequently occur.

Quite often one finds that localized fluctuations in electrode potential and surface concentration of electroactive species associated with surface features causes the growth of selected regions to be retarded. In extreme cases, localized dissolution may even occur. This is particularly possible in molten salt processes where the reaction kinetics are generally reversible and small differences in overpotential may give rise to large differences in local current density. Close examination of a nodule which was found protruding from an otherwise specular amorphous deposit indicates that the base of the nodule is quite smooth while the top of the nodule appears rough (fig 3 in ref (5)). The preferential growth at the nodule tip may have resulted in a much lower current density along the base. Such growth conditions may be responsible for the appearance of the icosahedral phase in an otherwise amorphous alloy deposited at 150 °C.

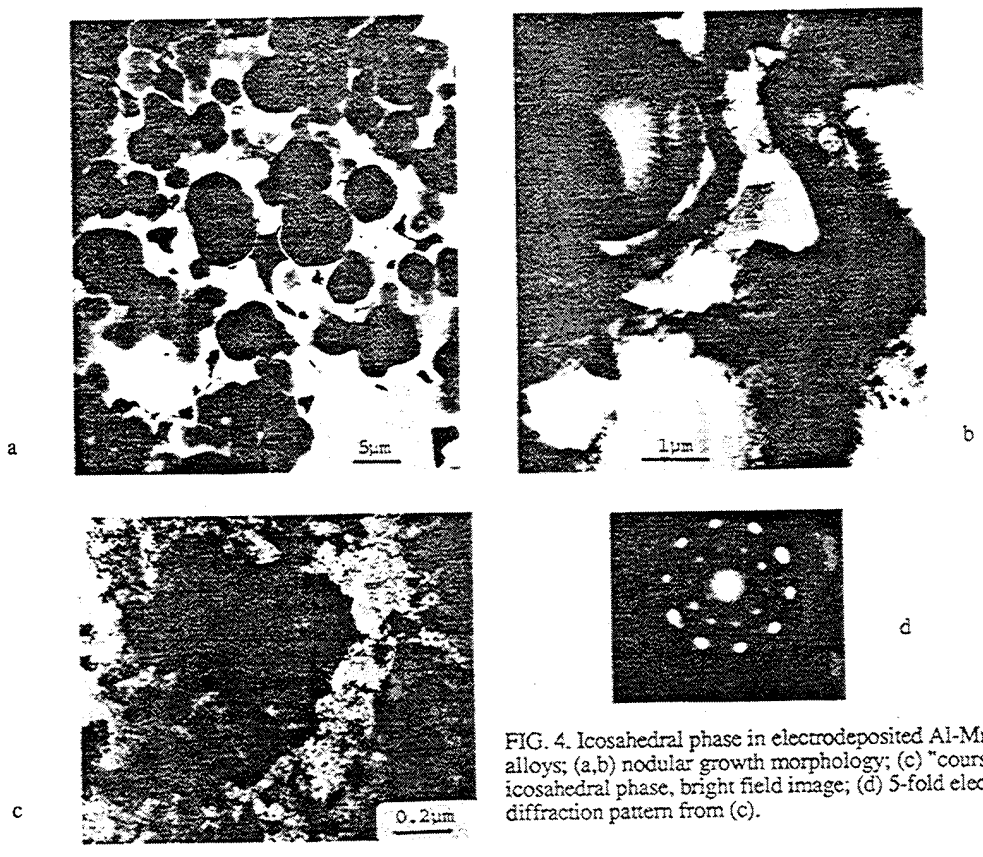

FIG. 4. Icosahedral phase in electrodeposited Al-Mn alloys; (a,b) nodular growth morphology; (c) "course" icosahedral phase, bright field image; (d) 5-fold electron diffraction pattern from (c).

The direct formation of completely quasicrystalline single-phase material requires rigorous control of several processing variables such as alloy composition, temperature, and current density which is proportional to the deposition rate. Since the average deposition rate is controlled externally and the temperature at the cathode-electrolyte interface is constant, the primary concern should be the ability to form alloys of uniform composition under conditions of uniform, lateral growth.

The manganese composition of the electrodeposited alloy can be controlled by several parameters, the most dramatic of which is the relative concentration of the electroactive species, $Al_2Cl_7^-$ and Mn^{++}, in the electrolyte (10). As the ratio of Mn^{++} to $Al_2Cl_7^-$ is increased, the manganese composition of the alloy increases proportionally under deposition conditions where both species are diffusion limited. The effect of electrolyte composition on alloy composition is seen in specimens 2-4 (Table I).

Below 250 °C, there does not appear to be a significant change in alloy composition with temperature. As the temperature approaches 300 °C however, an appreciable increase in the Mn content of the alloy is observed (specimen 5). This enhanced reduction in Mn^{++}, and the inability to predict the dependence of the kinetics of each electroactive species on temperature, resulted in depositing from an electrolyte dilute in Mn^{++} (specimens 6 and 7). Adjustments to alloy composition can be made by increasing the deposition current beyond the diffusion limiting current for Mn^{++} reduction. Since the rate of manganese deposition is limited by mass transport, the increase in total deposition current results in an increase in the aluminum current efficiency, thereby making the resultant alloy aluminum rich.

Depositing from an electrolyte in which either of the electroactive species is limited by mass transport generally results in deposits which are compositionally non-homogeneous and are subject to morphological instabilities (nodules or dendrites). The nodular morphology of the icosahedral phase (fig 4a,b) may be the result of depositing at the manganese limiting current and not inherent in the technique.

Increasing the $MnCl_2$ content of the electrolyte to a level which allows for the deposition of alloys in the icosahedral composition range under kinetic control should improve deposit morphology and might lead to larger icosahedral grains. In addition, uniformity in alloy composition can be promoted by controlling the hydrodynamics at the electrode-electrolyte interface by utilizing a rotating disk or rotating cylinder cathode. Though these techniques are commonly practiced in aqueous electrochemistry, their use in molten salt electrolytes has been limited.

Acknowledgements

The authors would like to thank Alexander Shapiro, and Leo Bendersky for their technical contributions. The technical assistance of Sandra Clagget is gratefully acknowledged. One of the authors (B.G.) would like to acknowledge the financial support of the Israel National Council for Research and Development. This work was jointly supported by the Office of Naval Research (Contract N00014-88-F-0091) and the NIST metal matrix competence building program.

References

1. D.A. Lilienfeld, M. Nastasi, H.H. Johnson, D.G. Ast and J.W. Mayer, Phys. Rev. Lett. 55, 1587 (1985).
2. D.M. Follstaedt and J.A. Knapp, Mat. Sci. Eng. 90, 1 (1987).
3. K. Urban, N. Moser and H. Kronmuller, Phys. Stat. Sol. (a) 91, 411 (1985).
4. K.G. Kreider, F.S. Biancaniello and M.J. Kaufman, Scripta Met. 21, 657 (1987).
5. B. Grushko and G.R. Stafford, Metall. Trans., In Press.
6. D.M. Follstaedt and J.A. Knapp, Nucl. Instrum. Meth. Phys. Res. B24/25, 542 (1987).
7. R.J. Schaefer, L.A. Bendersky, D. Shechtman, W.J.Boettinger and F.S. Biancaniello, Metall. Trans. 17A, 2117 (1986).
8. B. Grushko and G.R. Stafford, Scripta Met., In Press.
9. G.R. Stafford, Proc. Corr., Electrochem. and Cat. of Metallic Glasses, 172 Meet. Electrochem. Soc., Honolulu, Hawaii, p. 348 (1987).
10. G. R. Stafford, J. Electrochem. Soc. 136, 635 (1989).

Reprinted from JOURNAL OF THE ELECTROCHEMICAL SOCIETY
Vol. 136, No. 3, March 1989
Printed in U.S.A.

The Electrodeposition of an Aluminum-Manganese Metallic Glass from Molten Salts

Gery R. Stafford*

Institute for Materials Science and Engineering, National Institute of Standards and Technology, Gaithersburg, Maryland 20899

ABSTRACT

The electrodeposition of binary aluminum-manganese alloys from chloroaluminate molten salts is reported. The manganese content of the electrodeposit varies from 7 to 30 w/o and is dependent upon deposition potential and the relative concentrations of $Al_2Cl_7^-$ and Mn^{++} in the melt. At small cathodic overpotentials the deposition process, with respect to alloy composition, is kinetically controlled. At larger cathodic overpotentials, it becomes mass transport limited in Mn^{++} and then $Al_2Cl_7^-$. The most uniform and brightest deposits are obtained at a constant potential of −0.3V with respect to an aluminum wire in the same electrolyte. The potential dependence of alloy composition allows one to create homogeneous, graded and modulated structures from a single electrolyte. The structure of the as-deposited alloy appears to be that of a metallic glass above 27 w/o manganese and a mixture of glass and supersaturated aluminum below 27 w/o. Heating to 400°C converts the deposit containing less than 26 w/o Mn to a mixture of the orthorhombic Al_6Mn intermetallic and aluminum. The ability to electrodeposit intermetallic compounds on a near atomic scale presents interesting possibilities for high temperature alloys.

Metallic glasses have received widespread attention because of their promising chemical, electrical, and mechanical properties. These single-phase alloys can be of the metal-metalloid type where late transition metals such as Fe, Co, Ni, Pd, or Au are combined with B, C, Si, P, or Ge. Binary metal-metal glasses such as Cu-Zr, Ni-Nb, Ti-Be, and Ca-Mg have also been demonstrated (1). Aluminum containing metallic glasses (Ca-Al, La-Al, and Y-Al) have been investigated recently for their electrical properties (2-5), but very little work has been reported on the properties of Al-rich metallic glasses.

Aluminum and some of its alloys can be electrodeposited from molten salt electrolytes. The chemical equilibria operative in $AlCl_3$/NaCl melts under a wide range of $AlCl_3$ concentrations above the equimolar point are well known (6-9), and extensive work has been reported on the deposition of pure aluminum from these electrolytes (10-20). The electroactive species in 2:1 mole ratio $AlCl_3$:NaCl melts is $Al_2Cl_7^-$ and is present at concentrations approaching 3.5*M*. Its reduction occurs by the following

$$4Al_2Cl_7^- + 3e^- \longrightarrow Al + 7AlCl_4^- \qquad [1]$$

The reduction of $AlCl_4^-$ occurs at potentials more negative than that required for $Al_2Cl_7^-$ reduction and becomes prominent as the acidity ($AlCl_3$ content) of the melt is reduced. The kinetics for the aluminum deposition reaction are quite fast, and exchange current densities on the order of 20 A/cm² have been measured at 450°C using the galvanostatic double-pulse method (21). With exchange currents of this magnitude, the aluminum cathode is essentially at equilibrium even at deposition currents approaching 100 mA/cm². Consequently, one has little electrochemical control over deposit morphology which is generally nodular and quite often dendritic (22).

Efforts to obtain bright aluminum deposits from chloroaluminate electrolytes have included studies of deposition onto various substrates, the use of ac superposition (19) and the addition of agents including water (14), organics and metal chlorides (23). The most remarkable improvement has been seen with the addition of small amounts of $MnCl_2$ (24, 25). Specular deposits containing 16-45 weight percent (w/o) Mn have been obtained from molten salt electrolytes containing 0.4 w/o $MnCl_2$ at current densities as high as 100 mA/cm². The manganese content of the electrodeposit was reported to increase with increasing $MnCl_2$ and an empirical relationship was developed so that the manganese content of the electrodeposit could be predicted from melt composition. These investigators found alloy composition to be independent of current density. Hayashi reported a similar increase in Mn composition of the deposit as well as an increase in the activation overpotential with increasing $MnCl_2$ (26).

The structures of these electrodeposited aluminum-manganese alloys have been investigated (27). Low manganese deposits (arbitrarily chosen as less than 16 w/o Mn) consisted entirely of a supersaturated solid solution of manganese in aluminum. High manganese deposits were reported to contain the supersaturated solid solution and also exhibited electron diffraction patterns consistent with that of a glassy structure. The diffuse band could not be identified directly from electron diffraction, but other data (27) suggested that it was due to the Al_6Mn intermetallic. A crystallite size for the intermetallic was not reported.

The purpose of this paper is to describe our work on aluminum-manganese alloy deposition from a eutectic $AlCl_3$/NaCl melt. Our efforts have concentrated on characterizing the aluminum-manganese deposition process and determining the parameters influencing alloy composition, deposit quality, and structure. Contrary to the previously cited literature, we find that the manganese content of the deposit is clearly potential dependent; consequently, the deposition of some very interesting structures is possible.

Experimental Procedure

The $AlCl_3$ was obtained from Aldrich[1] (99.99% pure) and was used as received. The NaCl (Mallinckrodt, Reagent) was dried for 4h at 500°C. The manganous chloride (Fisher, Reagent) was received in the hydrated form, $MnCl_2 \cdot 4\,H_2O$, and was heated to 225°C for 4h to remove the water (dehy-

*Electrochemical Society Active Member.

[1]Certain trade names are mentioned for experimental information only; in no case does it imply a recommendation or endorsement by NIST.

dration temperature is 198°C). The reagents were then transferred to an argon dry box. The composition of all melts was 2:1 mole ratio $AlCl_3$:NaCl. The powders were thoroughly mixed in the dry box before being transferred to the cell, which has been described elsewhere (22). The temperature of the mixture was increased to 150°C and the resultant melt was pre-electrolyzed for 48h using a platinum screen working electrode held at a potential of +0.01V with respect to an aluminum wire in the same electrolyte. After pre-electrolysis, the background current density at a tungsten indicator electrode was 340 $\mu A/cm^2$ at +0.1V *vs.* Al at a sweep rate of 0.1 V/s. The desired amount of $MnCl_2$ was then added. The melt temperature for all experiments was 150°C.

Potential control was maintained with a PAR Model 363 potentiostat/galvanostat and a PAR Model 175 universal programmer. The counter and reference electrodes were 2 mm aluminum wire (99.99%) while the substrate for the electrodeposits was copper (OFHC) either in the form of a 0.76 mm wire or 1 cm × 2.5 cm × 0.05 cm wafer. In all cases the copper was electropolished in 50% H_3PO_4 and then thoroughly dried. After introduction into the melt, the working electrode was allowed to come to thermal equilibrium at a potential of +0.2V *vs.* Al to cathodically protect the copper. The deposition process was controlled galvanostatically at 40 mA/cm^2 until a charge of one C/cm^2 had passed to eliminate problems associated with nucleation overpotentials. At this time the PAR 363 was manually switched to the potentiostat mode (while the cell was disabled) and further deposition was controlled potentiostatically.

X-ray diffraction (Cu-Kα) patterns were measured for the deposited films after the copper wafer substrate was removed by concentrated HNO_3. The manganese content of these free standing films was determined by atomic absorption. Deposits on copper wires were overplated with bright copper (after a room temperature zincate treatment and cyanide copper strike) and were then mounted in epoxy to expose the cross section. Alloy composition of these alloys was determined by energy dispersive spectroscopy (EDS) quantitative analysis using pure aluminum and manganese standards. Deposit hardness was measured on these polished cross sections using a Knoop indenter under a 10g load; the values reported are the average of four measurements.

Results

Steady-state current-potential measurements and linear sweep voltammetry at slow scan rates normally yield little kinetic information in molten salt systems since ohmic and mass transport contributions are significant when compared to the activation overpotential even at very low current densities. Figure 1 is a set of curves which qualitatively shows this effect and its dependence on $MnCl_2$. In aqueous electrolytes, the reversible potential for manganese deposition is positive of that for aluminum. In contrast, manganese is less noble than aluminum in this chloroaluminate electrolyte and the reduction of Mn^{++} occurs at a potential more negative than the reversible potential for aluminum deposition; consequently discrete reduction peaks for the two reactions are not seen. At low $MnCl_2$ concentrations, the curve is similar to that for pure aluminum where the entire scan is dominated by solution resistance, resulting in a linear current-potential curve in this region. As the $MnCl_2$ concentration is increased, the activation overpotential increases dramatically and dominates at the lower current densities. It is this shift from ohmic to activation control which is at least partially responsible for promoting lateral growth and eliminating the nodular and dendritic morphology.

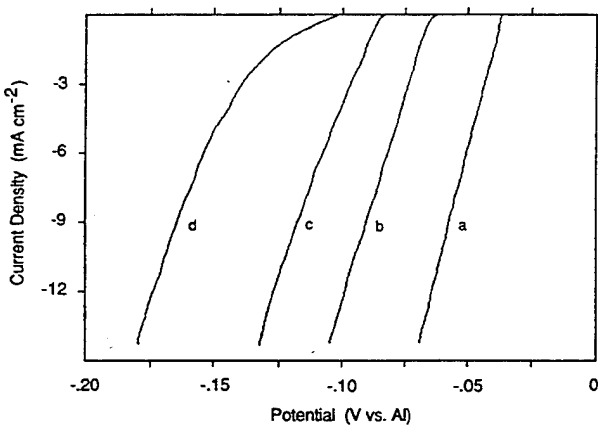

Fig. 1. Linear sweep voltammetry in 2:1 mole ratio $AlCl_3$:NaCl electrolyte with (a) 0.25 w/o $MnCl_2$; (b) 0.50 w/o $MnCl_2$; (c) 0.75 w/o $MnCl_2$; (d) 1.0 w/o $MnCl_2$. One C/cm^2 was first deposited onto a copper substrate at 40 mA/cm^2 to eliminate problems associated with nucleation overpotentials. Sweep rate = 5 mV/s and T = 150°C.

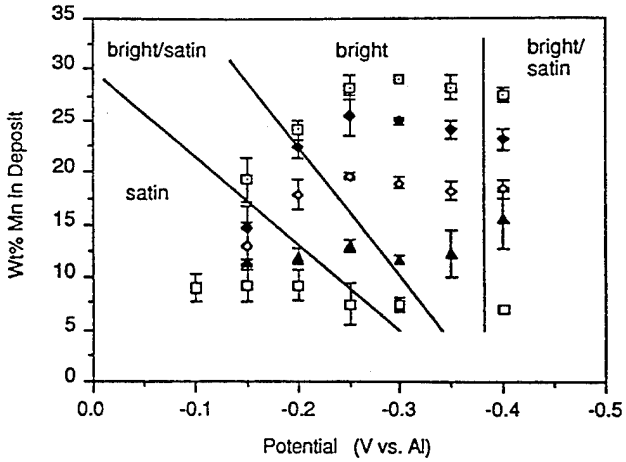

Fig. 2. Alloy composition and deposit quality as a function of deposition potential for a 2:1 $AlCl_3$:NaCl melt containing 0.25 w/o (□); 0.50 w/o (▲); 0.75 w/o (◇); 1.0 w/o (◆); and 1.25 w/o (⊡) $MnCl_2$. Each reported alloy composition is the average of 12 EDS readings. Substrate was a 0.76 mm diameter copper wire. Melt temperature was 150°C.

Figure 2 is a set of curves relating alloy composition and deposit quality to deposition potential and $MnCl_2$ concentration. The manganese content of the deposit varies from 7 to 30 w/o and increases with increasing $MnCl_2$. Contrary to reports in the literature (24), there is a dramatic dependence of alloy composition on potential, particularly at the higher $MnCl_2$ concentrations. At all concentrations, the manganese content of the deposit drops slightly at a critical potential. The potential at which this occurs shifts to more negative values with increasing $MnCl_2$, suggesting that Mn^{++} is becoming mass transport limited. At a potential of −0.35 V/Al the deposition current is seen to approach a constant value, indicating that $Al_2Cl_7^-$ is nearly diffusion limited as well.

The deposit quality of all of the alloys depicted in Fig. 2 is much superior to that of pure aluminum and generally improves with increasing $MnCl_2$ and at more negative potentials. Specular deposits were obtained at −0.3 V/Al for nearly all $MnCl_2$ concentrations and the alloy composition ranged from 12 to 29 w/o. At potentials negative of −0.35 V/Al, deposit quality drops without an appreciable change in alloy composition. These results clearly indicate that a high manganese alloy is not required and is certainly not a sufficient condition for generating bright deposits. The deposition potential is the key to obtaining bright deposits with the favorable potential window broadening with increasing $MnCl_2$ concentration. It is also interesting to note that the standard deviation of the reported alloy compositions (average of 12 EDS readings) can be related to deposit quality. The most uniform deposits are also the brightest and were deposited at −0.3 V/Al.

X-ray diffraction patterns were measured for the electrodeposited films. Some of the patterns are shown in Fig. 3. Deposits containing greater than 27 w/o Mn have patterns consistent with that of a metallic glass structure, *i.e.*, a broad, diffuse peak is seen rather than sharp Bragg diffraction peaks. As the manganese content of the deposit is reduced, the (111) and (200) Bragg diffraction peaks for aluminum begin to appear and reveal a lattice constant

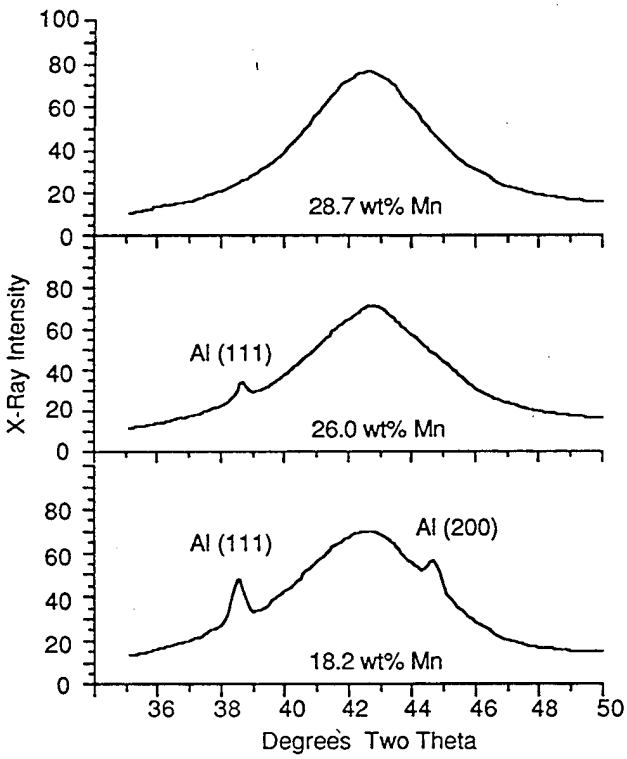

Fig. 3. X-ray (Cu-Kα) diffraction of electrodeposited aluminum-manganese alloys.

smaller than that for pure aluminum. This lattice reduction is due to the substitution of aluminum by manganese in solid solution. The equilibrium phase diagram for the aluminum-manganese system shows that aluminum and orthorhombic Al_6Mn are in equilibrium up to 25 w/o Mn, beyond which Al_6 Mn and the λ phase (hexagonal Al_4Mn) are in equilibrium (28). The diffraction patterns in Fig. 3 indicate that the electrodeposited alloys are subject to some of the same stoichiometric limitations as those shown in the equilibrium phase diagram since fcc aluminum is not seen in alloys containing greater than 27 w/o Mn. These results suggest that the glassy structure has a stoichiometry similar to that of Al_6Mn. Though metallic glasses can be expected to show short range order, none of the diffraction techniques used by us or reported in the literature (27) have positively identified this glass as the Al_6Mn intermetallic.

When electrodeposits containing less than 26 w/o Mn are heat-treated to 400°C, the alloy is converted to a mixture of the Al_6Mn intermetallic and aluminum. After crystallization, alloy hardness increases significantly and becomes widely scattered due to segregation of aluminum and the intermetallic, Fig. 4. The intermetallic grain size was not determined and its distribution in the aluminum and crystallization kinetics are not presently known.

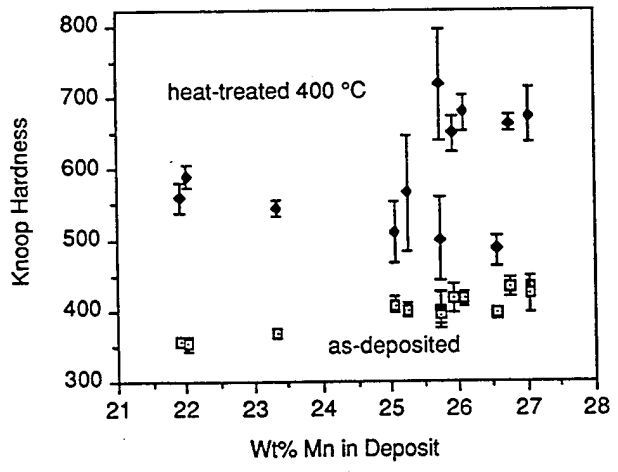

Fig. 4. Knoop hardness (10g load) vs. alloy composition for electrodeposited alloys before and after crystallization.

The potential dependence of manganese incorporation allows one to deposit some very interesting structures. Figure 5 is a set of EDS linescans from deposit cross sections showing the relative intensities for aluminum and manganese under different deposition conditions from the same melt containing 1.5 w/o $MnCl_2$. When the potential is held constant with respect to an aluminum wire in the same electrolyte, the concentrations of the two species are constant throughout the 20 μm deposit. Under galvanostatic control, the manganese concentration drops radially. As the deposit thickens, the surface area increases resulting in a lower current density and overpotential. In the potential dependent range, Fig. 2, the smaller cathodic overpotential causes a reduction in the manganese content of the alloy. Steeper concentration gradients are possible through computer control by stepping the potential at a rate proportional to the deposition current.

Control over composition provides a means of precisely modulating the microstructure to produce finely spaced layers alternately depleted and rich in manganese. Microstructures of this type have been shown to have significantly enhanced mechanical properties (29), and after heat-treatment, would allow one to produce alternating layers of ductile Al-Mn and Al_6Mn intermetallic. Modulated structures were obtained through potential modulation between −0.3 and −0.15 V/Al. The manganese rich layers shown in Fig. 5 contain about 30 w/o Mn (EDS, quantitative analysis) while the adjacent layers contain 20 w/o. The layer spacings in this example are approximately 3 μm so they could be resolved by EDS, but much smaller layer spacings are possible. An optical micrograph of a modulated structure is shown in Fig. 6; the layers are continuous with very sharp interfaces.

Discussion

The data shown in Fig. 2 suggest that the deposition process becomes diffusion limited in Mn^{++} at a potential dependent upon $MnCl_2$ concentration and the deposition current indicates that $Al_2Cl_7^-$ is diffusion limited at −0.35 V/Al. At any time during the deposition process, the alloy

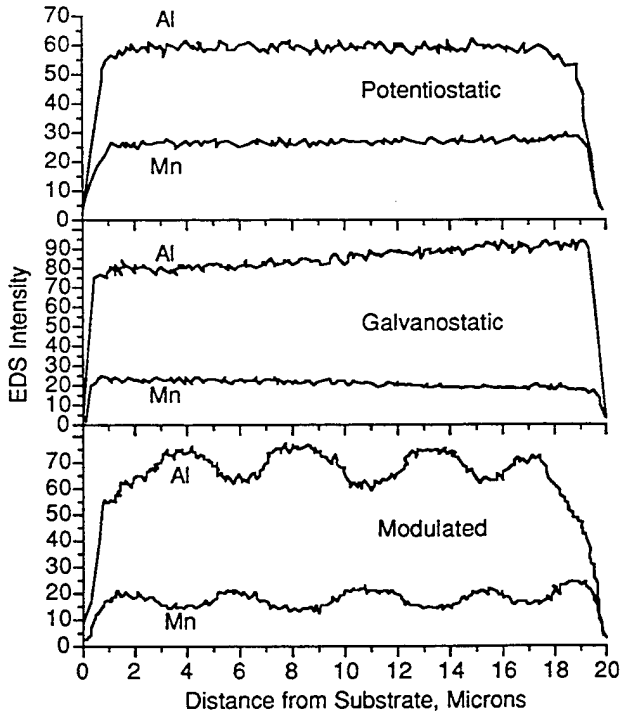

Fig. 5. Distribution of manganese and aluminum radially through the electrodeposit under various deposition conditions; (a) potentiostatic, $E = -0.3$ V/Al; (b) galvanostatic, $I = 40$ mA/cm^2; and (c) modulated, pulsed between −0.3 and −0.15 V/Al for 5 C/cm^2 at each potential.

composition can be expressed as the ratio of the partial currents

$$W_{f,Mn} = \frac{\frac{N_{Mn}\, i_{Mn}}{n_{Mn}}}{\frac{N_{Mn}\, i_{Mn}}{n_{Mn}} + \frac{N_{Al}\, i_{Al}}{n_{Al}}} \quad [2]$$

where N_{Mn} and N_{Al} are the molecular weights, i_{Mn} and i_{Al} are the partial currents, and n_{Mn} and n_{Al} are the equivalents per mole for manganese and aluminum. When both electroactive species are diffusion limited, the partial currents can be expressed as limiting currents (from Fick's second law assuming conditions of linear diffusion)

$$i_{Mn} = \frac{n_{Mn^{++}}\, \mathbf{F}\, A\, D_{o,Mn^{++}}\, C_{o,Mn^{++}}^{\bullet}}{\delta}, \qquad i_{Al} = \frac{n_{Al_2Cl_7^-}\, \mathbf{F}\, A\, D_{o,Al_2Cl_7^-}\, C_{o,Al_2Cl_7^-}^{\bullet}}{\delta} \quad [3]$$

where n are the equivalents for the electroactive species, $\mathbf{F}$ is Faraday's constant, A is the electrode area, D_o are diffusion coefficients, $C_o^{\bullet}$ are the bulk concentrations of the electroactive species, and δ is the diffusion layer thickness which is assumed to be equal for the two species. Since the substrate in these experiments is a 0.76 mm wire, the electrode radius is only about a factor of five greater than the steady-state diffusion layer thickness and enhanced cylindrical diffusion may be a factor. Unfortunately, an exact solution to the diffusion equation for the cylindrical case does not exist (solutions may be obtained in terms of Bessel functions chosen to satisfy the boundary conditions for the experiment). Assuming δ is less than 100 μm, we estimate that this contribution will be less than about 10% of the limiting current for the case of linear diffusion. Since it is assumed that the diffusion conditions are the same for both Mn^{++} and $Al_2Cl_7^-$, then δ and the cylindrical terms will cancel and consequently will not affect the following results. Substitution of Eq. [3] into Eq. [2] yields the following

$$W_{f,Mn} = \frac{\frac{N_{Mn}\, n_{Mn^{++}}\, \mathbf{F}\, A\, D_{o,Mn^{++}}\, C_{o,Mn^{++}}^{\bullet}}{n_{Mn}\, \delta}}{\frac{N_{Mn}\, n_{Mn^{++}}\, \mathbf{F}\, A\, D_{o,Mn^{++}}\, C_{o,Mn^{++}}^{\bullet}}{n_{Mn}\, \delta} + \frac{N_{Al}\, n_{Al_2Cl_7^-}\, \mathbf{F}\, A\, D_{o,Al_2Cl_7^-}\, C_{o,Al_2Cl_7^-}^{\bullet}}{n_{Al}\, \delta}} \quad [4]$$

Assuming that the diffusion coefficients for Mn^{++} and $Al_2Cl_7^-$ are equal [reported to be 5×10^{-6} cm²/s for $Al_2Cl_7^-$ (15)], then upon rearranging, Eq. [3] becomes

$$\frac{1}{W_{f,Mn}} = 1 + \frac{N_{Al}\, n_{Al_2Cl_7^-} n_{Mn}\, C_{o,Al_2Cl_7^-}^{\bullet}}{N_{Mn}\, n_{Mn^{++}}\, n_{Al}\, C_{o,Mn^{++}}^{\bullet}} \quad [5]$$

For a two electron Mn^{++} reduction and assuming the aluminum deposition reaction is that given in Eq. [1], then Eq. [5] reduces to

$$\frac{1}{W_{f,Mn}} = 1 + 0.123\, \frac{C_{o,Al_2Cl_7^-}^{\bullet}}{C_{o,Mn^{++}}^{\bullet}} \quad [6]$$

The concentration of $Al_2Cl_7^-$ for melts of varying $AlCl_3$ composition was calculated by Boxall (6) and was reported to be 3.5*M* for 2:1 $AlCl_3$:NaCl melts. Figure 7 shows the solution to Eq. [6] as well as our data for two different deposition potentials assuming a $Al_2Cl_7^-$ concentration of 3.5*M*. At −0.15 V/Al and high $MnCl_2$ concentration, the alloy composition is richer in aluminum than that predicted by melt composition assuming diffusion control. In this region, neither species is diffusion limited and alloy composition is governed by electrochemical kinetics. At low $MnCl_2$ concentrations, Mn^{++} reduction is mass transport limited while $Al_2Cl_7^-$ is reduced at a rate well below its limiting current; consequently, alloy composition is richer in manganese than that predicted by melt composition.

At −0.4 V/Al, alloy composition is that predicted by Eq. [6] for all melt compositions suggesting that the deposition process is mass transport limited in both Mn^{++} and $Al_2Cl_7^-$ and that the composition of the electrodeposit is exactly what one would expect from the bulk compositions of the electroactive ions. Since we ran these experiments at a constant $AlCl_3$ composition and never varied the $Al_2Cl_7^-$ concentration, it is possible that the process is linear only with respect to Mn^{++}. Austin has shown however (24) that the manganese content of the electrodeposit increases with decreasing acidity which proves that the $Al_2Cl_7^-$ concentration is indeed a factor.

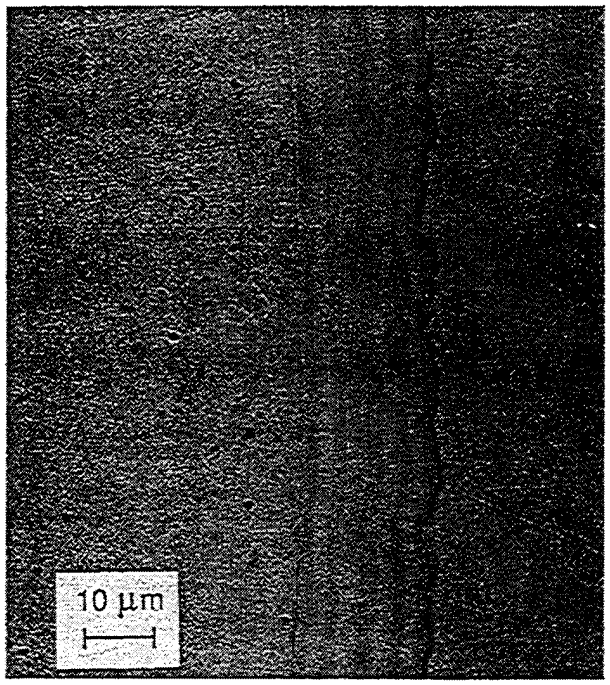

Fig. 6. Optical cross section of potential modulated aluminum-manganese electrodeposit. Potential was modulated between −0.3 and −0.1 V/Al for 5 C/cm² at each potential. The dark layers contain 30 w/o Mn (EDS, quantitative analysis) while the adjacent layers contain 15 w/o Mn.

It is the above mechanism which allows for the deposition of modulated alloys from a single electrolyte. When $Al_2Cl_7^-/MnCl_2$ is small, manganese rich layers are obtained at potentials where the deposition process is diffusion controlled and alloy composition is therefore determined by melt composition. Layers depleted in manganese can then be achieved at small cathodic overpotentials where both electroactive species are under kinetic control and $Al_2Cl_7^-$

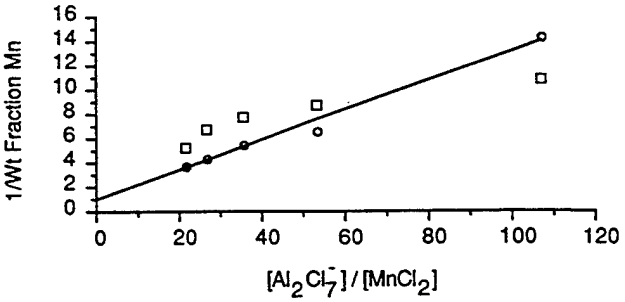

Fig. 7. Dependence of alloy composition on melt composition at deposition potentials of −0.15 V/Al (□) and −0.40 V/Al (○); solution to Eq. [6] (———).

is preferentially reduced. When $Al_2Cl_7^-/MnCl_2$ is large, a modulated alloy with a lower average Mn content is deposited. In this case, Mn^{++} reduction is diffusion limited at nearly all deposition potentials so the partial current for Mn is essentially constant. Potential modulation alters the Al partial current, thus creating layers of different composition and structure.

The effects of migration must often be considered in treating the flux of ions to and from an electrode during steady-state processes. In the case of aluminum deposition from chloroaluminates, migration would hinder the diffusion of electroactive anions to the negative electrode, thereby lowering the limiting current predicted by the diffusion equation. Transference numbers have been measured for the $AlCl_3$-NaCl system (30, 31), and were found to be quite low for $AlCl_4^-$. The mobilities of the rather large $AlCl_4^-$ and $Al_2Cl_7^-$ ions are quite small compared to Na^+. Since these anions contribute little to the overall conductivity of the electrolyte, migration effects can be ignored.

Conclusions

The addition of small quantities of $MnCl_2$ (0.25-1.5 w/o) to acidic mixtures of $AlCl_3$ and NaCl dramatically increases the activation overpotential for the deposition of aluminum, thereby promoting lateral growth and eliminating the tendency to form dendrites. The mechanism for nucleation and growth normally operative during $Al_2Cl_7^-$ reduction changes dramatically; the extent of which is not presently known. Alloys containing up to 30 w/o manganese have been deposited and alloy composition is dependent upon potential and $MnCl_2$ concentration of the melt. At small cathodic overpotentials, the deposition process, with respect to alloy composition, is kinetically controlled for both species. At a potential dependent upon $MnCl_2$ concentration, it then becomes mass transport limited in Mn^{++}. At potentials approaching -0.35 V/Al, $Al_2Cl_7^-$ also becomes diffusion limited. In this region, alloy composition is exactly what one would expect from the bulk compositions of the electroactive ions assuming linear diffusion to the electrode. The most specular, homogeneous deposits were obtained at a potential of -0.3 V/Al; however, the potential dependence of alloy composition allows one to create graded and modulated structures from a single electrolyte.

Deposits containing greater than 27 w/o Mn have x-ray diffraction patterns similar to that observed for metallic glasses. As the manganese content of the deposit is reduced, supersaturated aluminum is detected in addition to the glassy material. The structure of the glassy phase has not been directly determined, but data suggest it has a stoichiometry similar to that of the Al_6Mn intermetallic. Heating to 400°C converts the glass to Al_6Mn and results in increased alloy hardness, possibly through a dispersion/precipitation hardening mechanism.

Our ability to form a variety of structures (homogeneous, graded, and modulated) coupled with the materials potentially inherent strengthening mechanisms might lead to the electrodeposition of alloys with very interesting mechanical properties. The ability to electrodeposit intermetallic compounds on a near atomic scale presents interesting possibilities for high temperature alloys.

Acknowledgments

The experimental assistance of Sandra Claggett, David Kelley, Perry Sharpless, and Christian Turner is gratefully acknowledged. The author would also like to express appreciation to Carlos Beauchamp, Christian Johnson, David Lashmore, and Alexander Shapiro for their technical contributions.

Manuscript submitted April 11, 1988; revised manuscript received July 25, 1988. This was Paper 227 presented at the Honolulu, HI, Meeting of the Society, Oct. 18-23, 1987.

The National Institute of Standards and Technology assisted in meeting the publication costs of this article.

REFERENCES

1. M. D. Archer, C. C. Corke, and B. H. Harji, *Electrochim. Acta*, **32**, 13 (1987).
2. M. Olivier, J. O. Strom-Olsen, Z. Altounian, R. W. Cochrane, and M. Trudeau, *Phys. Rev. B*, **33**, 2799 (1986).
3. D. G. Naugle, R. Delgado, H. Armbruster, C. L. Tsai, T. O. Callaway, D. Reynolds, and V. L. Moruzzi, *ibid.*, **34**, 8279 (1986).
4. R. Delgado, H. Armbruster, D. G. Naugle, C. L. Tsai, W. L. Johnson, and A. Williams, *ibid.*, **34**, 8288 (1986).
5. J. Laakkonen and R. M. Nieminen, *ibid.*, **34**, 567 (1986).
6. L. G. Boxall, H. L. Jones, and R. A. Osteryoung, *This Journal*, **120**, 223 (1973).
7. B. J. Welch and R. A. Osteryoung, *J. Electroanal. Chem.*, **118**, 455 (1981).
8. A. A. Fannin, Jr., L. A. King, and D. W. Seegmiller, *This Journal*, **119**, 801 (1972).
9. B. Tremillon and G. Letisse, *J. Electroanal. Chem.*, **17**, 371 (1968).
10. J. Bouteillon and A. Marguier, *Surf. Technol.*, **22**, 205 (1984).
11. B. S. Del Duca, *This Journal*, **118**, 405 (1971).
12. B. Nayak and M. M. Misra, *J. Appl. Electrochem.*, **7**, 45 (1977).
13. B. Nayak and M. M. Misra, *ibid.*, **9**, 699 (1979).
14. R. C. Howie and D. W. Macmillan, *ibid.*, **2**, 217 (1972).
15. P. Rolland and G. Mamantov, *This Journal*, **123**, 1299 (1976).
16. T. Sato, T. Ishikawa, and R. Midorikawa, *Denki Kagaku*, **41**, 446 (1973).
17. R. Midorikawa, *ibid.*, **24**, 366 (1956).
18. R. Midorikawa, *ibid.*, **24**, 457 (1956).
19. R. Midorikawa, *ibid.*, **24**, 511 (1956).
20. R. Midorikawa, *ibid.*, **24**, 562 (1956).
21. K. Schulze and H. Hoff, *Electrochim. Acta*, **17**, 119 (1972).
22. G. R. Stafford and C. Turner, Proc. AESF, Chicago (1987).
23. K. Matiasovsky and M. Paucirova, *Povrchove Upravy*, **13**, 10 (1973); Chem Abstr., **80**, 22000d (1974).
24. L. W. Austin, M. G. Vucich, and E. J. Smith, *Electrochem. Technol.*, **1**, 269 (1963).
25. E. J. Jankowsky, NADC Final Report no. NADC-83127-60 (1983). Gov. Rep. Announce. Index (U.S.) **84** (5), 222 (1984).
26. T. Hayashi, Proc. Int. Symp. Molten Salt Chem. Technol., pp. 53-56 (1983).
27. H. J. Read and D. A. Shores, *Electrochem. Technol.*, **4**, 526 (1966).
28. A. J. McAlister and J. L. Murray, *Bull. Alloy Phase Diagrams*, **8** (5), 438 (1987).
29. D. Baral, J. B. Ketterson, and J. E. Hilliard, *J. Appl. Phys.*, **57**, 1076 (1985).
30. Y. V. Baimakov and V. I. Shelomov, *Trans. Leningrad. Inst. Sect. Met.*, (1):36-48 (1938).
31. J. Braunstein, G. Mamantov, and G. P. Smith, "Advances in Molten Salt Chemistry," Vol. 1, Plenum Press, New York (1971).

Phase Formation in Electrodeposited and Thermally Annealed Al-Mn Alloys

BENJAMIN GRUSHKO and GERY R. STAFFORD

Aluminum-manganese alloys with compositions ranging from 0 to 50 wt pct Mn were electrodeposited onto copper substrates from a chloroaluminate molten salt electrolyte containing $MnCl_2$ at temperatures of 150 °C to 325 °C. The structures of these electrodeposits were then compared to those observed when metastable electrodeposits were thermally annealed at 200 °C to 610 °C. The alloys were characterized by scanning electron microscopy, transmission electron microscopy (TEM), energy dispersive spectroscopy, and X-ray diffraction. At deposition temperatures of 150 °C to 250 °C, no stable structure other than the strongly supersaturated and highly dislocated Al-face-centered cubic (fcc) solid solution is observed. An amorphous phase and body-centered cubic (bcc) Al_8Mn_5 are observed at higher manganese compositions. In the temperature range of 250 °C to 325 °C, some of the phases predicted by the equilibrium phase diagram, such as Al_6Mn and $Al_{11}Mn_4$, are electrodeposited. The direct deposition of the icosahedral and decagonal phases has been demonstrated at 325 °C. Thermal annealing of the amorphous phase at temperatures higher than 225 °C results in its transformation to the icosahedral phase with a grain size much smaller than that obtained in the electrodeposited icosahedral phase. Additional annealing at higher temperatures does not result in any detectable coarsening of the icosahedral phase; instead, crystals of Al_6Mn or $Al_{11}Mn_4$ grow into the regions once occupied by the icosahedral phase. The crystalline Al_6Mn phase which forms as the result of thermal annealing shows a structural deviation from the equilibrium phase. As-deposited alloys comprised of 2- to 3-nm-thick amorphous regions separated by fcc-Al grains failed to crystallize after 30 minutes annealing at 500 °C.

I. INTRODUCTION

THE deposition of certain alloys at relatively low process temperatures generally results in the formation of metastable structures. Metastable amorphous, quasicrystalline, and crystalline phases in Al-Mn alloys have been obtained by sputtering, ion-beam mixing, and electrodeposition.[1–7]

Results of previous studies on Al-Mn alloys containing up to 50 wt pct Mn and electrodeposited from chloroaluminate electrolytes at 150 °C[5,6,7] have shown the following. The lower Mn alloys consist of the face-centered cubic (fcc) solid solution of Mn in Al, and the compositional limit of the fcc phase is extended up to about 9 wt pct Mn. With additional Mn, the fcc order cannot be maintained, and amorphous alloys are deposited. The amorphous phase has a lower Mn composition limit quite close to that of Al_6Mn, and its appearance results in a dramatic decrease in the Mn concentration of the coexisting fcc phase. Completely amorphous specimens are obtained in the range of composition between 26 and 39 wt pct Mn. At higher Mn composition, the amorphous phase is gradually replaced by a crystalline body-centered cubic (bcc) phase.[7] This phase has the Al_8V_5 structure with a lattice parameter of 0.9012 nm and appears to be the high-temperature $\gamma 1$ phase, which according to the phase diagram in Reference 8, is stable at temperatures above 950 °C. The structure of $\gamma 1$ is presently unknown.[8]

Studies of alloys electrodeposited at higher temperatures[9,10] indicate that in the composition range of 26 to 35 wt pct Mn, completely amorphous deposits are obtained at electrolyte temperatures up to 250 °C. At a deposition temperature of 325 °C, the formation of quasicrystalline phases has been observed in alloys containing 16 wt pct Mn.[9,10]

It has been established that annealing amorphous Al-Mn alloys at temperatures above 250 °C transforms these structures into crystalline phases[1–5] and, under similar annealing conditions, can transform them into the icosahedral phase, having a level of free energy between that of an amorphous and a stable crystalline phase.[11] Consequently, the metastable phases which are electrodeposited at elevated temperatures are affected by the thermal anneal during the deposition of the subsequent layers.

The present study was initiated in an effort to compare the structure of phases formed by electrodeposition at elevated temperatures (greater than 225 °C) to that which is observed when electrodeposited metastable phases are annealed in the same temperature range. The Al-Mn alloys were electrodeposited from a molten salt electrolyte comprised of a 2:1 mole ratio of $AlCl_3$:NaCl with controlled additions of $MnCl_2$. Films measuring 6- to 10-μm thick were electrodeposited galvanostatically at a current density of 50 mA/cm^2, corresponding to a deposition rate of approximately 1 μm/min, though some alloys produced at 325 °C were deposited at lower current densities in an effort to alter the Mn content of the

BENJAMIN GRUSHKO is with the Department of Materials Engineering, Technion-Israel Institute of Technology, Haifa, Israel. GERY R. STAFFORD is with the Metallurgy Division, National Institute of Standards and Technology, Gaithersburg, MD 20899.

Manuscript submitted January 15, 1990.

electrodeposit. The experimental procedure for melt handling, electrodeposition, and sample preparation has been described elsewhere.[5-7,9,12]

II. RESULTS OF ELECTRODEPOSITION

At any given temperature, alloy composition is found to vary with both the electrode potential and the relative concentration of the electroactive species, $Al_2Cl_7^-$ and Mn^{++}, in the electrolyte.[12] At small cathodic overpotentials (low current density), the deposition process, with respect to alloy composition, is kinetically controlled for both species. As the overpotential is increased, the reduction of Mn^{++} is favored, and alloys richer in Mn are produced. At larger cathodic overpotentials, the deposition process becomes mass transport-limited, first in Mn^{++} and then in $Al_2Cl_7^-$. In this region, alloy composition is exactly what one would expect from the bulk compositions of the electroactive ions, assuming linear diffusion to the electrode. The composition of the alloy can be predicted by the following equation,[12] where $W_{f,Mn}$ is the weight fraction manganese in the electrodeposit and the terms C^* are the bulk concentrations of the two electroactive species:

$$\frac{1}{W_{f,Mn}} = 1 + 0.123\,\frac{C^*_{Al_2Cl_7^-}}{C^*_{Mn^{++}}} \qquad [1]$$

Equation [1] has been verified experimentally in alloys electrodeposited under diffusion-limiting conditions at 150 °C.[12]

In the temperature range of 150 °C to 200 °C, little change in alloy composition is observed with an increase in temperature (Figure 1). A further increase in the deposition temperature results in a rather dramatic increase in the Mn content of the alloy. At temperatures approaching 300 °C, the Mn content increases by a factor of 2 over that which is observed at 150 °C. This enhanced reduction in Mn^{++} can result from preferential enhancement of the Mn^{++} diffusion coefficient or sufficient diffusion enhancement for both species such that the deposition process is once again kinetically controlled, thereby favoring Mn^{++} reduction.

Adjustments to alloy composition can also be made by depositing from an electrolyte dilute in Mn^{++} and increasing the deposition current beyond the diffusion-limiting current for Mn^{++} reduction. Since the rate of manganese deposition is limited by mass transport, the increase in total deposition current results in an increase in the aluminum current efficiency, thereby making the resultant alloy aluminum-rich. At any time during the deposition process, the alloy composition can be expressed as the ratio of the partial currents,

$$W_{f,Mn} = \frac{\dfrac{N_{Mn} i_{Mn}}{n_{Mn}}}{\dfrac{N_{Mn} i_{Mn}}{n_{Mn}} + \dfrac{N_{Al} i_{Al}}{n_{Al}}} \qquad [2]$$

where $W_{f,Mn}$ is the manganese weight fraction of the electrodeposited alloy, N_{Mn} and N_{Al} are the molecular weights, i_{Mn} and i_{Al} are the partial currents, and n_{Mn} and n_{Al} are the equivalents per mole for manganese and aluminum, respectively. Normally, unless the kinetics for alloy deposition are well characterized, the partial currents are not known and can only be inferred from alloy composition. If the electrolyte is dilute in one of the species and the deposition current is greater than the diffusion-limiting current for that species, then its partial current can be assumed constant and equal to the limiting current. For an electrolyte dilute in Mn^{++}, Eq. [2] becomes

$$W_{f,Mn} = \frac{\dfrac{N_{Mn} i_{Mn,lim}}{n_{Mn}}}{\dfrac{N_{Mn} i_{Mn,lim}}{n_{Mn}} + \dfrac{N_{Al}(i - i_{Mn,lim})}{n_{Al}}} \qquad [3]$$

where $i_{Mn,lim}$ is the limiting current for Mn^{++} reduction and i is the total applied current density.

Several alloys were deposited at 325 °C at different applied current densities in an electrolyte dilute in $MnCl_2$ to characterize the effects on alloy composition and to see if aluminum-rich alloys could be produced at this elevated temperature; the results are shown in Figure 2. Contrary to what is observed when both electroactive species are under kinetic control, an increase in current

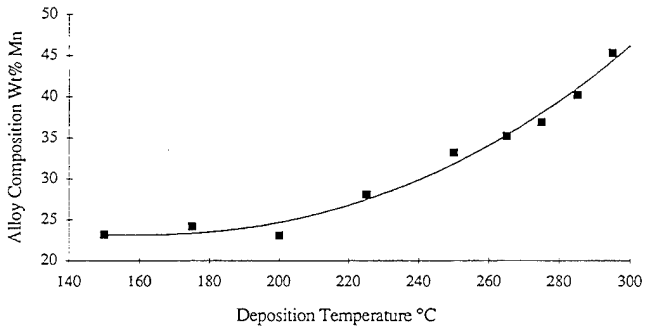

Fig. 1—The dependence of alloy composition on deposition temperature for an electrolyte containing 1.2 wt pct $MnCl_2$ at a current density of 50 mA/cm^2.

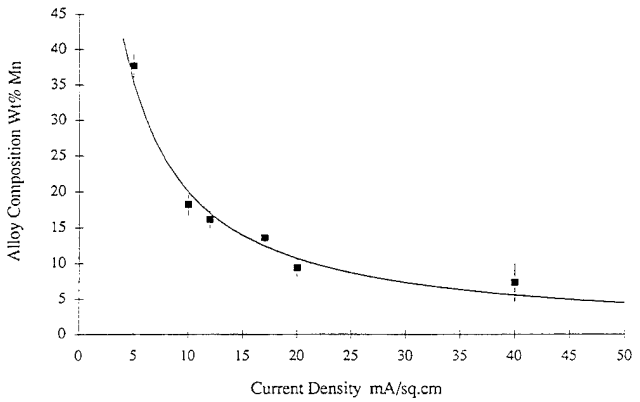

Fig. 2—Composition of electrodeposited Al-Mn alloys as a function of current density in an electrolyte dilute in $MnCl_2$ (0.2 wt pct) and at a temperature of 325 °C; (——) solution to Eq. [3] for $i_{Mn,lim}$ = 0.75 mA/cm^2.

density when Mn^{++} is diffusion-limited produces an alloy containing significantly less Mn. The solid line in Figure 2 is the solution to Eq. [3] which provides the best fit for the data by varying $i_{Mn,lim}$. The limiting current providing the best fit was 0.75 mA/cm^2, very close to what one would estimate for steady-state linear diffusion of 0.026 molar Mn^{++} assuming a diffusion coefficient of 5×10^{-6} cm^2/s and a diffusion layer thickness of 100 μm. Consequently, when the current efficiency for Mn^{++} is limited by mass transport, the applied current density becomes an effective way of changing the alloy composition without altering the electrolyte composition. Though this is an effective way of making adjustments to the overall alloy composition, depositing from an electrolyte in which either of the electroactive species is limited by mass transport generally results in deposits which are compositionally nonhomogeneous and are subject to morphological instabilities (nodules or dendrites).

A structural study of as-deposited aluminum-manganese alloys reveals the formation of several phases with varying degrees of deviation from equilibria. The phase constitution depends strongly on alloy composition and deposition temperature. Variations in current density between 5 and 50 mA/cm^2 dramatically affect alloy composition, as described previously, but appear to have a negligible effect on the structure of the electrodeposits. For instance, two alloys of identical composition, deposited at the same temperature but at different current densities from electrolytes containing different amounts of Mn^{++}, have essentially the same structure. The experimental results (Figure 3) indicate that there are basically two temperature regions which show some differences in the deviation from the state predicted by the equilibrium phase diagram.[8] At lower temperatures (150 °C to 250 °C), no stable structure other than the strongly supersaturated and highly dislocated Al-fcc solid solution was observed. In the temperature range of 250 °C to 325 °C, some of the phases predicted by the phase diagram at these temperatures are deposited.

The structures of alloys electrodeposited at temperatures up to 250 °C do not differ significantly from that reported previously for deposition at 150 °C.[6] X-ray diffraction indicates the presence of fcc-Al and an amorphous phase in compositions of 10 to 26 wt pct Mn (Figure 4(a)). The electrodeposited alloys are completely amorphous in the 26 to 39 wt pct Mn composition range (Figure 4(b)). Above 39 wt pct Mn, bcc Al_8Mn_5 is seen to coexist with the amorphous phase (Figure 4(c)). Alloys containing 50 wt pct Mn and deposited at 150 °C contain an additional cubic phase (Figure 4(d)) which, from X-ray diffraction, can be indexed to an fcc structure with a lattice parameter of 0.385 nm. In addition, a shift in the reflections for bcc Al_8Mn_5 to larger values of 2θ (see 330 peak in Figures 4(c) and (d)) with the increase in manganese suggests a range of composition for Mn in this phase.

When the deposition temperature for low Mn alloys

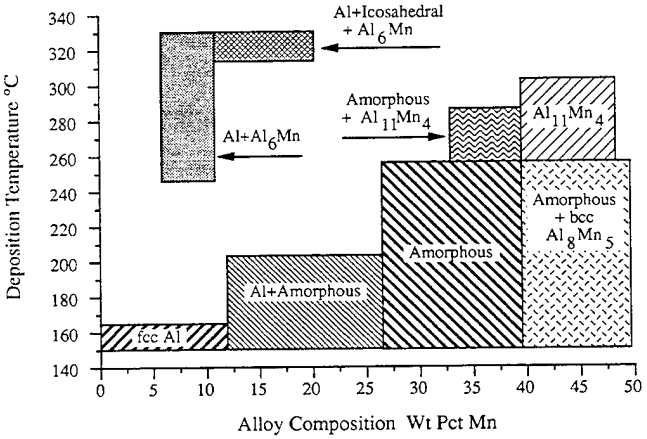

Fig. 3—Phases observed in electrodeposited Al-Mn alloys.

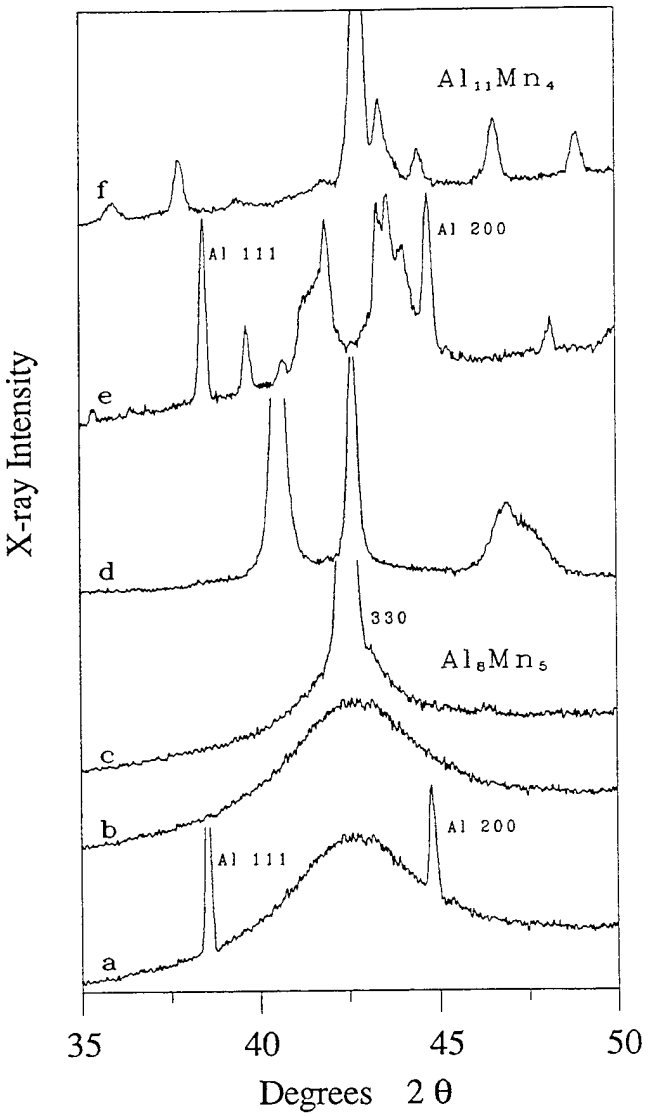

Fig. 4—X-ray diffraction patterns (Cu K_α) of electrodeposited Al-Mn alloys: (*a*) 17.6 wt pct Mn alloy deposited at 250 °C, (*b*) 39.0 wt pct Mn alloy deposited at 250 °C, (*c*) 45.7 wt pct Mn alloy deposited at 250 °C, (*d*) 49.6 wt pct Mn alloy deposited at 150 °C, (*e*) 16.0 wt pct Mn alloy deposited at 325 °C, and (*f*) 48.0 wt pct Mn alloy deposited at 275 °C.

(supersaturated Al when deposited at 150 °C) is increased, additional reflections other than those due to fcc-Al begin to appear in the X-ray diffraction patterns from samples containing 7 to 10 wt pct Mn and deposited at 250 °C to 325 °C. The phase was identified as Al_6Mn in these lower Mn alloys. Alloys deposited at 325 °C and having an average composition of 15 to 20 wt pct Mn are composed of a mixture of fcc-Al, Al_6Mn, and the icosahedral phase.[9,10] Examination by transmission electron microscopy (TEM) reveals areas which are completely icosahedral, and spot selected area diffraction (SAD) has confirmed the icosahedral symmetry.[9,10] The X-ray diffraction pattern for such a deposit is shown in Figure 4(e). The amorphous and decagonal phases were also observed in this specimen.

Formation of the metastable Al_8Mn_5 phase for alloys containing more than 39 wt pct Mn was not observed at temperatures above 250 °C. At temperatures of 275 °C to 300 °C, a phase identified as triclinic $Al_{11}Mn_4$ appears in these alloys (Figure 4(f)). A typical transmission electron micrograph of this phase is shown in Figure 5(a) and reveals that the structure of the electrodeposited material is strongly faulted. The electron diffraction pattern in Figure 5(b) is consistent with the above triclinic structure. According to the equilibrium phase diagram,[8] triclinic $Al_{11}Mn_4$ is stable up to about 900 °C and is a stoichiometric compound; *i.e.*, it has no range of solubility. The electrodeposited $Al_{11}Mn_4$ phase, however, has a composition somewhat richer in Mn (46 to 47.5 wt pct Mn) than that of stoichiometric $Al_{11}Mn_4$ (42.5 wt pct Mn), which may result in lattice parameter deviations. Our data (Table I) is consistent with the following lattice parameters: $a = 0.5052$ nm, $b = 0.8873$ nm, $c = 0.5034$ nm, $\alpha = 89.7$ deg, $\beta = 99.8$ deg, and $\gamma = 104.9$ deg. Lattice parameters of the equilibrium $Al_{11}Mn_4$ phase are $a = 0.5095$ nm, $b = 0.8879$ nm, $c = 0.5051$ nm, $\alpha = 89.35$ deg, $\beta = 100.47$ deg, and $\gamma = 105.08$ deg.[8] The strongly faulted structure revealed in the TEM image may also account for the deviation in lattice parameters. This electrodeposit, when thermally annealed, shows a shift in the main X-ray reflections and the appearance of additional reflections due to the presence of a second phase.

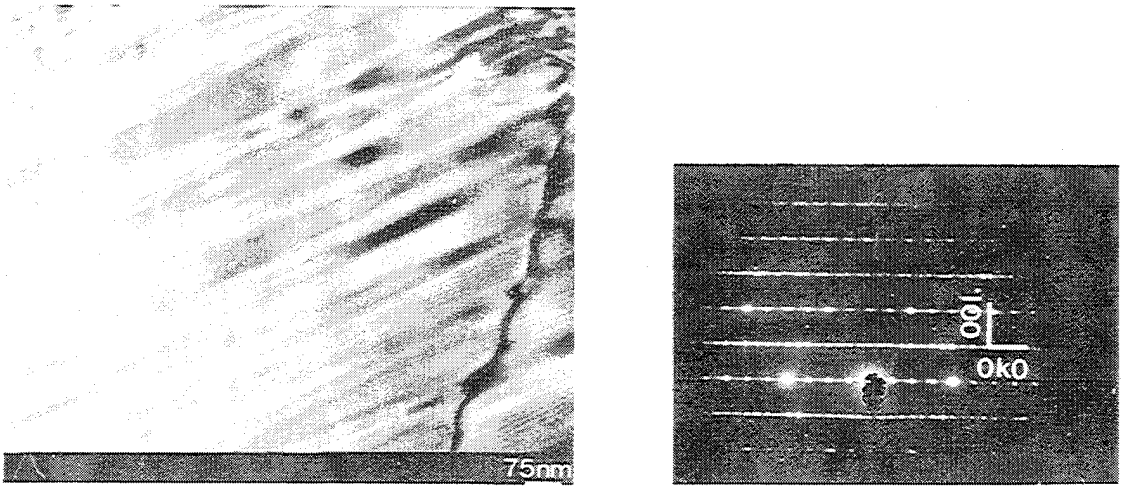

Fig. 5—Transmission electron micrographs of the crystalline $Al_{11}Mn_4$ phase: (*a*) bright-field image and (*b*) typical SAD pattern.

Table I. Experimental X-ray Diffraction Data (Cu K_α) for Proposed $Al_{11}Mn_4$ Compared to Calculated 2θ Values for a Triclinic Primitive Cell with $a = 0.5052$ nm, $b = 0.8873$ nm, $c = 0.5034$ nm, $\alpha = 89.7$ deg, $\beta = 99.8$ deg, and $\gamma = 104.9$ deg

Experimental		Calculated			
2θ	I (Pct)	2θ	h	k	l
35.990	38	35.992	2	−1	0
37.825	49	37.822	1	−3	1
42.785	100	42.787	0	2	2
46.645	21	46.641	1	3	1
48.955	25	48.956	2	−4	0
53.350	10	53.351	0	5	0
62.030	39	62.031	3	−1	1
64.785	16	64.785	3	−3	−2
71.045	29	71.045	2	4	1

III. RESULTS OF THERMAL ANNEALING

The electrodeposited 28 wt pct Mn amorphous alloy, which has a composition quite close to that of Al_6Mn, was studied after annealing at 200 °C to 345 °C in purified argon. Transmission electron microscopy of the as-deposited alloy does not reveal any contrast, and typical electron diffraction patterns for the specimen consist of one strong and two to three weaker rings. A normalized line scan plot of a ring SAD pattern is shown in Figure 6(a). The ratios of the ring radii yield values which are essentially the same as those found in vapor-deposited, liquid-quenched, and radiation-transformed amorphous alloys.[3] The electrodeposited amorphous Al-Mn alloy is therefore similar in structure to that obtained by other methods. Annealing in an external furnace at 345 °C for 10 minutes results in the appearance of fine contrast modulation in the TEM image which is related to the icosahedral phase. The formation of the fine-grained icosahedral phase is confirmed by the appearance of additional rings in the electron diffraction pattern (Figure 6(d)).

The icosahedral grain size obtained by annealing the amorphous phase at 345 °C is very similar to that observed in the interfacial area (deposit/substrate interface) of alloys electrodeposited at 250 °C (Figure 6(b)).[9] Consequently, the electron diffraction patterns shown in Figures 6(b) and (d) are very similar. In both cases, the strongest reflections are not quite separated, in contrast to that observed for the bulk alloy electrodeposited at 325 °C (Figure 6(c)), which clearly shows the two strongest reflections for the icosahedral phase. The icosahedral grain sizes resulting from the thermal annealing of amorphous alloys electrodeposited at 150 °C and 225 °C were the same, having electron diffraction patterns similar to that shown in Figure 6(d).

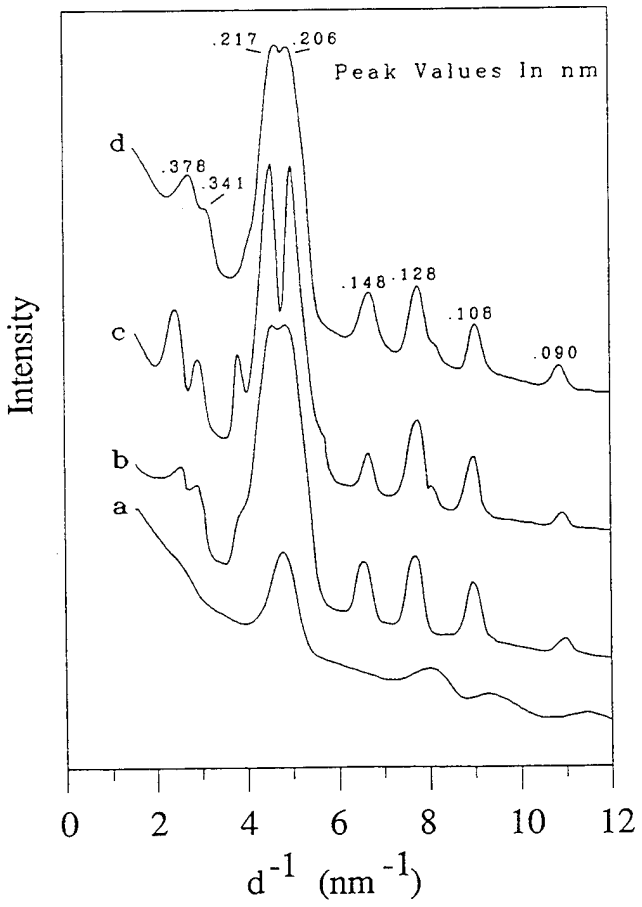

Fig. 6—Normalized line scan plots of ring electron diffractograms obtained from (*a*) amorphous alloy electrodeposited at 150 °C, (*b*) fine-grained icosahedral phase observed at the substrate-deposit interface in an alloy electrodeposited at 250 °C, (*c*) icosahedral phase observed in the bulk of an alloy electrodeposited at 325 °C, and (*d*) fine-grained icosahedral phase observed in an amorphous alloy annealed at 345 °C.

In addition to the above transformation, the growth of elongated grains of a crystalline phase is observed after annealing for 10 minutes at 345 °C (Figure 7(a)). The crystalline phase was identified as Al_6Mn (Figures 7(d) and (e)). The *d*-spacings of the crystalline phase, determined by X-ray diffraction, are also consistent with the Al_6Mn structure (Figure 8(d)). Additional annealing at 345 °C does not result in any significant coarsening of the icosahedral phase. Instead, crystals of Al_6Mn grow into the regions once occupied by the icosahedral phase. After 1-hour annealing time at 345 °C, the crystallization was not complete (Figure 7(b)).

Annealing experiments at lower temperatures indicate that the alloy remains amorphous after 40 hours at 200 °C (Figure 8(a)). The transformation of the amorphous phase, as discussed above, begins at 225 °C after about 30 hours (Figure 8(b)). At 250 °C, no transformation was observed after 10 to 30 minutes; however, the alloy was completely crystalline after 10 hours (Figure 8(c)). Thermal annealing at 610 °C also results in the formation of Al_6Mn as well as the appearance of an additional phase, the reflections of which are designated by (?) in Figure 8(e). Transmission electron microscopy examination of the specimen annealed at 345 °C also reveals this additional phase which nucleates separately from Al_6Mn (Figure 7(c)) and suggests that compositional inhomogeneities exist in the electrodeposited amorphous material. The second phase has yet to be identified, but the *d*-spacings of the strongest reflections in X-ray diffraction patterns are similar to those for $Al_{11}Mn_4$ observed in specimens of higher Mn concentration.

The highest Mn content measured in the amorphous phase electrodeposited at 150 °C was 39 wt pct Mn. Transformation of completely amorphous alloys of this composition occurs much faster than that of the amorphous phase containing less Mn. The 39 wt pct Mn alloy was completely crystallized after 30 minutes annealing at 345 °C. A TEM image and typical electron SAD pattern of this specimen are shown in Figure 9. This Mn-rich amorphous phase transforms into a two-phase structure which does not contain Al_6Mn. The identity of these phases is presently under investigation.

The presence of fcc-Al grains embedded in an amorphous matrix (the duplex structure is present in alloy compositions of 10 to 26 wt pct Mn) appears to have no effect on the amorphous-icosahedral transformation but causes an increase in the formation rate of the crystalline phase over that which is observed for the transformation of completely amorphous material. The crystallization of the amorphous phase into Al_6Mn was observed during *in situ* thermal annealing in the transmission electron

(a)

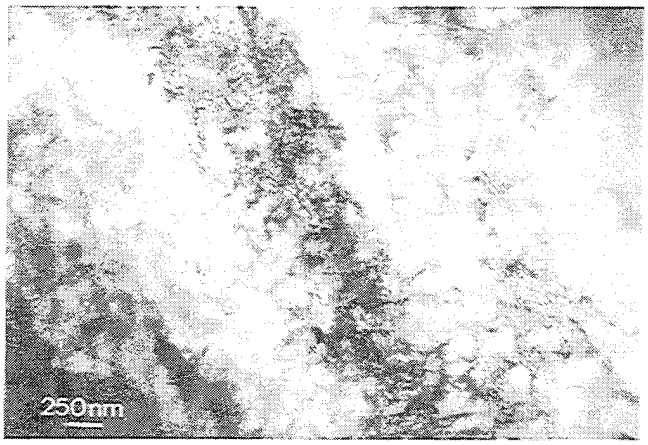

(c)

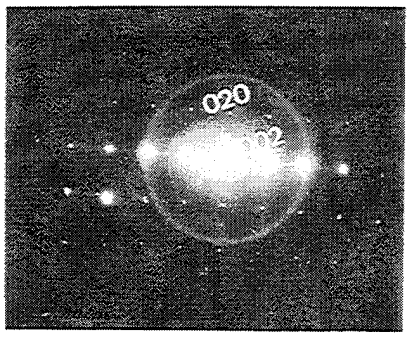

(d)

(b)

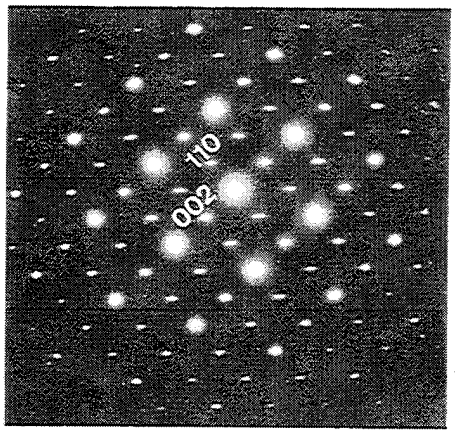

(e)

Fig. 7—Transmission electron micrograph of amorphous alloy containing 28 wt pct Mn partially transformed to Al_6Mn following thermal annealing at 345 °C: (*a*) initial stage of crystallization showing elongated grains of Al_6Mn; (*b*) dark-field image of Al_6Mn in an alloy annealed for 1 h, (*c*) morphology of an additional (unidentified) crystalline phase; and (*d*) and (*e*) electron diffraction patterns from (a) and (b), respectively. Ring diffraction reflections are from the fine-grained icosahedral region.

microscope. At temperatures approaching 230 °C to 250 °C, crystallization begins at the fcc-amorphous interface and "spreads" along the boundary.[5] Transmission electron micrographs of the duplex alloys with the partially transformed amorphous phase are shown in Figure 10.

The electron diffraction patterns obtained from Al_6Mn grains formed during the annealing of the fcc-amorphous duplex structure contain 001 reflections for odd values of 1 (compare Figures 10(d) and 7(e)). These reflections are forbidden in the Cmcm space group designated for the stable Al_6Mn structure. The Al_6Mn phase obtained from the thermal annealing of completely amorphous electrodeposited alloys can also show additional reflections of the (001) ($2n + 1$) type (Figure 7(d)) but at significantly lower relative intensity. Such electron diffraction

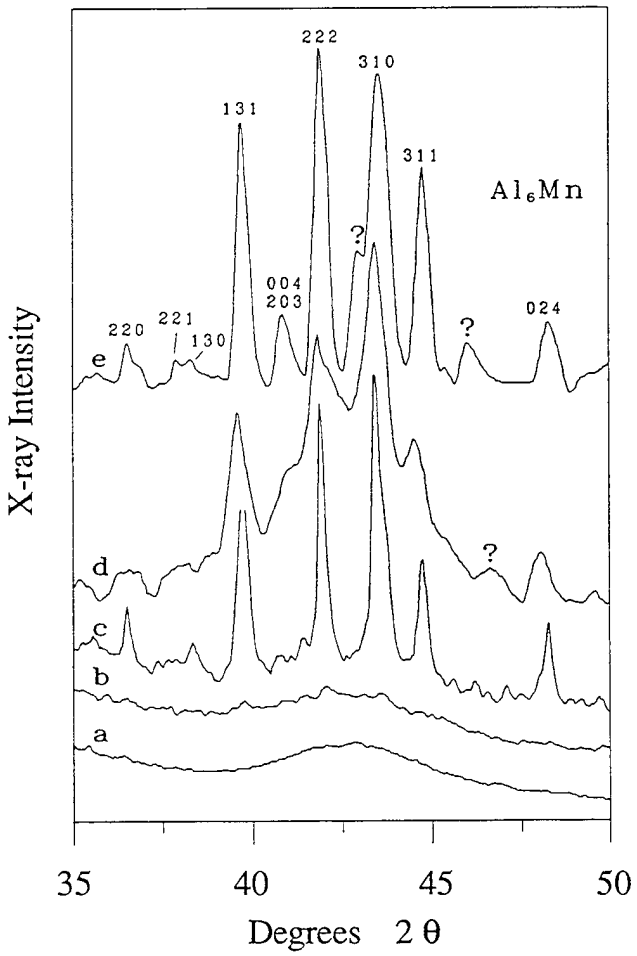

Fig. 8—X-ray diffraction patterns (Cu K_α) obtained from a 28 wt pct Mn amorphous alloy annealed at the following temperatures and times: (*a*) 200 °C for 40 h, (*b*) 225 °C for 35 h, (*c*) 250 °C for 10 h, (*d*) 345 °C for 10 min, and (*e*) 610 °C for 2 h.

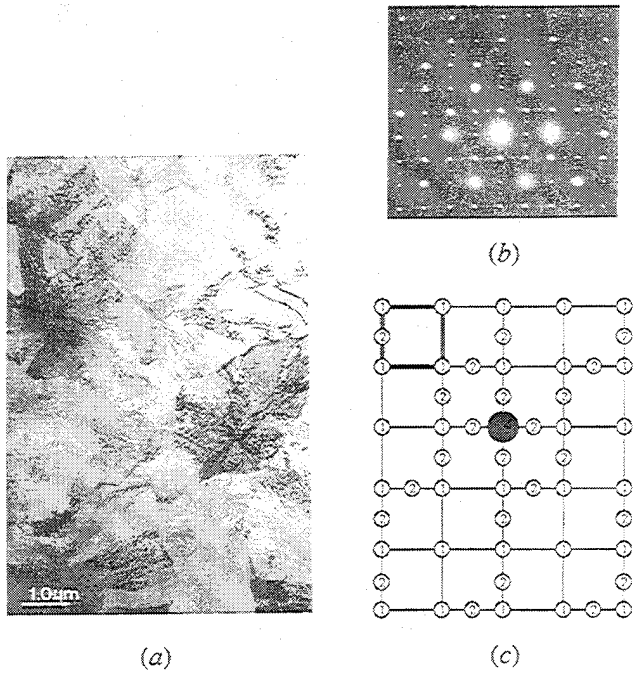

Fig. 9—Transmission electron micrographs of amorphous 39 wt pct Mn alloy after 30 min annealing at 345 °C: (*a*) bright-field image, (*b*) typical electron diffraction pattern, and (*c*) schematic representation of the above electron diffraction showing patterns of two phases. Reflections designated by ① are from the matrix, while those designated by ② are from the minor phase.

patterns have been observed by others.[1,4,13] The tendency to form circular Al_6Mn grains,[1] is seen in transformed electrodeposited alloys (22 wt pct Mn) with the duplex structure (Figure 10(a)). This type of growth is not universal, however, and elongated grains of Al_6Mn are also observed in this specimen (Figure 10(b)). Preferential formation of elongated grains occurs in higher Mn alloys (25 wt pct Mn) which contain a lower volume fraction of the fcc phase (Figure 10(c)). The composition of the amorphous phase in the two alloys, as calculated by quantitative metallography, is nearly identical. Visual observation suggests that the amorphous phase completely transforms into Al_6Mn, while the fcc phase is unaffected in this temperature region.

In situ thermal annealing experiments were performed on a fine mixture of amorphous and fcc-Al grains obtained in Al-Mn electrodeposits.[5] A typical structure is shown in Figure 11(a) and consists of fcc grains smaller than 10 nm separated by amorphous gaps of 2- to 3-nm thickness. The electron diffraction pattern of such a region (Figure 11(b)) consists of a sharp ring pattern for the fcc phase and a diffuse halo for the amorphous phase. Crystallization did not occur after 30 minutes at 500 °C in the TEM, although coarsening of the fcc grains could be observed. Additional heat treatment resulted in changes in the diffraction pattern inconsistent with the formation of Al_6Mn and the icosahedral phase (Figure 11(c)).

IV. DISCUSSION

Despite the general phenomena of nonequilibria in electrodeposited alloys at all compositions studied, the most interesting result is the qualitative differences in alloy structure which result from variations in the process parameters. Depending on the deposition temperature, the level of free energy of the deposited structure can be significantly higher than that of the equilibrium configuration, and transformation to the stable phase can be either direct or involve intermediate stages.

Alloys with composition of about Al-26 wt pct Mn can be electrodeposited directly in the amorphous, quasicrystalline, or crystalline states. Additional thermal annealing of these alloys results in transformation to the phase with a lower free energy, *i.e.*, amorphous to quasicrystalline and quasicrystalline to crystalline.

As it follows from the metastable nature of the amorphous phase, its transformation into phases of lower free energy can occur at a temperature below the temperature required for its direct deposition; consequently, annealing at the deposition temperature could indeed cause transformation. During deposition, the first deposited regions are essentially subject to an isothermal anneal for the duration of the deposition. It should be noted,

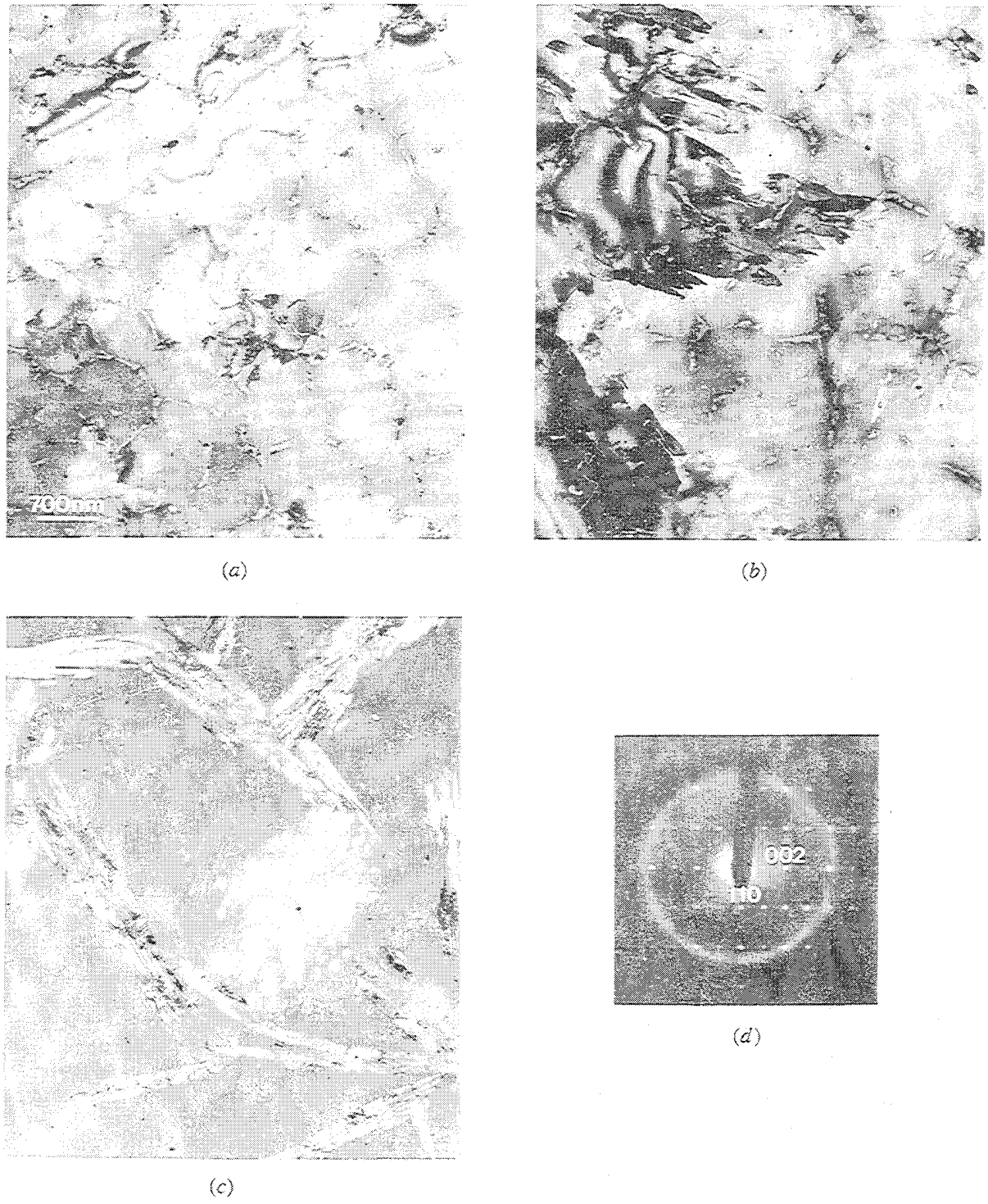

Fig. 10—Transmission electron micrographs of the annealed duplex amorphous-fcc alloy: (*a*) and (*b*) in a 22 wt pct Mn alloy, (*c*) in a 25 wt pct Mn alloy, and (*d*) typical electron diffraction pattern showing reflections forbidden in Cmcm Al_6Mn.

however, that the interfacial icosahedral phase observed in samples deposited at 225 °C and 250 °C is not the result of a thermal anneal during the deposition of subsequent layers, as discussed in Reference 9. Though the temperature is sufficient to cause transformation, the deposition time (10 minutes) is not. Based on the annealing results reported in this study, one would expect such a transformation to begin after about 30 minutes at 250 °C. At relatively high deposition temperature, the thickness of an amorphous layer may be limited as a result of the transformation process. However, if the deposition temperature can be decreased, the thickness of the amorphous phase can be practically unlimited.

The direct formation of completely quasicrystalline

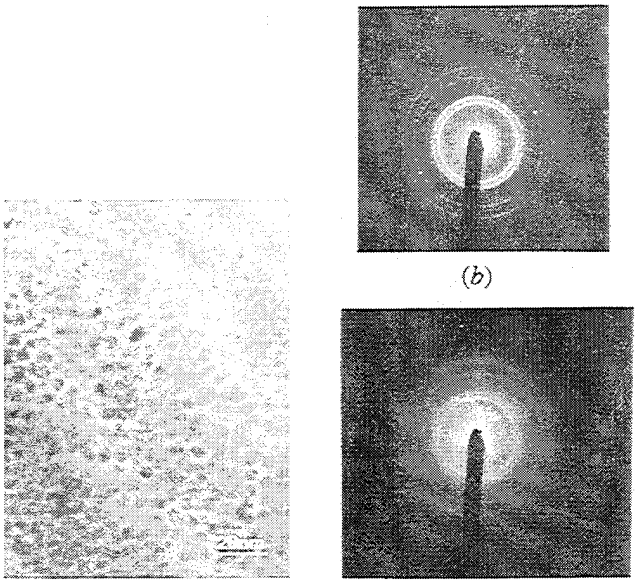

Fig. 11—Transmission electron micrograph of a fine duplex amorphous-fcc alloy: (*a*) bright-field image, (*b*) electron diffraction pattern obtained from above structure before thermal annealing, and (*c*) after annealing at 500 °C for 30 min.

single-phase material, having a level of free energy between that of an amorphous and a stable crystalline phase,[11] requires rigorous control of several processing variables. A coarser icosahedral phase can be produced at higher deposition temperatures[9,10] (relatively coarse icosahedral grains have been obtained by rapid solidification at uncontrolled temperatures). An increase in the deposition temperature may limit the thickness of the quasicrystalline layer due to transformation by thermal annealing. A decrease in deposition temperature results in the formation of the amorphous phase.

Let us now examine the fact that a significantly coarser icosahedral phase can be obtained directly by electrodeposition than by the thermal annealing of the amorphous phase at the same temperature. Indeed, the electrodeposition of Al-Mn alloys at 325 °C results in an icosahedral structure with regions of coherency up to 0.5 μm.[9] In contrast, the amorphous phase which has been thermally annealed at 345 °C results in icosahedral regions which cannot be reliably resolved in the transmission electron microscope.

Generally, one finds that a decrease in the processing temperature results in an increase in the nucleation density of the resultant crystals. The similar grain size obtained in annealed amorphous alloys deposited at 150 °C and 225 °C suggests that the icosahedral phase nucleates at about the same temperature and above 225 °C. The fact that a similar grain size of icosahedral phase was observed in alloys deposited at 250 °C and in amorphous alloys annealed at 345 °C can be understood if one assumes that significant nucleation of the icosahedral phase in the latter case starts at some temperature below 345 °C. The temperature at which transformation begins in the annealing experiment may not be determinable from the deposition experiments, since one has to be careful comparing a transformation requiring bulk diffusion to that of direct deposition. Isothermal annealing experiments indicate that the transformation temperature is greater than 250 °C, since at this temperature, the transformation is still fairly slow (recall that no transformation was observed after 10 minutes at 250 °C). Growth of icosahedral grains is completed before the material achieves the final annealing temperature (345 °C in our experiments). The additional annealing at 345 °C does not increase the grain size, since growth of the icosahedral phase by grain boundary motion does not occur. Evidently, the heating rate in our experiments on relatively thick specimens (6 to 10 μm) was not rapid enough to restrict transformation at the lower temperature; thus, a higher nucleation density than expected was observed.

Preliminary results of amorphous phase transformation using a heat-pulse technique[14] indicate that a significantly coarser icosahedral phase can be obtained when the temperature is increased to 350 °C in less than 1 second. The two strongest reflections are clearly resolved in the electron diffraction pattern. This suggests that the coarsening is the result of nucleation at a higher temperature in the heat-pulse experiment.

The solid-state transformation of the amorphous to icosahedral phase occurs homogeneously and does not appear to be affected by the presence of a second (crystalline) phase in the amorphous matrix. On the other hand, the presence of fcc grains seems to favor the nucleation of Al_6Mn from the amorphous phase; this transformation was observed at relatively low temperatures, 230 °C to 250 °C. Initially, the conversion to Al_6Mn occurs along the fcc-amorphous interphase boundary, eventually spreading into the interior of the amorphous grains.

Transformation initiation at the fcc-amorphous interface and a decrease in the temperature at which the amorphous phase crystallizes, however, were not confirmed for a very fine duplex structure consisting of fcc grains less than 10 nm, separated by 2- to 3-nm-thick amorphous regions. The amorphous phase in this structure failed to crystallize after 30 minutes at 500 °C. Either thin layers of the amorphous phase located between fcc grains have increased thermal stability in this configuration or the limited thickness of these layers does not allow one to detect the resultant crystalline phase by electron diffraction. The latter may be rejected, however, since disoriented icosahedral grains of similar dimension (1 to 2 nm) have been detected in the transformed amorphous phase of other specimens.

Naturally, the minimal thickness of a crystalline layer is limited by the size of its unit cell, about 1 to 2 nm for the crystalline phases pertinent to this study.[8] Since crystallization of the amorphous phase first requires the formation of a critical nuclei, the thickness of the amorphous layer must certainly be of the same order as a few lattice parameters of the crystalline phase being formed. An icosahedral phase of similar dimensions forms in a thermally annealed amorphous phase. This was not detected, however, during annealing of the fine mixture of the phases. Annealing experiments on somewhat similar Al-Mn duplex structures produced by vacuum codeposition[1] do not report an increase in transformation temperature over that observed in coarser structures. The fcc

grains reported in this study[1] are 10 to 30 nm in diameter, and it appears that the amorphous regions are appreciably coarser than the electrodeposited duplex alloy.

The higher thermal stability (up 500 °C) in the high Mn amorphous phase (35 wt pct Mn) reported in Reference 1 was not confirmed in our experiments. In fact, the crystallization of a 39 wt pct Mn alloy was significantly more rapid than that containing 28 wt pct Mn.

It should be noted that the crystalline phases which form as the result of thermal annealing are not necessarily those that are predicted by the equilibrium phase diagram. They can, in fact, be metastable, with an intermediate level of free energy. In several cases, electron diffraction patterns obtained from Al_6Mn grains which crystallize from the amorphous phase contain reflections which are forbidden in the Cmcm space group for the stable Al_6Mn structure. Similar diffraction patterns have been observed in annealed amorphous Al-Mn alloys produced by vacuum deposition[1] and in annealed multilayered Al-Mn alloys.[13]

The appearance of these "forbidden" reflections was discussed in Reference 13 and attributed to a multiple diffraction effect. Conversely, it has been suggested in Reference 1 that a more plausible explanation is that these reflections arise because there is more than one kind of atomic layer in the lattice. According to Reference 1, orthorhombic Al_6Mn forms from annealed amorphous alloys under a wide range of compositions (15 to 35 wt pct Mn), and the perfection of the resultant crystalline phase varies with Mn concentration. These disorders are suggested to be mainly in the stacking of atomic layers parallel to the (001) plane. This hypothesis is criticized in Reference 4, where it is suggested that the 29 wt pct Mn amorphous phase transforms completely into a hexagonal phase identified as $Al_{10}Mn_3$. The composition of this phase, however, deviates appreciably from that of stoichiometric $Al_{10}Mn_3$. Though the morphology of this phase is very similar to that observed in our study, the presence of hexagonal $Al_{10}Mn_3$ was not confirmed.

The results of our study confirm the presence of Al_6Mn in transformed amorphous alloys containing about 22 to 28 wt pct Mn by both X-ray and electron diffractometry. Both circular and bladelike grains were observed; however, the morphological dependence on the composition was not confirmed. The observed differences in the electron diffraction patterns could not be attributed to compositional differences nor to the presence of fcc-Al.

V. SUMMARY

The electrodeposited aluminum-manganese alloys reported in this study contain several phases which vary in their deviation from equilibria. The following deviations from equilibria have been observed in these electrodeposits: (a) an increased level of lattice defects and grain boundary density, (b) a widening of the solubility range of stable phases, (c) the formation of a crystalline phase which is probably stable at temperatures greater than the formation temperature (high-temperature modification appearing in the equilibrium phase diagram), (d) the formation of quasiperiodic phases (icosahedral, decagonal), and (e) the formation of an amorphous phase.

The phase constitution in these electrodeposits depends strongly on the deposition temperature and composition. At temperatures of 150 °C to 250 °C, no stable structure other than the strongly supersaturated and highly dislocated Al-fcc solid solution is observed. An amorphous phase and bcc Al_8Mn_5 (believed to be $\gamma 1$ on the phase diagram[8]) are observed at higher manganese compositions. In the temperature range of 250 °C to 325 °C, some of the phases predicted by the equilibrium phase diagram, such as Al_6Mn and $Al_{11}Mn_4$, are electrodeposited. The direct deposition of the icosahedral and decagonal phases have been demonstrated at 325 °C.

The amorphous phase begins to transform to the icosahedral phase in a temperature range below the upper limit of its deposition temperature. Thermal annealing at 225 °C and higher results in the transformation of the as-deposited amorphous phase to the icosahedral phase with a grain size much smaller than that obtained in the electrodeposited icosahedral phase. Additional annealing at higher temperatures does not result in any significant coarsening of the icosahedral phase; instead, crystals of Al_6Mn or $Al_{11}Mn_4$ grow into the regions once occupied by the icosahedral phase. Preliminary results indicate that the grain size of the icosahedral phase which forms upon thermal annealing of the amorphous phase can be increased if very fast heating rates are applied. This would allow one to achieve a higher transformation temperature while suppressing icosahedral nucleation at a lower temperature.

Transformation of completely amorphous alloys containing 39 wt pct Mn occurs much faster than that of the amorphous phase containing 28 wt pct Mn. The Mn-rich amorphous phase transforms into a two-phase structure. The identity of these phases is presently under investigation.

The presence of fcc-Al grains embedded in an amorphous matrix appears to have no effect on the amorphous-icosahedral transformation but causes an increase in the formation rate of the crystalline phase. Crystallization begins at the fcc-amorphous interface and "spreads" along the boundary. On the other hand, 2- to 3-nm-thick amorphous regions separated by grains of fcc-Al were not crystallized after 30 minutes annealing at 500 °C. The crystalline Al_6Mn phase which forms as the result of thermal annealing shows a structural deviation from the equilibrium phase. The electron diffraction patterns obtained from the above grains contain 001 reflections for odd values of 1 which are forbidden in the Cmcm space group designated for the stable Al_6Mn structure.

ACKNOWLEDGMENTS

The authors would like to thank Alexander Shapiro, Leo Bendersky, and Dan Shechtman for their technical contributions. The technical assistance of Sandra Clagget is gratefully acknowledged. One of the authors (B.G.) would like to acknowledge the financial support of the Israel National Council for Research and Development. This work was jointly supported by the Office of Naval Research (Contract No. N00014-88-F0091) and the

National Institute of Standards and Technology (Metal Matrix Competence Building Program).

REFERENCES

1. K. Yoshida and A. Takekawa: *Thin Solid Films*, 1978, vol. 48, pp. 293-308.
2. D.A. Lilienfeld, M. Nastasi, H.H. Johnson, D.G. Ast, and J.W. Mayer: *Phys. Rev. Lett.*, 1985, vol. 55, pp. 1587-90.
3. K. Urban, N. Moser, and H. Kronmuller: *Phys. Status Solidi A*, 1985, vol. 91, pp. 411-22.
4. M.J. Kaufman, F.S. Biancaniello, and K.G. Kreidèr: *J. Mater. Res.*, 1988, vol. 3, pp. 1342-48.
5. B. Grushko and G.R. Stafford: *Metall. Trans. A*, 1989, vol. 20A, pp. 1351-59.
6. B. Grushko and G.R. Stafford: *Proc. IV Israel Mater. Eng. Conf.*, Beer-Sheva, Israel, 1988, pp. 523-27.
7. B. Grushko and G.R. Stafford: *Scripta Metall.*, 1989, vol. 23, pp. 557-62.
8. A.J. McAlister and J.L. Murray: *Bull. Alloy Phase Diagrams*, 1987, vol. 8, pp. 438-47.
9. B. Grushko and G.R. Stafford: *Scripta Metall.*, 1989, vol. 23, pp. 1043-48.
10. G.R. Stafford and B. Grushko: *Proc. 3rd Int. Conf. on Quasicrystals and Incommensurate Structures*, Vista Hermosa, Mexico, May 27–June 2, 1989.
11. D.M. Follstaedt and J.A. Knapp: *Nucl. Instrum. Meth. Phys. Res.*, 1987, vol. B24/25, pp. 542-47.
12. G.R. Stafford: *J. Electrochem. Soc.*, 1989, vol. 136, pp. 635-39.
13. D.M. Follstaedt and J.A. Knapp: *J. Less-Common Met.*, 1988, vol. 140, pp. 375-84.
14. B. Grushko: Technion-Israel Institute of Technology, Haifa, Israel, unpublished research, 1989.

Structural Study of Electrodeposited Aluminum-Manganese Alloys

BENJAMIN GRUSHKO and GERY R. STAFFORD

Aluminum-manganese alloys with compositions ranging between 0 and 27 wt pct Mn were electrodeposited at 150 °C onto copper substrates from a chloroaluminate molten salt electrolyte with a controlled addition of $MnCl_2$. The specimens were studied by scanning electron microscopy (SEM), transmission electron microscopy (TEM), energy dispersive spectroscopy (EDS), and X-ray diffraction. The addition of small amounts of Mn results in the formation of a supersaturated fcc solid solution of Mn in Al. At the higher Mn content, an amorphous phase is established. The highly faceted crystalline surface of pure Al and Al-Mn solid solution becomes smooth and nearly specular when the amorphous phase is present. The amorphous phase appears in the form of rounded grains and has a lower limit of Mn concentration close to the Al_6Mn composition. There is a concentration discontinuity between the above limit and the higher Mn concentration limit of the fcc phase (about 9 wt pct). Appearance of the amorphous phase in the alloy results in a decrease in the Mn concentration in solid solution to about 2 wt pct. Crystallization of the amorphous phase starts at the fcc-amorphous phase interface at 230 °C. As a result of treatment at 230 °C to 340 °C, the amorphous phase completely transforms into Al_6Mn, while the fcc phase is unaffected. Prior to crystallization, the amorphous phase shows a modification that could be interpreted as the formation of a fine-grained icosahedral phase. The formation and distribution of phases by electrodeposition and rapid solidification are discussed.

I. INTRODUCTION

INTEREST in aluminum-manganese alloys (and a number of other transition metals) has dramatically increased with the recent discovery of quasicrystal phenomena[1] in many of these alloys. The essentially uncontrolled conditions present during rapid solidification have resulted in a search for alternative methods of preparing alloys containing quasicrystals such as solid-state processing[2,3] and sputtering deposition.[4] Al-Mn alloys produced from these methods at room temperature are amorphous. Heat treatment of the amorphous phase at 270 °C to 350 °C results in the amorphous-to-quasicrystalline transformation in the solid state.[3] The *in situ* formation of a fine-grained icosahedral phase has been observed in thin layers of alloys which were sputter deposited at 230 °C to 370 °C.[4]

Aluminum alloys can also be electrodeposited from molten salt electrolytes containing $AlCl_3$, NaCl, and the chloride salt of the solute metal at temperatures as low as 110 °C. The addition of small quantities of $MnCl_2$ to the chloroaluminate melt produces a binary aluminum-manganese alloy with a near-specular surface finish.[5] The manganese content of the electrodeposit can be rigorously controlled and is dependent upon deposition potential and the relative bulk concentrations of the electroactive species $Al_2Cl_7^-$ and Mn^{++} in the melt.[6] Alloy compositions ranging from 0 to 30 wt pct Mn have been reported,[6,7,8] and higher manganese compositions are possible.

The electrodeposition of these alloys offers many advantages over conventional solidification techniques. Since the deposition process is isothermal, one has rigorous control of the temperature at the electrolyte/electrode interface; hence, alloys of uniform composition and structure are possible. One also has an *in situ* measure of the deposition rate, which is proportional to the applied or measured current density.

Earlier structural studies of electrodeposited Al-Mn alloys[7] indicate that alloys of lower manganese composition consist of a supersaturated solid solution of manganese in aluminum. Alloys with greater manganese content were reported to contain an additional phase which produced a diffuse ring between the aluminum (111) and (200) reflections in electron diffraction patterns. It was proposed that this phase was a very fine-grained Al_6Mn intermetallic.[7] In this study,[7] well-defined reflections of this phase were observed in diffraction patterns of the heat-treated alloys.

More recent work has characterized the electrochemical parameters pertinent to alloy composition and suggests that the structure of the as-deposited high-manganese alloy is that of a metallic glass,[6,8] which corresponds to the second phase in Reference 7. The relevance of the amorphous phase to the question of icosahedral phase formation has been emphasized by a number of authors employing a variety of fabrication techniques,[3,9,10] and it has been suggested that the Al-Mn amorphous phase does, in fact, have a microquasicrystalline structure.[9]

In this paper, we report on the microstructure of Al-Mn alloys electrodeposited from a chloroaluminate

BENJAMIN GRUSHKO, Postdoctoral Fellow, is with the Department of Materials Engineering, Technion-Israel Institute of Technology, Haifa, Israel. GERY R. STAFFORD, Research Chemist, is with the Metallurgy Division, National Institute of Standards and Technology, Gaithersburg, MD 20899.

Manuscript submitted August 30, 1988.

melt at 150 °C with particular emphasis on the formation and distribution of the amorphous and fcc phases.

II. EXPERIMENTAL

The Al-Mn alloys were deposited onto planar copper (OFHC) substrates from a chloroaluminate melt comprised of 2:1 mole ratio $AlCl_3$:NaCl, with controlled additions of $MnCl_2$. Methods for electrolyte handling and preparation are given elsewhere.[6,8] The temperature of the melt was held at 150 °C ± 0.1 °C for all experiments. The electrodeposition of all alloys was controlled potentiostatically using a pure Al wire placed in the same melt as a reference electrode. Deposition potentials were chosen so that initial current densities ranged from 20 to 60 mA/cm^2. The pertinent melt and deposition parameters are shown in Table I.

The specimens were studied by SEM, TEM, EDS, and X-ray diffraction. The copper substrate was removed from selected samples by dissolution in concentrated HNO_3. For the short times required for copper dissolution, the HNO_3 has little effect on the electrodeposited alloy. EDS analysis was performed at 12 KeV to suppress possible copper interaction in samples where the substrate was present. X-ray diffraction was carried out on as-deposited samples as well as those in which the substrate had been removed. In the former case, the copper substrate was used as an internal standard for the determination of changes in the lattice constant of the fcc phase. Transmission electron microscopy was performed on specimens punched from deposits which had been removed from the substrate and electropolished by a twin-jet technique using 20 pct perchloric acid in methanol at −20 °C.

III. RESULTS

Analysis of X-ray diffraction patterns obtained from a series of electrodeposits (Figure 1) shows that increasing the manganese content in the alloy results in the following:

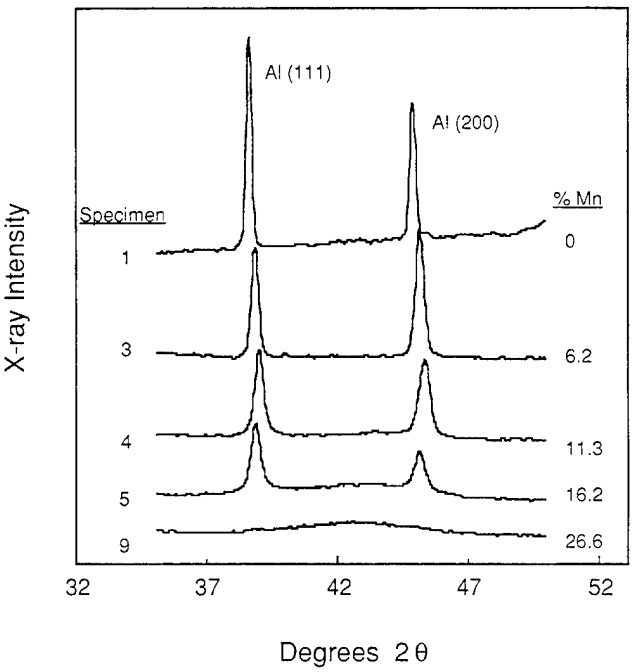

Fig. 1—X-ray diffractograms of as-deposited Al-Mn alloys. The pattern numbers are from Table I.

(a) *A shift in the fcc reflections*: The variation of *d* spacing for Al (111) obtained from the X-ray diffraction patterns in Figure 1 is shown in Table I. Initially, the lattice parameter decreases with increasing manganese content (specimens 1 through 4) as the manganese is incorporated substitutionally into aluminum. Specimen 5, however, shows an increase in lattice parameter indicative of a decreased manganese content in the fcc phase despite the higher bulk manganese content. The maximum manganese content observed in the solid solution, based on calculated *d* spacings,[11] was 8.8 wt pct (Table I). The solid solution composition is reduced to 2 wt pct Mn

Table I. Parameters of Electrodeposition, Composition, and Selected Diffractometric Data for Studied Specimens

Specimen No.	1	2	3	4	5	6	7	8	9
$MnCl_2$ wt pct in melt	0	0.17	0.25	0.50	0.75	1.00	1.00	1.25	1.25
Potential, −V/Al	0.20	0.25	0.15	0.20	0.25	0.30	0.20	0.20	0.30
Initial current density, mA/cm^2	33	50	26	40	42	48	24	20	46
Final to initial current ratio	—	2.8	2.3	2.5	1.6	1.5	1.0	1.2	1.2
Total charge deposited, C/cm^2	28	6	30	—	40	40	10	20	20
Wt pct Mn in alloy (EDS)	0.0	5.2	6.2	11.3	16.2	21.6	21.6	24.7	26.6
d_{111}, Å	2.338	2.327	2.326	2.317	2.333	2.331	—	—	—
Calculated wt pct Mn in fcc*	0.0	5.5	6.0	8.8	2.0	2.0	—	—	—
I_{200}/I_{111}, pct	57	175	115	92	64	72	—	—	—
Appearance of amorphous phase in X-ray diffraction	—	—	—	?**	+	+	+	+	+

*Calculated from d_{111} from Ref. 11.
**Amorphous phase is revealed by TEM.

in specimen 5. This decrease in d spacing with increasing manganese composition has been reported for rapidly solidified Al-Mn alloys[11] and is well established for this supersaturated solid solution. These investigators also report that the d spacing of the Al (111) planes increases to a value indicative of a manganese content of less than 4 wt pct in ribbons in which the icosahedral phase begins to appear.[11] They conclude that the icosahedral phase grows with a manganese content greater than the average composition of the alloy, leaving the intercrystalline liquid depleted in manganese.

(b) *A decrease in the intensities for the fcc reflections and appearance of a broad reflection due to the presence of an amorphous phase*: TEM examination of electrodeposited films indicates that the amorphous phase begins to appear in specimens containing 11.3 wt pct Mn. According to X-ray diffraction, the amorphous and crystalline phases coexist until the Mn content reaches about 25 wt pct, above which the deposit is essentially completely amorphous. It should be noted, however, that very small quantities of the fcc phase are revealed by TEM in specimens 8 and 9, which contain 24.7 and 26.6 wt pct Mn, respectively.

(c) *A change of the relative intensities of the fcc reflections*: The relative intensities for the as-deposited pure Al and Al-6.2 wt pct Mn are compared in Table II with the standard diffraction data for Al powder. The pattern for the pure Al electrodeposit does not show any significant deviation from the standard. On the other hand, the electrodeposited Al-Mn alloys shows a significant (200) texture in the solid solution. This texture is less significant in high-manganese alloys containing an appreciable fraction of the amorphous phase.

The surface morphology of the electrodeposit changes significantly with increasing manganese composition, as shown in Figure 2. The highly faceted crystalline surface of pure Al and the Al-Mn solid solution becomes a smooth, nearly specular surface when the amorphous phase is present. Further evidence for the decrease in surface roughness with increasing manganese is seen in the ratios of the final to initial deposition current in Table I. The steady-state current density for potentiostatically controlled deposition is constant. An increase in the total current is indicative of an increase in the roughness factor and, consequently, the electrochemically active surface area. The ratios of the final to initial current are seen to decrease with increasing manganese and approach a value of 1.0, an indication that the electrochemically active surface area of the electrodeposit is essentially that of the electropolished copper substrate.

Table II. Relative Intensities of the First Five Reflections of the Electrodeposited Pure Al and Al-Mn Solid Solution

	I/I_1		
Reflection	Pure Al	6.2 Wt Pct Mn	Al Powder Standard
111	100	100	100
200	57	115	47
220	33	25	22
311	40	26	24
222	10	—	7

The specular surface, indicative of an appreciable amorphous phase content, often contains regions where smooth nodules are present (Figure 3(a)). One of these nodules is shown under higher magnification (Figure 3(b)). The surface at the top of the nodule appears quite rough, while the bottom is smooth. The electrolytically etched surface (Figure 3(c)) reveals that the nodule is present in the early stages of growth and quite possibly might be an extension of the original nuclei.

Transmission electron microscopy shows that the supersaturated fcc solid solution grows as fine, highly dislocated grains. The amorphous phase appears in the form of rounded grains. Selected transmission micrographs of the as-deposited duplex Al-Mn alloys are shown in Figure 4. As the manganese content of the alloy increases, one sees an increased fraction of the amorphous phase and decreased grain size for fcc Al (Figures 4(a) and (b)). The amorphous and fcc phases are sharply separated in the high-manganese alloys (Figure 4(b)). The gaps between the amorphous growth nodules are filled by fine-grain fcc Al or are left unfilled (Figure 4(c)). The alloys of medium Mn percentages (about 12 wt pct), however, contain very fine fcc grains in the amorphous regions (Figure 4(d)).

A number of structures containing different fractions of sharply separated phases were studied by quantitative metallography to determine the relative amounts of fcc and the amorphous phase. The manganese contents in the fcc phase were calculated from the shift in the Al (111) reflection.[11] The composition of the amorphous phase was then calculated from the above data and the bulk composition of the deposit. A composition of 25 to 26 wt pct Mn was obtained for the amorphous phase, equal to that of stoichiometric Al_6Mn.

The amorphous grains show a typical diffraction pattern consisting of one strong and two or three weak rings (Figure 5(a)). The same patterns have been obtained in experiments for rapid solidification and ion beam mixing of Al-Mn alloys.[3,9] A diffraction pattern of the fine-grain structure shown in Figure 4(d) is shown in Figure 5(b).

The duplex electrodeposited Al-Mn alloy was heat-treated *in situ* during observation in the TEM. No transformation was observed up to 230 °C. In the temperature range of 230 °C to 340 °C, the amorphous phase crystallizes to Al_6Mn. It should be noted that the transformation was completed in the thicker parts of the specimen; the thinner parts were only partially transformed since they still contained a significant fraction of the amorphous phase (Figure 6(a)). This is probably due to the poor thermal conductivity in the thin regions. The remaining amorphous areas, however, are modified by the above heat treatment (Figure 6(b)). Additional rings in electron diffraction (Figure 6(c)) have a d spacing consistent with the fine-grained icosahedral phase (Table III).[20]

The crystallization of the amorphous phase starts at the fcc-amorphous interface. Visual observation in the transmission electron microscope suggests that the amorphous phase is completely transformed into Al_6Mn, while the fcc phase seems to be unaffected in this temperature region. This suggests that the composition of the amorphous phase is close to that of Al_6Mn and is consistent with the value calculated by quantitative metallography.

(a)

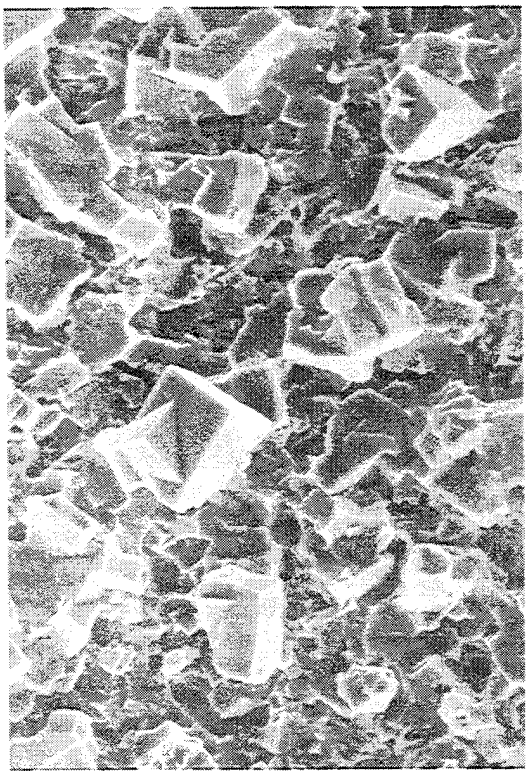

(b)

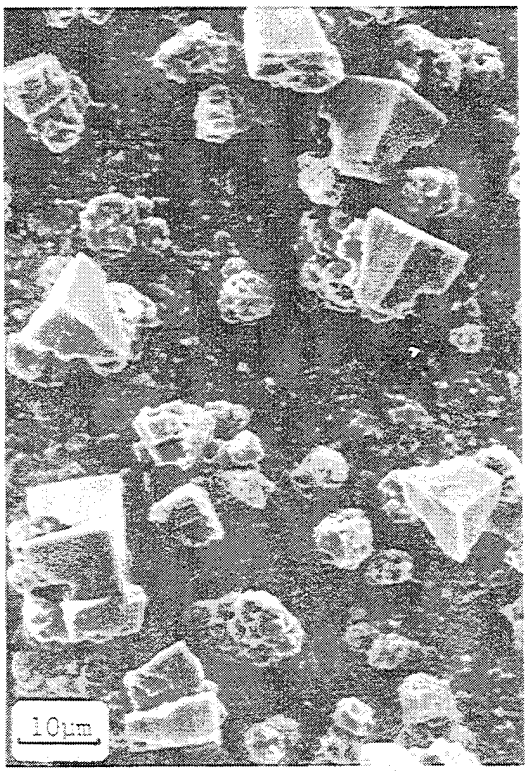

(c)

(d)

Fig. 2—Free surface of as-deposited specimens: (*a*) No. 1, (*b*) No. 3, (*c*) No. 4, and (*d*) No. 9 (see Table I).

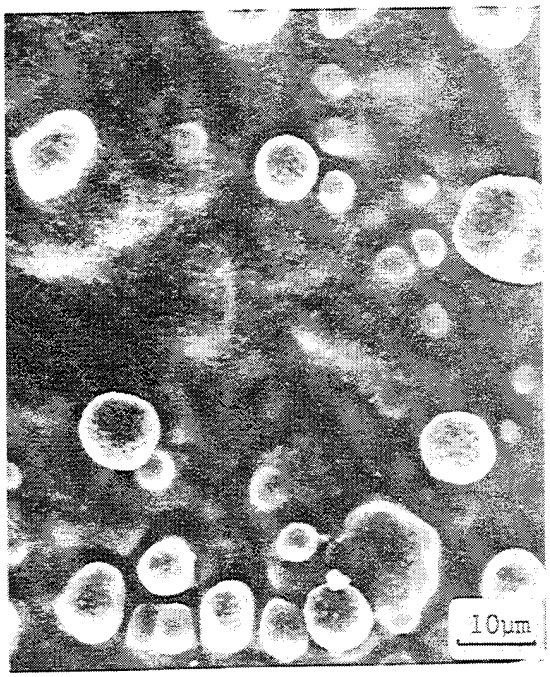

(a)

(b)

(c)

Fig. 3—Nodular growth of electrodeposited, partially amorphous Al-Mn alloy No. 6 (see Table I): (*a*), (*b*) free surface and (*c*) electrolytically etched surface.

A small area of as-deposited specimen 9 showed a diffraction pattern consistent with that of the fine-grained icosahedral phase (Table III).[20] The pattern is very close to that shown in Figure 6(c) for the heat-treated specimen. The possibility of heat treatment by the electron beam cannot be totally excluded. This effect, however, was not observed in other regions of the specimen.

IV. DISCUSSION

Growth of the solid phases in the above electrodeposition experiments occurs at temperatures which do not allow for significant bulk diffusion. The extent of the deviation from equilibrium, as well as the degree of ordering, is defined by the concurrent processes of new

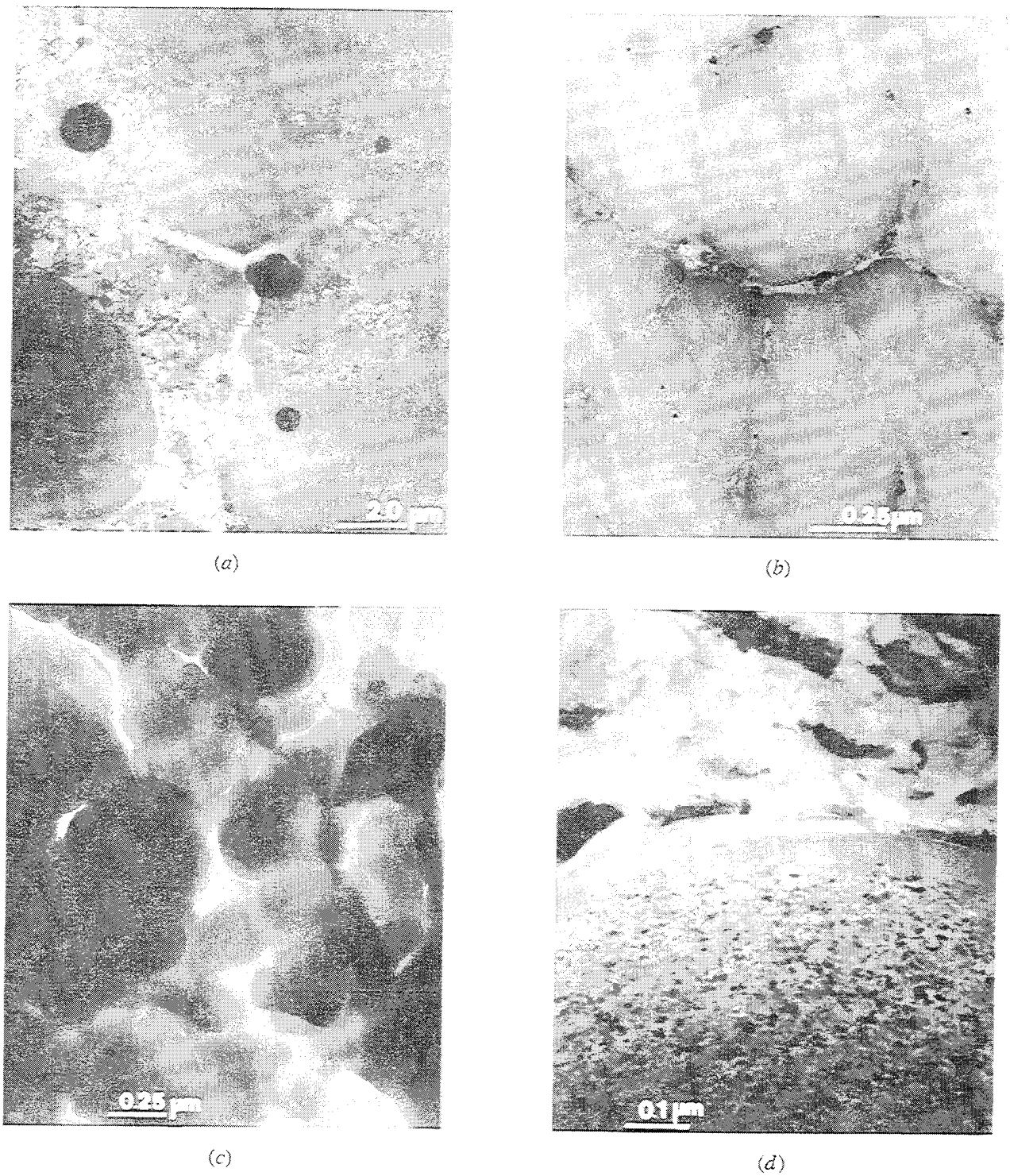

(a) (b) (c) (d)

Fig. 4—TEM micrographs of as-deposited alloys: (*a*) duplex structure of specimen 5 (black grains are unidentified); (*b*) duplex structure of specimen 6; (*c*) single-phase amorphous region in specimen 5; and (*d*) structure of specimen 4 containing fcc region (top) and fine mixture of amorphous and fcc phases (there seems to be a strictly amorphous layer between the above regions).

layer formation and surface diffusion. Segregation of manganese in the solid phase does not occur under these deposition conditions. Consequently, a high level of supersaturation of manganese into aluminum is obtained as a solid solution. At the high Mn content, the fcc order cannot be maintained, and an amorphous phase is established.

The preferential nucleation of the amorphous phase results in dramatic microstructural changes with increasing manganese, particularly in the composition region where the amorphous phase just begins to appear. Up to approximately 9 wt pct Mn, the deposit is entirely crystalline. With increased manganese, the amorphous phase deposits preferentially, resulting in a lower Mn content in the coexisting crystalline phase. Using the rule of mixtures relationship and assuming that the amorphous

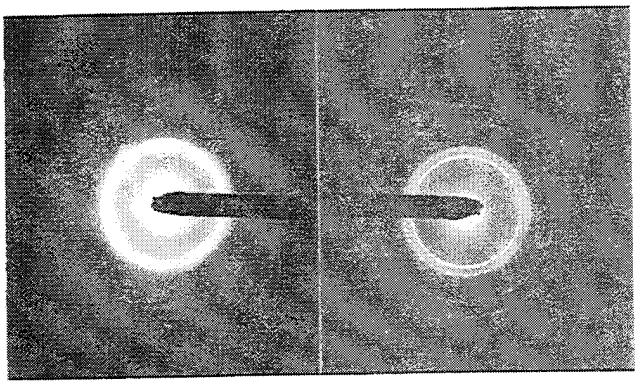

(a) (b)

Fig. 5—(*a*) Electron diffraction pattern of the amorphous phase and (*b*) fine-grained fcc plus amorphous phase in Fig. 4(d).

Table III. Electron Diffraction Reflections from Modified Amorphous Phase (A), Electrodeposited Fine-Grained Icosahedral Phase (B), and Reference X-Ray Data from (C).[20]

A	B		C	
d, Å	*d*, Å	Int.*	*d*, Å	Int.
3.82	3.81	m	3.85	22
3.32	3.30	vw	3.35	8
2.53	2.50	w	2.52	3
2.20** to 2.06	2.20** to 2.05	s	2.17	100
			2.07	78
1.51	1.49	m	1.50	11
1.29	1.28	m	1.28	20
1.10	1.10	m	1.10	5

*Intensities are similar in both patterns: strong (s), medium (m), weak (w), and very weak (vw).

**Single broad ring from 2.20 to 2.05 Å; two reflections are not resolved.

phase contains 25 wt pct Mn while the crystalline phase in the duplex structure contains 2 wt pct Mn (Table I), one can calculate that the 12 wt pct Mn two-phase alloy is 44 wt pct amorphous. The relative amount of the amorphous phase then increases linearly with overall Mn content until at 25 wt pct Mn, the deposit is entirely amorphous. This sharp discontinuity in the microstructure may result in dramatic property changes in alloys containing 10 to 13 wt pct Mn. Preliminary results indicate that substantial changes in the corrosion properties of these alloys in chloride environments do indeed occur in this region of manganese content.[12]

The above observations are consistent with the hypothesis of primary amorphous phase formation in the duplex structure of Al-transition metal alloys,[9,10] where it has been proposed that formation of the amorphous phase occurs in rapidly solidified Al-Mn or Al-Fe-Si alloys by a first-order transformation from the liquid. The hypothesis was applied for the purpose of explaining the rounded morphology of the amorphous phase surrounded by the aluminum phase. Each nodule of the amorphous phase nucleates and grows outward isotropically with a composition different from the melt. Rejected aluminum saturates the liquid until the crystallization temperature of fcc Al is reached.

Nucleation of the amorphous phase from melts apparently requires a minimal concentration of Mn ions in the vicinity of the growing interface. The growth of the primary amorphous phase causes a decrease in the manganese concentration to a level less than that present when only the crystalline phase solidifies from the liquid. Accordingly, the concentration of Mn in the fcc phase which coexists with the amorphous phase is lower than that of the single-phase fcc alloy.

The possibility of obtaining the above solidification morphology through liquid-phase separation was also discussed.[10] In the case of Al-Fe-Si, the liquid would separate into Fe-rich and Al-rich liquids; the former undergoes glass formation, while the latter crystallizes

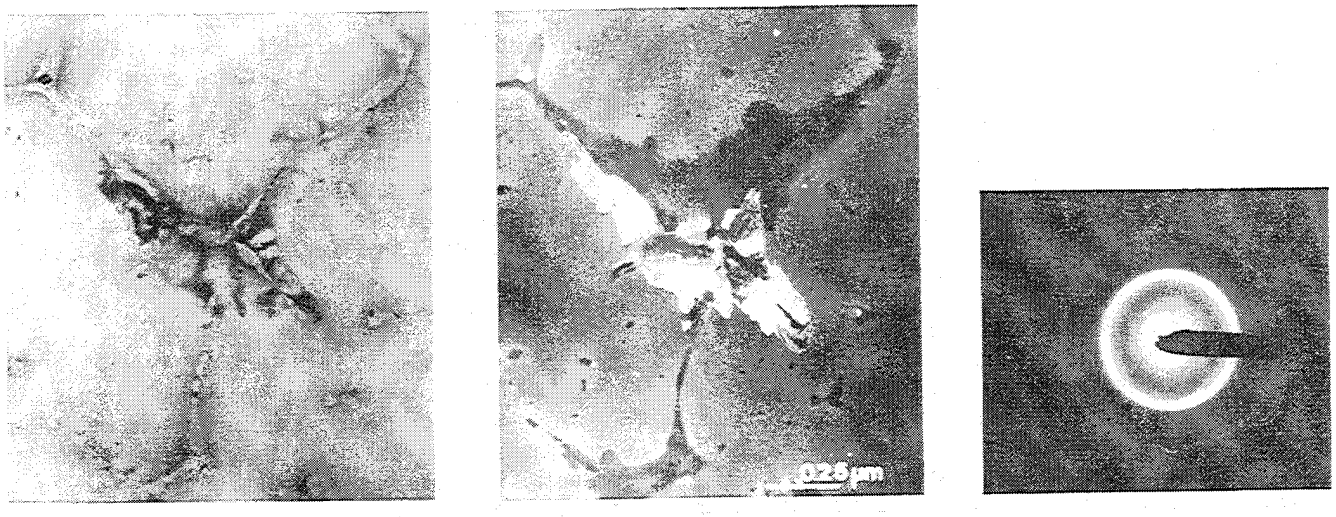

(a) (b) (c)

Fig. 6—Transformation of amorphous phase during *in situ* heat treatment in TEM specimen 5. (*a*) Growth of Al_6Mn on the fcc-amorphous interface. Bright-field image. (*b*) Dark-field image of the fcc-amorphous interface region. The changes in amorphous phase can be observed. (*c*) Diffraction pattern of the modified amorphous phase.

to aluminum. Analysis of the metastable and liquid phases in the binary systems does not show that a liquid miscibility gap is possible in the expected regions of composition and temperature.[10] Therefore, it was concluded that liquid-phase separation was not responsible for the observed solidification morphology.

The amorphous phase obtained through electrodeposition has the same characteristics as the amorphous phase in Reference 9. Its formation, however, occurs atom by atom; the supercooling of any liquid in the traditional sense does not occur in the electrochemical process. However, high free energy, nonequilibrium structures produced by electrodeposition have been widely observed in a number of pure metals and alloys, ranging from the formation of binary glasses to pure metals with varying degrees of texture.[13–17]

Electrodeposited Al-Mn alloys have structures that are very similar to rapidly solidified alloys of the same composition due to the similarity in mechanisms of phase growth. In both processes, the growth of the solid phase(s) occurs from the liquid of (as a rule) dissimilar composition, creating the problem of ion (atoms) transport to the growth interface. The bulk diffusion in the solid is restricted at the low temperature and does not play a significant role.

This mechanism may apply for electrodeposited alloys if the partial current for Mn^{++} exceeds that required to maintain the surface concentration required for deposition of the amorphous phase. In the absence of migration, the rate of mass transfer is proportional to the concentration gradient at the electrode surface and is equal to the electrodeposition rate. Under steady-state deposition, it is assumed that a stagnant layer of thickness δ exists near the electrode surface. Within this layer, mass transfer occurs only by diffusion; outside this layer, convective transport maintains the concentration uniform at the bulk concentration, C_0^*. Thus, the flux of each electroactive species at the electrode surface assuming linear diffusion is

$$-J_0(x=0) = \frac{i}{n\mathrm{FA}} = \frac{D_0}{\delta}[C_0^* - C_0(x=0)] \quad [1]$$

where $J_0(x = 0)$ is the flux, i is the current, n is the number of equivalents per mole of electroactive species, F is Faraday's constant, D_0 is the diffusion coefficient, and $C_0(x = 0)$ is the concentration at the surface.

Assuming a situation in which one wishes to electrodeposit the amorphous phase at a current density of 100 mA/cm^2, the deposition of the amorphous phase (25 wt pct Mn) would require a partial current for Mn^{++} reduction of 9.8 mA/cm^2 and for $Al_2Cl_7^-$ reduction of 90.2 mA/cm^2. This assumes the equivalents for Mn^{++} and $Al_2Cl_7^-$ to be 2 and 0.75, respectively.[6,8] If the concentration of $MnCl_2$ in a 2:1 $AlCl_3$:NaCl melt is 0.75 wt pct (0.1M) and if one assumes that both electroactive species have diffusion coefficients of 5×10^{-6} cm^2/s,[18] then the concentration profile for both Mn^{++} and $Al_2Cl_7^-$ would be that shown in Figure 7 for a diffusion layer thickness of 100 μm. This value for the diffusion layer thickness is an estimate for the case of a stationary electrode under conditions of natural convection; no attempt was made to control the electrolyte hydrodynamics in these experiments. Under these conditions of deposition, which are similar to the experimental conditions shown in Table I, the $Al_2Cl_7^-$ concentration is sufficient to support aluminum deposition; however, the surface concentration of Mn^{++} approaches zero, and the species becomes mass transport limited. The deposition of the amorphous phase can no longer be supported, and a crystalline phase depleted in Mn is then deposited. It is quite possible that deposition of the amorphous phase shuts down when the surface concentration of Mn^{++} drops below some critical value and that partial currents approaching the diffusion-limited current do not need to be reached. The fact that the crystalline phase of the duplex structure contains 2 wt pct Mn supports this.

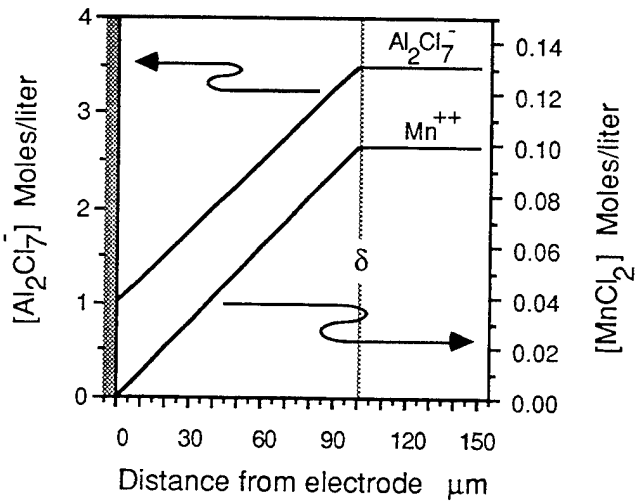

Fig. 7—Concentration profile for Mn^{++} and $Al_2Cl_7^-$ in the diffusion layer in the vicinity of the growing interface.

In rapid solidification, both growth velocity and surface diffusion, which determine the structure of growing layers, depend on the temperature of the process, which is essentially uncontrolled. In electrodeposition, however, the process is isothermal, and growth velocity (current) depends on the overpotential and surface concentration of the electroactive species at the electrode.

One might suggest that for the same growth velocity, an amorphous phase showing SRI ordering forms at lower temperatures, an icosahedral phase (LRI ordering) at higher temperatures, and a crystalline phase at still higher temperatures. This has been reported for sputter deposition of Al-Mn and Al-Mn-Si.[4] The direct electrodeposition of stable and metastable alloys may then be possible by increasing the melt temperature during electrodeposition. Chloroaluminate electrolytes containing somewhat less $AlCl_3$ than that reported here are quite stable at temperatures exceeding 400 °C.[19]

For suitable alloys produced isothermally by electrodeposition without mass transport limitations, one might expect high overpotentials (high growth velocities) to produce amorphous alloys, moderate overpotentials to produce the icosahedral phase, and very low overpotentials to result in crystalline deposits. Changes in the cathodic overpotential, however, do not merely alter the deposition current in some stoichiometrically uniform way. Alloy composition is seen to vary dramatically with

overpotential due to changes in the driving force for reduction of each electroactive species and the resultant adjustment in their surface concentrations. Consequently, different structures are produced at different potentials, because the stoichiometry of the deposited alloy changes. The relative amounts of crystalline and amorphous material in the duplex structure are seen to vary in alloys of equal composition deposited at different potentials, because different mass transport conditions exist. X-ray diffraction patterns of amorphous deposits of the same composition deposited under different conditions are identical and give no indication of microstructural differences; however, it is likely that any differences may not be resolved by X-ray diffraction.

V. SUMMARY

Results of a structural investigation of electrodeposited aluminum alloys containing 0 to 27 wt pct Mn are reported. The addition of small amounts of Mn results in the formation of a supersaturated fcc solid solution and at higher Mn concentrations, the appearance of an amorphous phase. A maximum Mn content of 8.8 wt pct was observed in the solid solution. The first appearance of the amorphous phase was observed in alloys containing 11.3 wt pct Mn. The composition of the amorphous phase is close to that of Al_6Mn (25 to 26 wt pct Mn), while the aluminum-rich fcc phase contains about 2 wt pct Mn in the regions adjacent to the amorphous phase. Fine grains of the fcc phase were observed in 11.3 wt pct Mn alloys.

The highly faceted crystalline surface of electrodeposited pure Al and Al-Mn solid solution becomes smooth and nearly specular when the amorphous phase is present. Deposition of the aluminum-manganese solid solution shows a significant texture that decreases with an increase in the relative amounts of the amorphous phase. Pure aluminum electrodeposits show no preferred orientation.

In the temperature range of 230 °C to 340 °C, the amorphous phase crystallizes, starting at the fcc-amorphous phase interface. The amorphous phase is completely transformed into Al_6Mn, while the fcc phase appears to be unaffected in the above temperature region. The remaining amorphous areas are modified prior to crystallization. Electron diffraction of the modified region is consistent with the fine-grained icosahedral phase.

The structures of Al-Mn alloys obtained by electrodeposition are similar to the structures of rapidly solidified alloys of similar composition. Formation of the duplex structure is controlled in both processes by diffusion of atoms (ions) in the liquid phase. The amorphous phase forms atom by atom; the supercooling of any liquid that could be proposed for rapid solidification does not occur in the electrochemical process. Consequently, the extent of the deviation from equilibrium, as well as the degree of ordering, is defined by the concurrent processes of new layer formation and surface diffusion. The direct electrodeposition of stable and metastable alloys may be possible by increasing the melt temperature during electrodeposition.

ACKNOWLEDGMENTS

The authors would like to thank Alexander Shapiro, David Lashmore, and Leo Bendersky for their technical contributions. The technical assistance of Sandra Clagget and Perry Sharpless is gratefully acknowledged. One of the authors (BG) would like to acknowledge the financial support of the Israel Council for Research and Development and the NIST Guest Scientist Program. This work was jointly supported by the Office of Naval Research (Contract No. N00014-88-F-0091) and the NIST Metal Matrix Competence Building Program.

REFERENCES

1. D. Shechtman, I. Blech, D. Gratias, and J.W. Cahn: *Phys. Rev. Lett.*, 1984, vol. 53, pp. 1951-53.
2. D.A. Lilienfeld, M. Nastasi, H.H. Johnson, D.G. Ast, and J.W. Mayer: *Phys. Rev. Lett.*, 1985, vol. 55, pp. 1587-90.
3. D.M. Follstaedt and J.A. Knapp: *Mater. Sci. Eng.*, 1987, vol. 90, pp. 1-8.
4. K.G. Kreider, F.S. Biancaniello, and M.J. Kaufman: *Scripta Metall.*, 1987, vol. 21, pp. 657-62.
5. L.W. Austin, M.G. Vucich, and E.J. Smith: *Electrochem. Tech.*, 1963, vol. 1, pp. 269-72.
6. G.R. Stafford: *Proc. Corr., Electrochem. and Cat. of Metallic Glasses*, 172nd Meet. Electrochem. Soc., Honolulu, HI, 1987, pp. 348-58.
7. H.J. Read and D.A. Shores: *Electrochem. Tech.*, 1966, vol. 4, pp. 526-30.
8. G.R. Stafford: *J. Electrochem. Soc.*, 1989, vol. 136, pp. 635-39.
9. L.A. Bendersky and S.D. Ridder: *J. Mater. Res.*, 1986, vol. 1, pp. 405-14.
10. L.A. Bendersky, F.S. Biancaniello, and R.J. Schaefer: *J. Mater. Res.*, 1987, vol. 2, pp. 427-30.
11. R.J. Schaefer, L.A. Bendersky, D. Shechtman, W.J. Boettinger, and F.S. Biancaniello: *Metall. Trans. A*, 1986, vol. 17A, pp. 2117-25.
12. D.E. Hall and G.R. Stafford: National Institute of Standards and Technology, Gaithersburg, MD, unpublished research, 1988.
13. K.R. Lawless: *J. Vac. Sci. Tech.*, 1965, vol. 2, pp. 24-34.
14. C.A. Snavely: *Trans. Electrochem. Soc.*, 1947, vol. 92, pp. 537-77.
15. A. Brenner, D.E. Couch, and E.K. Williams: *Plating*, 1950, vol. 37, pp. 36-42.
16. E. Vafaei-Makhsoos and E.L. Thomas: *Metall. Trans. A*, 1978, vol. 9A, pp. 1449-60.
17. K. Masui, T. Yamada, and Y. Hisamatsu: *J. Metal Finishing Soc. Japan*, 1980, vol. 31, pp. 667-72.
18. P. Rolland and G. Mamantov: *J. Electrochem. Soc.*, 1976, vol. 123, pp. 1299-303.
19. Allen J. Bard: *Encyclopedia of Electrochemistry of the Elements*, Marcel Dekker, Inc., New York, NY, 1976, vol. VI, p. 88.
20. P.A. Bancel, P.A. Heiney, P.W. Stephens, A.I. Goldman, and P.M. Horn: *Phys. Rev. Lett.*, 1985, vol. 54, pp. 2422-25.

PATENTS

US005158653A

United States Patent [19]

Lashmore et al.

[11] Patent Number: 5,158,653

[45] Date of Patent: Oct. 27, 1992

[54] METHOD FOR PRODUCTION OF PREDETERMINED CONCENTRATION GRADED ALLOYS

[76] Inventors: **David S. Lashmore**, 5506 Woodlyn Rd., Frederick, Md. 21701; **Moshe P. Dariel**, 55 Rotem Street, Omer 84965, Israel

[21] Appl. No.: **249,531**

[22] Filed: **Sep. 26, 1988**

[51] **Int. Cl.**[5] **C25D 5/10**

[52] **U.S. Cl.** **205/103**; 204/192.12; 204/192.15; 204/DIG. 9; 427/255.7; 427/404; 427/405; 205/176

[58] **Field of Search** ..... 204/40, DIG. 9, 192.1, 204/192.11, 192.12, 192.15; 428/610, 635; 427/255.7, 404, 405, 406

[56] **References Cited**

U.S. PATENT DOCUMENTS

4,093,453	6/1978	Makino et al.	75/129
4,461,680	7/1984	Lashmore	204/41
4,576,699	3/1986	Sato et al.	204/192 M
4,652,348	3/1987	Yahalom et al.	204/40
4,666,567	5/1987	Loch	204/14.1
4,851,095	7/1989	Scobey et al.	204/192.12
4,869,971	9/1989	Nee et al.	428/635

FOREIGN PATENT DOCUMENTS

2062552	9/1971	Fed. Rep. of Germany	428/635
1420078	8/1988	U.S.S.R. .	

OTHER PUBLICATIONS

Lashmore et al., "Electrodeposition of Artificially Layered Materials," Proc. of the AESF 1986 Pulse Plating Symposium.

Yahalom et al., "Formation of Composition-Modulated Alloys by Electrodeposition," 22 J. Materials Science 499 (1987).

Ogden, "High Strength Composite Copper-Nickel Electrodeposits," 73 Plating and Surface Finishing 130 (1986).

Tench et al., "Enhanced Tensile Strength for Electrodeposited Nickel-Copper Multilayer Composites," 15A Metallurgical Transactions A 2039 (1984).

Goldman et al., "Short Wavelength Compositionally Modulated Ni/Ni-P Films Prepared By Electrodeposition," 60 J. Appl. Phys. 1374 (1986).

Cohen et al., "Electroplating of Cyclic Multilayered Alloy (CMA) Coatings," 130 J. Electrochem. Soc. 1987 (1983).

W. Fedrowitz, Chrome/Copper Laminated Stud Via, IBM Technical Disclosure Bulletin, vol. 19, No. 6, Nov., 1976, p. 2060.

Primary Examiner—John F. Niebling
Assistant Examiner—William T. Leader

[57] **ABSTRACT**

A process for the production of a composition modulated alloy having a predetermined concentration is disclosed, in which alternating layers of at least two metals are successively deposited upon a substrate by electrodeposition, vacuum deposition, vapor deposition, or sputtering. The individual thicknesses of at least one metal's layers are varied in a predetermined manner. Pulsed galvanostatic electrodeposition using a tailored waveform is preferred. A copper-nickel concentration graded alloy is disclosed. Concentration graded alloys of predetermined concentration having at least one region of local homogeneity are also disclosed. The region of local homogeneity has a thickness corresponding to the thickness of two adjacent layers of different metals which have been diffusion annealed together. A pulsed electrodeposition/diffusion anneal process for production of such alloys is also disclosed. An electrochemical deposition method is also disclosed for the production of a non-layered, continuous concentration graded alloy.

8 Claims, 4 Drawing Sheets

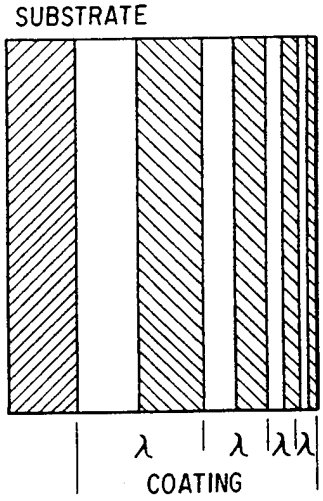

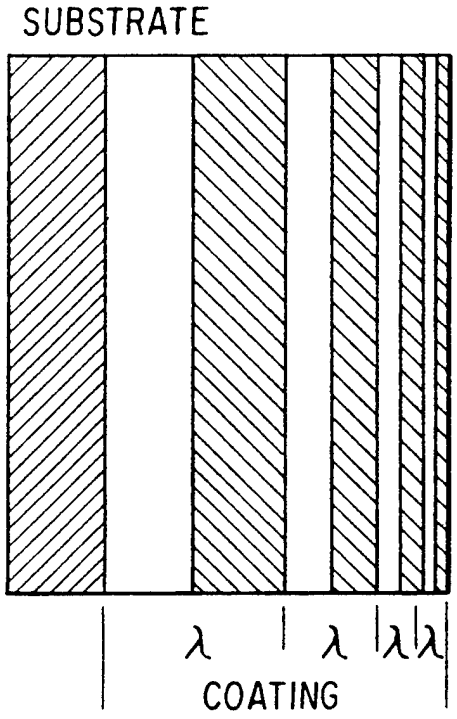

FIG. 1

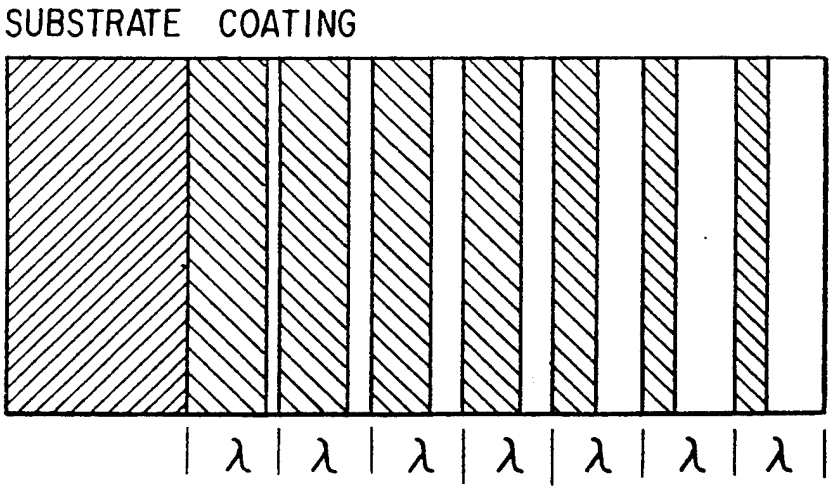

FIG. 2

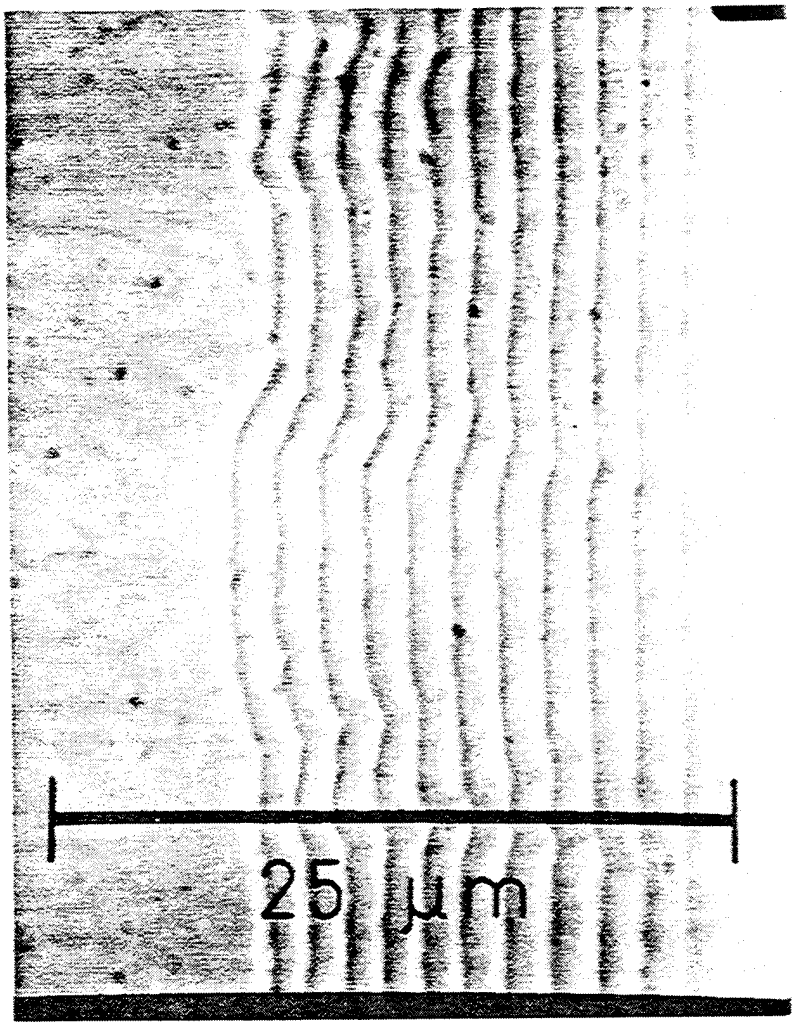

FIG. 3

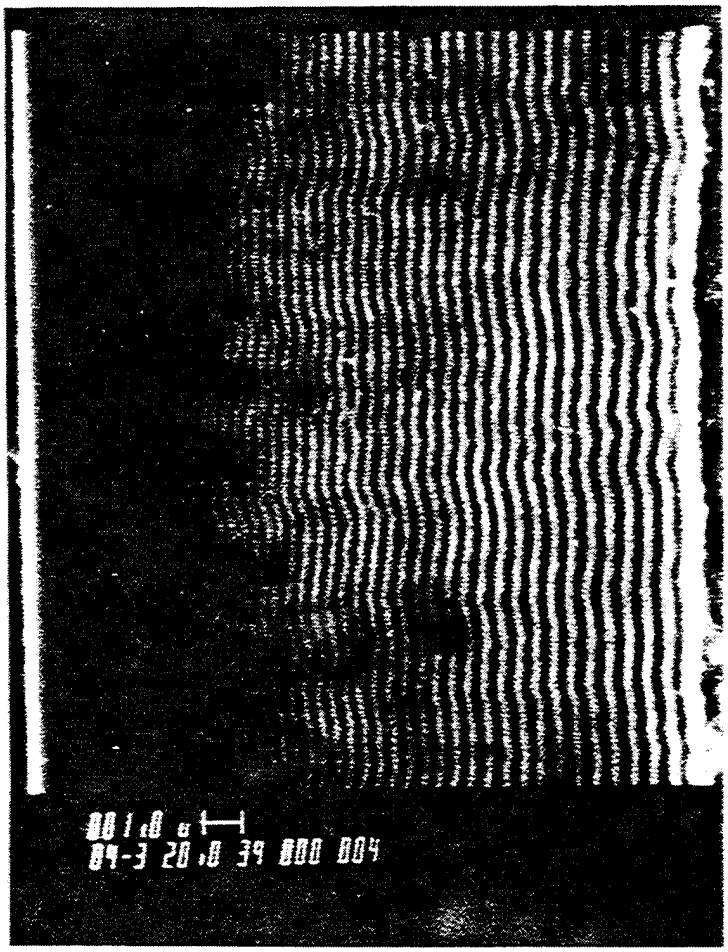

FIG. 4

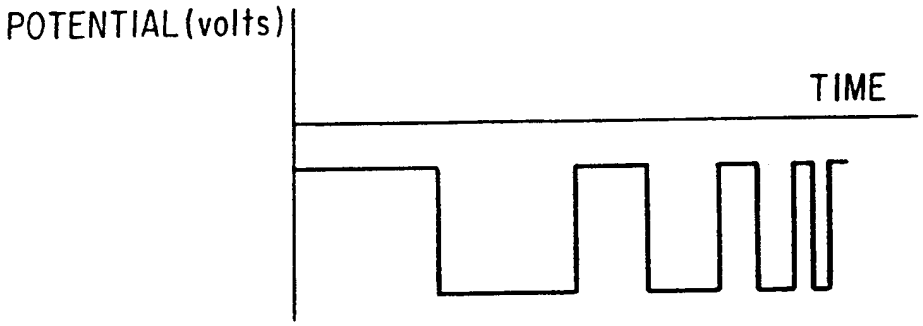

FIG. 5

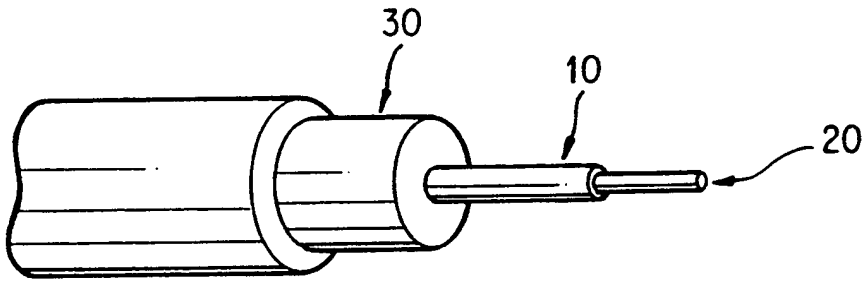

FIG. 6

METHOD FOR PRODUCTION OF PREDETERMINED CONCENTRATION GRADED ALLOYS

BRIEF DESCRIPTION OF THE TECHNICAL FIELD

The present invention relates to concentration graded alloys. More particularly, the present invention relates to predetermined concentration graded multilayer alloys and processes for the production of such alloys.

"Composition modulated alloys" are made of alternating layers of different metals or alloys and are typically prepared by vacuum deposition, molecular beam epitaxy or sputtering. For example, U.S. Pat. No. 4,576,699 discloses a periodic multilayer coating comprising a plurality of layers, each of which contains a rare earth metal and a transition metal, which have been simultaneously co-sputtered onto a substrate. The relative concentration ratio of the two metals may be cyclically varied with the thickness of the coating by providing relative movement between the substrate and the metal sources during co-sputtering.

Electrodeposition has been used successfully for the production of composition modulated materials having a layer thickness of less than 10 nm. For example, U.S. Pat. No. 4,461,680 discloses a pulsed electrodeposition process for production of composition modulated nickel-chromium alloys having a layer spacing of from 0.2 to 0.6 micron. See also U.S. Pat. No. 4,652,348. Both potentiostatic and galvanostatic electrodeposition techniques have been employed to produce composition modulated alloys. Potentiostatic electrodeposition typically produces a composition modulated alloy having sharp layer interfaces, but variable layer thickness. Galvanostatic electrodeposition typically produces a diffuse interface on one side of the layer. Galvanostatic electrodeposition employing "tailored" plating pulse waveforms has been suggested as a means to produce a composition modulated alloy having either sharp layer boundaries or graded interfaces between layers comprising a controlled concentration gradient. Lashmore et al, *Electrodeposition of Artificially Layered Materials,* Proc. 1986 AESF Third International Pulse Plating Symposium.

"Concentration graded alloys" are metallic or intermetallic materials which display a concentration gradient in a given direction. Such alloys can be prepared, in principle, as the outcome of a chemical diffusion reaction occurring between the two constituents of a diffusion couple. However, the concentration profile obtained as the result of a diffusion reaction is determined by the nature of the constituents of the diffusion couple, the equilibrium diagram of the system and the parameters (duration, temperature) of the diffusion anneal, and permits only limited latitude for designing a concentration gradient according to specific requirements.

Cohen et al, "Electroplating of Cyclic Multilayered Alloy (CMA) Coatings," 130 J. Electrochem. Soc'y 1937 (1983) employ square and triangular waveforms to galvanostatically electrodeposit a variety of Ag—Pd cyclic multilayered alloy deposits, and suggest modifying the alloy structure to obtain laminated coatings which may have desirable engineering properties.

An object of the present invention is to provide processes for the production of composition graded multilayer alloys having predeterminable concentration gradients.

Another object of the present invention is to provide composition modulated alloys comprising a plurality of alternating layers of at least two metals in which at least one metal's layer thickness is varied in a predetermined manner over the overall thickness of the alloy.

BRIEF SUMMARY OF THE INVENTION

In one aspect, the present invention relates to a process for the production of a composition modulated alloy having a predetermined variation of wavelength with thickness comprising depositing alternating layers of at least two metals upon a substrate such that the ratio of one layer's thickness to the other remains constant, and the wavelength changes in a predetermined manner over the overall thickness of the alloy.

In a preferred embodiment, the present invention relates to a process for the production of a composition modulated alloy having a predetermined concentration gradient, comprising:

i) providing an electrolyte containing a first metal and a second metal;

ii) providing a substrate upon which said first metal and said second metal are to be electrodeposited;

iii) at least partially immersing said substrate in said electrolyte;

iv) passing an electric current through said substrate, said electric current being alternately pulsed for predetermined durations between a first value corresponding to a reduction potential of said first metal and a second value corresponding to a reduction potential of said second metal to produce a composition modulated alloy having alternating layers of said first metal and said second metal on a surface of said substrate; such that the ratio of one layer's thickness to the other layer's thickness remains constant and the wavelength changes in a predetermined manner over the overall thickness of the alloy.

In another aspect, the present invention relates to a composition modulated alloy comprising a plurality of alternating layers of at least two metals, in which the ratio of at least one metal's layer thickness to the other remains constant, and the wavelength changes in a predetermined manner over the overall thickness of the alloy.

In still another aspect, the present invention relates to a process for the production of a composition modulated alloy having a constant wavelength and a predetermined variation in layer of at least two metals upon a substrate such that the wave-length of the layer remains constant, and the ratio of one layer's thickness to the other layer's thickness is varied in a predetermined manner.

In yet another aspect, the present invention relates to a composition modulated alloy comprising a plurality of alternating layers of at least two metals, in which the wavelength remains constant, and the ratio of the first metal layer thickness to the second metal layer thickness changes in a predetermined manner over the overall thickness of the alloy.

The present invention also relates to a process for the production of a continuously graded alloy having a predetermined concentration gradient, comprising:

providing an electrolyte containing a first metal and a second metal;

providing a substrate upon which said first metal and said second metal may be electrodeposited;

at least partially immersing said substrate in said electrolyte;

providing an electrical potential at said substrate, the magnitude of said potential being effective to cause codeposition of said first and second metals onto said substrate; and

varying said potential over time such that the relative amounts of said first and second metal being co-deposited onto said substrate varies in a predetermined manner.

BRIEF DESCRIPTION OF THE DRAWINGS

FIG. 1 is an enlarged schematic cross section which depicts a multilayer alloy of the present invention having a constant ratio of one layer's thickness to the other layer's thickness, and having a wavelength which changes in a predetermined manner over the overall thickness of the alloy.

FIG. 2 is an enlarged schematic cross section which depicts a multilayer alloy of the present invention having a constant wavelength and a ratio of one layer's thickness to the other layer's thickness which changes in a predetermined manner over the overall thickness of the alloy.

FIG. 3 is a photomicrograph of a Cu/Ni alloy having a "constant wavelength, variable ratio" structure.

FIG. 4 is a graph of microhardness of a Cu/Ni alloy having a "constant ratio, variable wavelength" structure;

FIG. 5 is a schematic illustration of a waveform produced by potentiostatic charge controlled electrodeposition of a Cu/Ni alloy.

FIG. 6 is a schematic illustration of a fiber application of the present invention.

DETAILED DESCRIPTION OF THE PREFERRED EMBODIMENTS

The total thickness of a multilayer composition modulated alloy is large compared with individual layer thicknesses. "Wavelength" (also known as "periodicity") means the combined thickness of two adjacent layers of a multilayer alloy. A "constant ratio" concentration gradient within a multilayer alloy can be produced by a deposition process in which the ratio of one layer's thickness to the other layer's thickness is maintained constant, but which varies the wavelength of the alloy in a predetermined manner over the overall thickness of the alloy. One possible structure of such a "constant ratio, variable wavelength" multilayer alloy is illustrated in FIG. 1. A desired concentration gradient within a multilayer alloy can also be achieved by carrying out a deposition process so that the wavelength of the multilayer alloy remains constant, but the relative thickness of two adjacent layers of different metals or alloys changes in a predetermined way. One possible structure of such a "constant wavelength, variable ratio" multilayer alloy is illustrated in FIG. 2. Multilayer alloys in which both the wavelength and the ratio are both varied over the overall thickness of the deposit are also within the scope of the invention.

The graded alloys of the present invention may be produced by a variety of deposition techniques including vapor depositing sputtering and pulsed electrodeposition. Pulsed electrodeposition is preferred.

Electroplating techniques are well known to those of ordinary skill in the deposition arts, and therefore need not be discussed in detail. In general, alternating layers of a first and second metal or alloy may be deposited upon a cathode substrate by pulsing from one deposition parameter (at which primarily the first metal or alloy is deposited on the substrate) to a second deposition parameter at which primarily only the second metal or alloy is deposited. Codeposition can be largely avoided by proper selection of deposition potentials and the relative concentrations of the metals to be deposited. This technique is described in more detail by U.S. Pat. No. 4,652,348, the disclosure of which is hereby incorporated by reference in its entirety herein.

The predetermined variation in wavelength or layer thickness ratio can be produced by intentionally varying the appropriate electrodeposition parameter during the course of the deposition. For example, a "constant wavelength, variable ratio" multilayer copper/nickel alloy can be produced by using a copper/nickel electrolyte similar to that described by Tench and White (Metall. Trans. A, 15, 2039 (1984). A square waveform is used which corresponds in potential to that for the more noble metal (copper) at one level and that for the less noble metal (nickel) at a second level. This waveform has a ratio (R) of the pulse lengths corresponding to the deposition of the more noble element to the less noble element respectively. The deposition time for each layer is determined by the charge required to deposit a preselected amount of the element or alloy. Once the desired amount of the first element has been deposited the potential is rapidly switched to the second value and continued for the time required to deposit the desired amount of the second element or alloy. The potential is then rapidly switched back to the first value in order to deposit a second layer of the first element or alloy. By repeating this process a multilayer alloy having hundreds of distinct layers may be formed.

In order to produce a "constant wavelength, variable ratio" multilayer alloy, the square waveform ratio R may be varied in a predetermined manner so that R is a function of the thickness. Such a waveform is shown schematically in FIG. 5. The deposition process may be carried out under potentiostatic conditions with the voltage levels being changed only after the preselected amount of charge has been passed. It is important that the amount of charge be measured with a very fast coulometer due to the small amount of charge required for each individual layer thickness. A computer is preferably employed to control the deposition process. FIG. 3 is an optical micrograph of an electrodeposited copper-nickel multilayer alloy whose wavelength was maintained constant at about 1–2 microns, and whose ratio R was changed from 1:10 to 10:1.

A "constant ratio, variable wavelength" multilayer alloy can be produced by using a copper/nickel electrolyte as described above with a waveform such that the ratio of the more noble to the less noble alloy remains constant (R=Constant) while the wavelength is deliberately varied with the thickness of the coating. FIG. 4 is an optical micrograph of an electrodeposited copper-nickel multilayer alloy whose wavelength was varied from 300 Angstroms to 3000 Angstroms. The ratio R was kept constant at 1:1.

In a preferred embodiment of the invention, the pulsed electrodeposition is controlled by actually measuring the amount of charge which has passed through the cathodic substrate, rather than by time control of the pulsed electrodeposition. An advantage of coloumetrically deposition is that individual layer thickness may be more precisely controlled, and that mass transport phenomena, solution effects, and other interfering

deposition phenomena are accounted for when measuring the actual amount of charge which has passed through the cathodic substrate.

The multilayer composition modulated structures of the present invention may be heated in order to promote local (i.e., on a nanometer thickness scale) homogeneity. The diffusion anneal may be carried out under vacuum to prevent oxidation and at a temperature to ensure that even though local homogenization is achieved, the desired macro-concentration gradient (i.e. over the overall thickness of the deposit) is maintained. The temperature of the diffusion anneal is dependent on the alloy system investigated. For example, multilayer Cu-Ni modulated structures may be diffusion annealed in the 200° to 300° C. range. In multi-layer Sn—Ni composition modulated structures, where amorphization is expected and desired, the diffusion anneal should be carried out at a lower temperature (<100° C.) to prevent premature crystallization of the amorphous alloy.

The present invention also comprises a process for production of continuously concentration graded (i.e. non-layered) alloys in which the relative concentrations of the alloy components varies as a function of the thickness of the alloy. Such alloys may be produced by slowly changing the potential of the cathodic substrate rather than by pulsing (rapidly switching) from one reduction potential to another.

The concentration graded alloys of the present invention are important because many properties of commercial interest may be varied by varying the layer spacing or wavelength of the alloy. By electroforming an alloy whose wavelength varies from about 30nm to about 300nm a material can be created having a predetermined gradient in tensile properties.

Another advantage of such a structure is the control of plastic deformation (i.e. the behavior of dislocations) near sharp interfaces, for example, in metal matrix composite structures. It can be expected that in homogeneous structures, dislocations will be concentrated at sharp interfaces and that voids may even form as a result. These voids can subsequently grow into cracks and result in failure of the material. In a graded structure, such plastic deformations can be distributed over a larger volume element, thereby reducing the possibility of crack formation. FIG. **6** illustrates a possible embodiment in which graphite fiber **20** is encased in an aluminum-manganese alloy. A nickel-tin graded structure alloy **10** of the present invention is interposed between graphite fiber **20** and an aluminum-manganese alloy **30** in order to enhance bonding of the alloy **30** to the fiber **10**, and to control plastic deformation. Other metal alloys can include aluminum-titanium, aluminum-vanadium, cobalt-tungsten, nickel-tungsten, nickel-molybdenum and copper. Suitable fibers may include graphite, silicon-copper and boron.

Enhanced ultimate tensile stress and wear resistance are two specific examples of how control over structure on virtually an atomic scale provides a high degree of control over properties which can be thereby tailored for a given materials application. There are many other applications for graded materials; for example, alloys which reflect different x-rays (x-ray mirrors) can be created because the effective index of refraction (in the x-ray region of the spectrum) can be tailored. Similarly, alloys capable of reflecting neutrons may be produced by electrodepositing graded layers of selected elements such as nickel/tin or nickel/manganese. Alloys with magnetic properties which can be controlled on an atomic scale may also have broad application for magnetic mirrors or in magnetic based memory devices. Yet another possible application of the graded alloys of the present invention is in electrical contacts. It is well known that in electrical contacts that the maximum stress in the counterface occurs at a distance below the surface [see, for example, Nam P. Suh, *Tribophysics* at p. 105-140 (Prentice-Hall, Inc. Englewood Cliffs, N.J. 07632)]. A graded structure may be produced of, for example, cobalt or nickel and gold such that the yield stress or resistance to deformation is maximized below the surface and the outer surface is pure gold to maximize the conductivity of the contact.

Though the discussion and examples provided herein are directed to metallic alloys it is understood that the instant disclosure is equally applicable for polymers, intermetallics, and ceramics (all of which can be produced using electrochemical techniques with or without subsequent processing, such as thermal, radiation or mechanical treatment).

EXAMPLES

The following examples are merely intended to illustrate the practice and advantages of specific embodiments of the present invention; in no event are they to be used to restrict the scope of the generic invention.

EXAMPLE I

Preparation of Copper Substrates

Cold rolled 150μm thick copper sheet and 15 mm diameter copper single crystals are used as substrate materials. Disks (0.5–0.8 mm) are cut from the single crystals using a slow speed diamond saw. Preliminary work had shown that appropriate surface preparation is a critical requirement for obtaining a short wavelength layered, coherent structure. The polycrystalline copper substrate disks are spark eroded from the cold rolled sheet. The disks are hand polished to the 0.25μm diamond paste stage. They are then mounted in a specially designed PTFE sample holder which leaves exposed a 10 mm diameter circular surface while providing electrical contact to the back of the substrate. The substrates are finally electropolished in 50% phosphoric acid, using a jet polisher set-up, at 110 V DC, for 20 sec. Just before plating, the sample holder is briefly immersed in 10% H_2SO_4 solution in order to remove the substrate surface oxide layer and rinsed in distilled water.

EXAMPLE II

Formation of a Constant Ratio, Variable Wavelength Ni-Cu Alloy

A sulfamate nickel electrolyte containing 1.5 Molar Nickel Sulfamate, 4 g/L Copper sulfate ($CuSO_4$ $5H_2O$) 30 g/L Boric acid 3 ml/L Triton X100 (surfactant) operated at a pH of 3 and a temperature of 30 degrees centigrade is used in this example.

The cell design incorporates a anodic chamber separated from the cathode chamber by an ion selective membrane (NAFION) to keep anodic reaction products from being incorporated into the coating. The temperature is held at 30 degrees and controlled to within 1 degree. Since the composition of the more noble element (copper) is a sensitive function of the transport condition within the cell, no stirring (or agitation) of the electrolyte is allowed during the deposition process.

The deposition is conducted under potentiostatic control, that is, the potential of the cathode is held constant with respect to an appropriate reference electrode such as a calomel electrode. The decision of when to change the potential level is governed by the amount of charge passed, rather than by elapsed time. The deposition process is controlled by a microcomputer connected to a hybrid analog/digital coulometer. Appropriate software communicates with the coulometer, establishes charge levels for each layer for a given graduation in structure, and outputs the appropriate voltage level to a potentiostat connected to the deposition cell.

What is claimed is:

1. A process for the production of a composition modulated alloy having a predetermined concentration gradient comprising depositing upon a substrate a plurality of adjacent sets of metal layers, each set comprising at least two adjacent layers, said two adjacent layers being formed of a first metal and a second metal respectively, such that the individual layer thicknesses of said first metal and said second metal are varied in a predetermined manner and are different in each successive set, wherein the ratio of the layer thickness of said first metal to the layer thickness of said second metal remains constant in all sets and the combined thickness of the adjacent layers of said first metal and said second metal varies from one set to the next.

2. The process of claim **1** wherein said metals are deposited upon said substrate by a method selected from the group consisting of vapor deposition, sputtering and pulsed electrodeposition.

3. The process of claim **2** wherein said deposition method is pulsed electrodeposition.

4. The process of claim **3** wherein said deposition method is pulsed galvanostatic electrodeposition.

5. The process of claim **3** wherein said deposition method is pulsed potentiostatic electrodeposition.

6. The process of claim **5** wherein said pulsed potentiostatic electrodeposition is coulometrically controlled.

7. The process of claim **4** wherein a cathode potential is varied as a function of deposition thickness.

8. A process for the production of a multilayer alloy having a predetermined concentration gradient, comprising:

providing an electrolyte containing a first metal and a second metal;

providing a substrate upon which said first metal and said second metal may be electrodeposited;

at least partially immersing said substrate in said electrolyte;

passing an electric current through said substrate, said electric current being alternately pulsed for predetermined durations between a value corresponding to a reduction potential of said first metal and a value corresponding to a reduction potential of said second metal, thereby producing a composition modulated alloy having adjacent pairs of layers of said first metal and said second metal on an immersed surface of said substrate wherein the ratio of the layer thickness of said first metal to the layer thickness of said second metal in each pair remains constant, and the wavelength of the alloy varies from one pair to the next with the overall thickness of the alloy.

* * * * *

US005171419A

United States Patent [19]

Wheeler et al.

[11] Patent Number: 5,171,419

[45] Date of Patent: Dec. 15, 1992

[54] METAL-COATED FIBER COMPOSITIONS CONTAINING ALLOY BARRIER LAYER

[75] Inventors: Nea S. Wheeler, Germantown; David S. Lashmore, Frederick, both of Md.

[73] Assignee: American Cyanamid Company, Stamford, Conn.

[21] Appl. No.: 466,800

[22] Filed: Jan. 18, 1990

[51] Int. Cl.[5] C25D 5/10; C25D 5/12

[52] U.S. Cl. 205/176; 205/181; 205/238; 205/255

[58] Field of Search 204/28, 38.1, 40, 44.5; 205/160, 161, 176, 181, 224, 238, 255, 150

[56] References Cited

U.S. PATENT DOCUMENTS

3,802,854	4/1974	Mueller-Dittmann et al.	204/44.5
4,525,248	6/1985	Landa et al.	204/44.5
4,609,449	9/1986	Morin	204/206

OTHER PUBLICATIONS

Chemical Abstract 82:117765n Yagubets et al.

Primary Examiner—John Niebling
Assistant Examiner—Brian M. Bolam
Attorney, Agent or Firm—Frank M. Van Riet

[57] ABSTRACT

The present invention disclosed metal-coated fibers and metal matrix composites made therefrom comprising metal-coated carbon or graphite fiber which have a layer of CoW or NiW alloy interposed between the fiber and its outer metal layer.

16 Claims, 1 Drawing Sheet

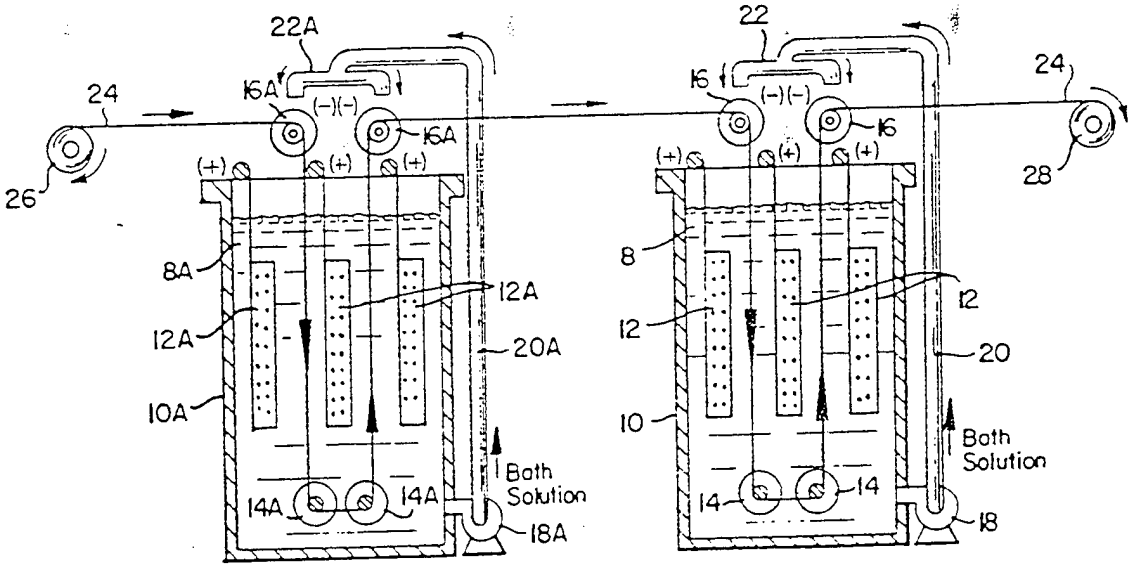

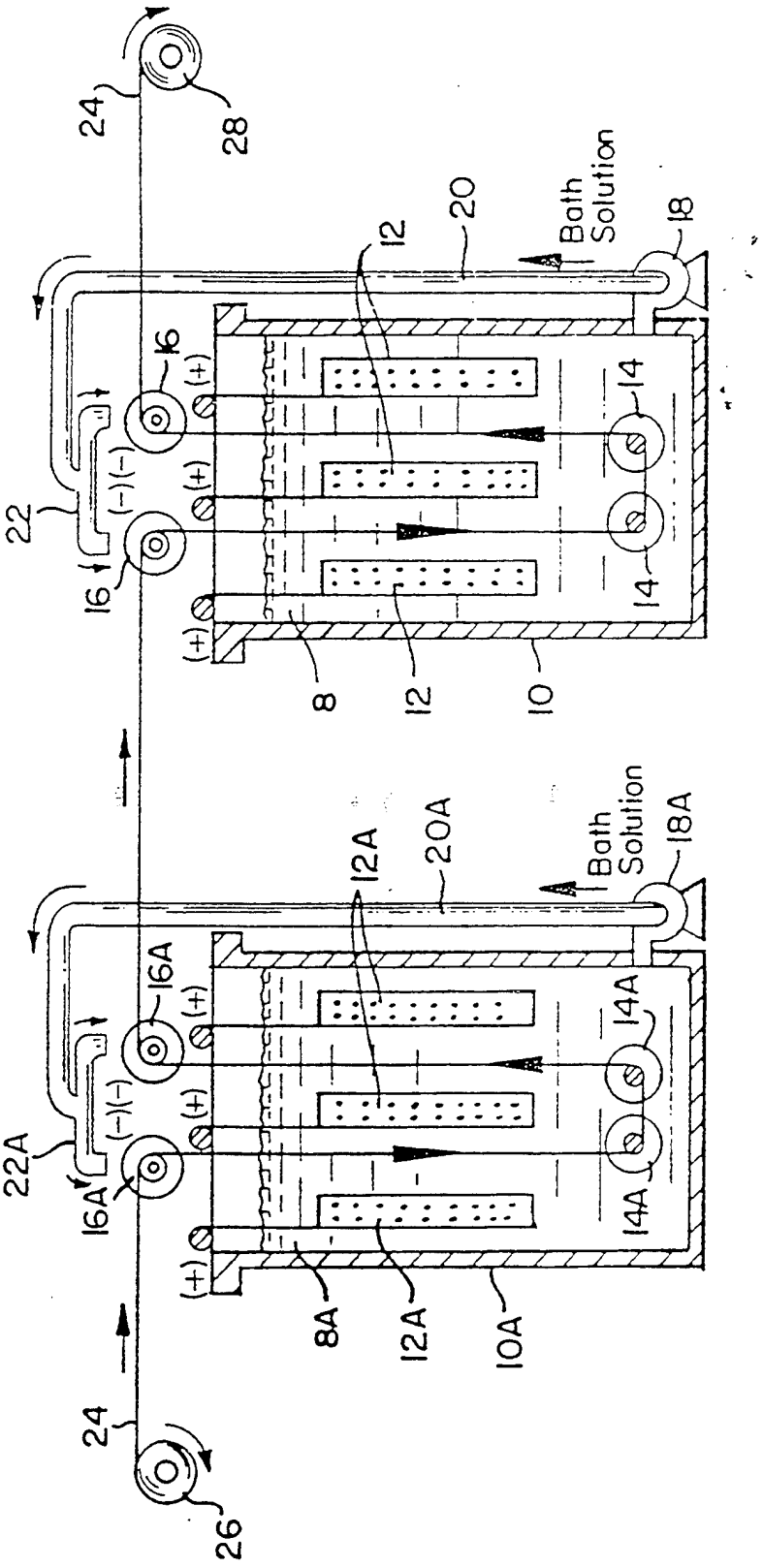
24
28
12
20
Bath Solution
18
16
(+)
14
(-)(-)
22
(+)
16
14
(+)
8
12
10
12A
20A
Bath Solution
18A
16A
14A
22A
16A
14A
8A
12A
10A
24
26

FIG. 1

METAL-COATED FIBER COMPOSITIONS CONTAINING ALLOY BARRIER LAYER

The invention described herein was made in the performance of work supported by the National Institute of Standard and Technology.

FIELD OF THE INVENTION

The present invention is directed to metal-coated fibers having a protective alloy barrier deposited thereon. In particular, the present invention is directed to metal-coated fibers and articles made therefrom comprising metal-coated graphite or carbon fibers having a layer of CoW or NiW electrodeposited thereon between said fiber and said metal coating.

BACKGROUND OF THE INVENTION

Carbon and graphite fibers are desirable for use in metal-matrix composites because of their high-temperature strength, high elastic modulus, and low density. Yet their use in certain matrices, such as those containing nickel, is limited by the degradation of their mechanical properties.

In the fiber interface of a nickel-containing matrix, for example, exposure of the composite to temperatures in excess of 600° C. for extended periods of time significantly reduces the tensile strength of the graphite fibers contained therein. The two mechanisms primarily responsible for the reduction of mechanical properties are reported to be: (1) decrease of fiber diameter due to diffusion of carbon from the fiber into the nickel matrix (as reported by Barclay R. B., *J. Mater. Sci.* 1971. 6, 1076-1083 and (2) nickel-catalyzed regraphitization of the fiber (as reported by Jackson, P. W. and Marjoram, J. R., *Nature* 1968, 218, 83-84). If the material is thermally cycled, the mismatch of thermal coefficients of expansion of the fiber and matrix material is also responsible for reduction in tensile strength. (as reported in U.S. Pat. No. 3,796,587)

Under constant thermal conditions, however, a diffusion barrier to suppress the interdiffusion of nickel and carbon has been reported to protect the mechanical properties of nickel-graphite matrices. Several such barriers have been proven to be beneficial, most notably those containing carbide-forming metals. Carbide-containing barrier coatings have been produced by a variety of methods, such as: by chemical vapor deposition (CVD) (Aggour, L., *Carbon* 1974, 12, 358-362); by soaking the fibers in a melt containing a carbide forming metal and an acid soluble metal, followed by an acid bath to remove the unreacted metal (U.S. Pat. No. 3,796,587); by precoating the fiber in a melt containing a refractory powder suspended in a low-melting-point metal [Rashid, 1974]; and by electrodeposition of a thin layer of nickel followed by another thinner layer of a carbide-forming metal (U.S. Pat. No. 3,807,996). The last two methods required the subsequent heating of the coated fibers to allow diffusion of the reactive metal to the graphite surface where a carbide interfacial zone was formed and therefore involves undesirable processing steps. Yagubets and Sherstkina (*Elektron. Obrab. Mater.* 1974, 5, 31-33, CA 82:117765n) electrodeposited, plastic cobalt-tungsten and nickel-tungsten coatings on graphite fibers from an aqueous bath.

SUMMARY OF THE INVENTION

The present invention is directed to metal-coated fibers and metal matrix composites comprising carbon or graphite fibers, said fibers having electrodeposited thereon a continuous coating of CoW or NiW.

The present invention is further directed to the production of such fibers and metal matrix composites.

DESCRIPTION OF THE DRAWINGS

FIG. 1 is a schematic representation of the apparatus which may be used to produce the fibers claimed herein.

DETAILED DESCRIPTION OF THE INVENTION

The core fibers used in the production of the claimed fibers of this invention include carbon, graphite and mixtures of such fibers. The choice of fiber will depend on the nature of the application envisioned for the coated fiber. Structural carbon fibers, such as those produced from polyacrylonitrile (PAN), having moduli in the range of 30 to 50×10^6 pound per square inch (psi), would be selected for applications where moderate strain to failure in the composite were needed. Graphite fibers such as those produced from pitch that have moduli from 55 to 146×10^6 psi might be used where very high thermal or electrical conductivity or very low thermal expansion were required.

If a batch process is to be used, it is convenient to use long cut sections of fiber tow (e.g. about 40 inches in length) tow and a glass weight placed halfway along the tow. The tow is then lowered into suitable vessels, e.g., 1 liter graduate cylinders containing the various baths described hereinafter, to provide that the weight rests on the bottom of the cylinder. In this way the fibers in the tows remain aligned.

If a continuous process is to be used for the production of the claimed fibers, it may be convenient to operate in the fashion described in U.S. Pat. No. 4,609,449 which will hereinafter be described in reference to FIG. 1.

Electrolytic bath solution 8A is maintained in tank 10A. Also included are cathode baskets 12A and idler rolls 14A near the bottom of tank 10A. Two electrical contact roller 16A are located above the tank. Tow 24 is pulled by means not shown off feed roll 26, over first contact roller 16A down into the bath under idler rollers 14A, up through the bath and over second contact roller 16A. By way of illustration, the immersed tow length may be about 6 feet. Optional, but very much preferred, is a simple recycle loop comprising pump 18A, conduit 20A, and feed head 22A. This permits recirculating the electroplating solution at a large flow rate, e.g. 2-3 gallons/min. and pumping it onto contact rollers 16A. Discharged just above the rollers, the sections of tow 24 and leaving the plating solution are totally bathed, thus cooling them. At the high current carried by the tow, in I^2R heat generated in some cases might destroy them before it reaches or after it leaves the bath surface without such cooling. The flow of the electrolyte overcomes anisotropy. Of course, more than one plating bath to effect electrodeposition of the alloy can be used in series.

Various electroplating baths may be used to effect electrodeposition of the CoW or NiW on the fibers. Such solutions and processes using said solutions are disclosed in *Modern Electroplating*, Third Edition,

Wiley - Interscience, New York, John Wiley & Sons, 1974. For example a solution for use in bath 10A contains:

cobalt sulfate and/or cobalt chloride	(25-200 g/l)
sodium tungstate	(5-100 g/l)
citric acid or sodium potassium tartrate	(5-100 g/l)

Optionally, the above solution may contain a wetting agent, such as sodium lauryl sulfate, and/or from 25-100 g/s of ammonium chloride. A preferred solution for bath 10A contains:

cobalt sulfate	(50-75 g/l)
sodium tungstate	(15-25 g/l)
citric cid	(60-79 g/l)
pH adjuted to 4.0 with sodium hydroxide	

The current density employed in the electrodeposition of the CoW or NiW alloy is generally maintained in the range of 15-120mA/cm^2, preferably between 30-60 mA/cm^2 and most preferably about 30mA/cm^2. The speed of tow 25 is maintained in the range of 0.1-25 ft/min, preferably 0.5-10ft/min and most preferably from 2-5ft/min. The voltage employed to maintain the desired current density range from about 5-30 volts.

The electrodeposition of the tungsten-containing alloy is maintained such that an alloy thickness is deposited which is sufficient to protect the fiber from the elevated-temperature degradation seen with uncoated fibers. This thickness generally varies from the minimum thickness which is detectable by scanning electron microscopy to about 0.3 microns. Expressed in another manner, this thickness can range from less than about 0.1 microns to about 0.3 microns. Preferably, the thickness of the alloy is no greater than 0.1 um. Most preferably, the thickness of the alloy is about 0.1 microns.

Electrolytic bath solution 8 useful in the electrodeposition of the outer metal coating on the alloy-coated fiber is maintained in tank 10A. Also included are anode/baskets 12 and idler roller 14A near the bottom of tank 10A. Two electrical contact roller 16A are located above the tank. Tow 24 is pulled by means not shown off feed roller 26 over contact roller 16A down into the bath under idler rolls 14A, up through the bath, over second contact roller 16A and into bath 10 by way of contact roller 16. Optional, but very much preferred, is a simple recycle loop comprising pump 18A, conduit 20A, and feed head 22A. This also permits recirculating the plating solution at a large flow rate, e.g. 2-3 gallons/min. and pumping it onto contact rolls 16A. Discharged just above the rolls, the sections of tow 24 and leaving the plating solution are totally bathed, thus cooling them. If high currents are carried by the tow, the I^2R heat generated in some cases might destroy them before they reach or after they leave the bath surface without such cooling. The flow of the electrolyte overcomes anisotropy. A serial array of more than bath can also be used.

Solutions and process conditions useful in the electrodeposition of the outer metallic layer on the alloy-coated fiber are well known in the electroplating art. Reference is again made to *Modern Electroplating*, supra. and U.S. Pat. No. 4,609,449, the contents of both sources being hereby incorporated by reference.

The metals useful in the outer layer of the claimed fibers may be any metal which may be electrodeposited. Its identity is therefore not critical. Among those metals useful in this regard include copper, aluminum, lead, zinc, silver, gold, magnesium, tin, titanium, iron, nickel, or a mixture of any of the foregoing. Preferred are nickel and copper.

The electrodeposition of the outer metallic layer is maintained for a time sufficient to produce a coating thickness sufficient for the intended application of the metal-coated fiber product. For instance, if the fiber is to be incorporated into a metal matrix composite, the thickness of the outer metallic layer may vary from about 0.1 to about 5.0 microns. Preferably, said layer has a thickness of about 0.2 to about 3.0 microns. Most preferably, the thickness ranges from about 1.5 to about 3.0 microns. However, if the fiber is to be used in electrical applications such as in providing electromagnetic shielding properties to molded articles, the thickness of the outer metallic layer on the fibers should range only from about 0.1 to about 0.3 microns.

Filtration of the solution within the baths is preferably performed by in-line filters and is very desirable to keep all solutions free of an accumulation of broken fibers.

The fiber is also preferably passed through an optional rinse station, desirable to remove any excess electroplating solution "drag-through" which can influence the chemistry of succeeding baths. A suitable rinse station consists of a table over which the fiber runs, and a water spray directed downward onto this table. The force of the water spray and subsequent run-off the edges of the "table" help to spread the fiber.

It should be understood that the plating line may have multiple tanks for each type of electroplating, and different current densities may be used therein. For example, a low current may be used in the first tank of each plating type to minimize the risk of fiber burnout. The remaining tanks can be operated at higher currents to facilitate more rapid plating in any of this remaining tanks. Solution agitation, such as by pumping from a reservoir, and oscillation resulting from the use a fiber spreading device may be employed to permit the current to be increased without evidence of hydrogen evolution, a symptom of overvoltages in plating operations, demonstrating that such agitation results in more efficient plating.

After the fiber has been electroplated with the outer metallic layer plated to a sufficient extent, the fiber optionally but preferably is rinsed as described above and then dried, such as through the use of an air knife, heat gun or rotary drum drier. Preferably, a heat gun is attached to a heating chamber (not shown). The fiber is then spooled, either onto a spool with other tows or preferably individually into separate spools by a fiber winder (e.g., graphite fiber winders made by Leesona Corp., South Carolina) (not shown).

As shown in the Examples contained herein, the alloy-coated fibers of the present invention markedly decrease temperature-induced deterioration of carbon and graphite fibers within a metal matrix. While not wishing to be bound by any theories presented herein, Applicants believe that such alloys present a barrier which presents interdiffusion of the fiber and matrix materials. This barrier is further believed to comprise a carbide composition of the alloy and fiber since preliminary x-ray diffraction studies have shown Co_3W_3C and

Co_6W_6C to be present at the interface of fibers coated with CoW alloy.

In a further embodiment of the present invention, a variety of types of composites of the invention can be produced using the fibers produced previously described. Methods for incorporating such fibers into polymeric and metallic matrices are contemplated. The methods include directly consolidating the metal coated fiber of this invention so that the coating becomes the matrix. Simply by hot pressing, for example, between 600° C. and 900° C., most preferably between 725° C. and 750° C., in a reducing atmosphere or a vacuum the fibers of this invention can be consolidated to form substantially void-free, uniform composites.

The fibers of this invention can be fabricated into composites by direct consolidation also by "laying up" the fibers. To do so, the fibers are aligned into single layer tow, which optionally may be held together by a fugitive binder or merely the capillary action of water. These layers are then stacked by either keeping the layers aligned in parallel or by changing the angle between adjacent layers to obtain a "cross-plied" laminate. Since the physical properties of the composite and fiber are anisotropic, a range of properties can be achieved by changing the orientation of the various layers of the composite.

Because the coated fibers of this invention have few agglomerations, it is possible to spread the fiber into very thin plies, as low as 3 mils. Thin plies are an advantage when large area structures are to be built, such as radiator structures. In such an application, the composite should be as thin as possible, yet to obtain sufficient stiffness in all directions, several layers, having several orientations, are required. Therefore, the thinner each ply is, the thinner the final, multi-layered composite can be. By making thinner structures, substantial weight savings can be effected which is crucial in any aerospace or transportation application.

Composites produced by direct consolidation of the fibers of this invention have the advantage that the metal remains in intimate contact with the fibers during hot pressing. This is possible because the carbon fibers are coated with metal by the plating process and are consolidated at relatively low temperatures (e.g. 750° C.) This assures that dewetting does not occur during consolidation of the fibers into the composite. The composites of this invention also have the advantage that they have a very uniform distribution of the base fiber throughout the thickness without undesirable matrix-rich regions. In addition, the void content of the composites is low because of the uniformity of coating and low agglomeration rate of the starting coated fiber. Also, the purity of the metal matrix can be very high. The very low agglomeration of the fibers of this invention makes possible thin metal matrix composites, filament wound composites, braided composites and woven composites. The composites of this invention have good mechanical properties due to their uniformity, and good thermal and electrical properties due to the purity of the copper component of the composite.

The organic polymeric materials for use as matrices in the composites of the invention are numerous and generally any known polymeric material may find application. By way of illustration, some of the known polymeric materials useful in the invention include: polyesters, polyethers, polycarbonates, epoxies, phenolics, epoxy-novolacs, epoxy-polyurethanes, ureatype resins, phenol-formaldehyde resins, melamine resins, melamine thiourea resins, urea-aldehyde resins, alkyd resins, polysulfide resins, vinyl organic prepolymers, multifunctional vinyl ethers, cyclic ethers, cyclic esters, polycarbonate-coesters, polycarbonate-co-silicones, polyetheresters, polyimides, bismalemides, polyamides, polyetherimides, polyamide-imides, polyetherimides, and polyvinyl chlorides. The polymeric material may be present alone or in combination with copolymers, and compatible polymeric blends may also be used. In short, any conventional polymeric material may be selected and the particular polymer chosen is generally not critical to the invention. The polymeric material should, when combined with the composite fibers, be convertible by heat or light, alone or in combination with catalysts, accelerators, cross-linking agents, etc., to form the components of the invention.

The fibers of the present invention are well-suited for incorporation with polymeric materials to provide electrically conductive components. The composite fibers have a very high aspect ratio, i.e., length to diameter ratio, so that intimate contact between the fibers to provide conductive pathways through the polymer matrix is achieved at relatively low loading levels of fibers, and more particularly at much lower levels than the metal-coated spheres and metal flakes utilized in prior art attempts to provide electrically conductive polymer compositions. This ability to provide electrical, and/or thermal conductivity at low concentrations of fiber, significantly reduces any undesirable degradation or modification of the physical properties of the polymer.

The metal coated fibers may be present in the composites as single strands, or bundles of fibers or yarn. The fibers or bundles may be woven into fabrics or sheets. In addition, the fibers, or bundles may be comminuted and dispersed within the polymeric material, may be made into nonwoven mats and the like, all in accordance with conventional techniques well-known to those skilled in this art.

The composites of the invention are convertible to many components. In one embodiment of the invention, a composite is prepared by immersing and wetting a nonwoven mat of the composite fibers, such as into a polymeric resin solution, such as one formed by dissolving an epoxy resin or a phenolic resin in an alcohol solvent. Other forms such as unidirectional fibers, woven fabrics, braided fabrics and knitted fabrics can be used, too. This composition may then be converted to an electrically conductive component in the form of a resin impregnated prepreg useful for forming electrically conductive laminates. More particularly, the polymer resin solution wetted mat may be heated to drive off the alcohol solvent. When the solvent removal is complete, a component is formed comprising a layer of randomly oriented and over-lapping composite fibers or bundles of fibers having a polymeric resin layer, and in this case epoxy or phenolic resin layer, coating said fibers and filling any voids or interstices within the mat. The resin impregnated prepreg so formed may be cut to standard dimensions, and several of the prepregs may be aligned one on top of the other, to form a conventional lay up. The lay up is then heated under pressure in a conventional laminating machine which causes the polymer resin to flow and then cure, thereby fusing the layers of the lay up together to form a hardened, unified laminate. The impregnating, drying, lay up, and bonding steps for preparing these laminates are conventional and well-known in the art. Further references as to

materials, handling and processing may be had from the *Encyclopedia of Polymer Science and Technology*, Volume 8, pages 121-162, Interscience, New York, 1969.

The laminates prepared in accordance with the invention may be cut, molded, or otherwise shaped to form many useful articles. For example, the laminate could be made to form a structural base or housing for an electrical part or device, such as a motor, and because the housing is electrically conductive, effectively ground the device.

In an alternate embodiment, the composition of the invention comprises a thin, normally non-conductive polymer film or sheet and a woven, nonwoven unidirectional sheet, etc., formed of the composite fiber. The polymeric film or sheet may be formed by conventional film forming methods such as by extruding the polymer into the nip formed between the heated rolls of a calendar machine, or by dissolving the polymeric material in a suitable solvent, thereafter coating the polymer solution onto a release sheet, such as a release kraft paper with for example a "knife over roll" coater, and heating to remove the solvent. The polymer film or sheet is then heated to between 100° and 200° F. and laminated with the nonwoven mat of composite fibers by passing the two layers between the heated nip of a calendar. The resulting component in the form of a fused polymer film supported with a conductive mat is useful, for example, as a surface ply for laminates.

Air foil structures made with such laminated composites provide an effective lightning strike dissipation system for aircraft. In the past, if lightning struck an aircraft, the non-metallic parts would be subject to significant damage because of their non-conductive nature. With such a laminate forming the outer surface of air foil, should lightning strike the aircraft, the resulting current will be conducted and dissipated through the conductive fiber mat and conductive base laminate, thereby reducing the risk and occurrence of damage to the airfoil.

The present invention is illustrated through the Examples which follow. These Examples should not, however, be construed as representing a limitation on the scope of the present invention or the claims appended hereto.

EXAMPLE 1

A nickel/graphite sample was prepared through the electrodeposition of a relatively heavy coating of nickel onto tows of polyacrylonitrile (PAN) fibers, which are marketed by Hercules under the designation AS4-3K. Application of this heavy electrodeposited coating allowed the simulation of a metal matrix composite. The electrodeposition was accomplished through the use of a plating bath of the following composition:

450 ml of 3.07 M concentrate Ni sulfamate
30 g/l of Boric Acid
0.5 g/l of Sodium Laurel Sulfate

The bath was found to have a pH of 4.0. Electrodeposition was conducted at a bath temperature of 50° C. and through the application of −1.1 V (vs SCE).

The resulting samples were then cut into 5-7 sections, each about one (1) centimeter in length. The samples were then sequentially degreased in acetone, hexane, methanol, hexane, and acetone followed by ultrasonic degreasing in ethanol. The samples were then individually encapsulated in quartz ampules under a vacuum of 10^{-5} Pa. The samples (with the exception of a control) were then heat treated. Only samples obtained from a single electrodeposition were used in any given test. Different batches were not mixed, and one sample from each batch was left unannealed for comparison purposes Annealing of a single batch (4-6 samples) was done at one time, with all samples being placed in the furnace at once. Samples were removed individually at the end of a specified time interval, which ranged from 9.2 minutes to 168 hours. After heat treatment, the samples were ground on silicon carbide paper through 2400 grit and polished with diamond paste through 0.25 um.

Measurement of fiber diameter and observation of the fibers were then performed using a JEOL JXA-840 electron probe x-ray microanalyzer and a Tracor-Northern image analyzer Typically, 5-10 fibers were used to determine the average fiber diameter of a sample. A total of 32 measurements were made on each fiber. The averages for all the fibers were then averaged to give the average diameter for the entire group of fibers.

The average diameter of the control sample of fibers were found to be about 7.01. This figure, as well as those for fibers following the application of elevated temperatures is set forth below in Table I.

TABLE I

Sample	Annealing Treatment	Average Diameter (μm)	# of Fiber Measured
Control	None	7.01 ± 0.27	13
1	1100° C., 24 hr	0.75 ± 0.31	3
2	800° C., 24 hr	6.36 ± 0.28	6
3	600° C., 24 hr	6.78 ± 0.15	8

It is apparent that annealing at from 600°-1100° altered the fiber morphology with the severity of the alteration varying directly with annealing temperature. At both 600° C. and 800° C., analysis with the scanning electron microscope did not reveal any morphological changes in the fibers while in Sample 2, nickel was shown to have entered the fiber itself.

EXAMPLE 2

In procedure of Example 1 was followed except that a layer of cobalt tungsten alloy (CoW) was electrodeposited on the PAN fibers prior to their receiving the nickel coating.

Electrodeposition was accomplished through the use of a bath having the following composition:

0.23 m/l (64.5 g/l) $CoSO_47H_2O$
0.057 m/l (66.0 g/l) Na_2WO_4-$2H_2O$
0.31 m/l (18.8 g/l) Citric Acid
pH 4 (adjusted with NH_4OH).

Pre-electrolysis of the solution was conducted at 1 m A/cm_2 for 48 hours to ensure purity of the solution. Electrodeposition of the CoW alloy was then conducted at about 22° C. and an applied current of 30 A/cm_2. The resulting fibers had a tungsten content of about 24-27 wt. %.

The average diameters of the fibers within the sample so produced is set forth in Table II below.

TABLE II

Samples	Annealing Treatment	Average Diameter (μm)	# of Fiber Measured
4	1100° C., 24 hr	3.79 ± 0.86	21
5	800° C., 24 hr	6.77 ± 0.17	5
6	800° C., 49 hr	6.25 ± 0.39	4
7	800° C., 168 hr	6.24 ± 0.21	8

Through comparison with Samples 1-3, it can be seen that the alloy coating protected the fibers even after annealing at 800° C. for 24 hours.

EXAMPLE 3

The procedure of Example 2 was followed except that electrodeposition of the CoW alloy was conducted such that the resulting fibers were coated with a thinner layer of alloy (<0.5 wt. % W).

The average diameter of the fibers within the sample so produced is set forth in Table III below.

TABLE III

Sample	Annealing Treatment	Average Diameter (μm)	# of Fibers Measured
8	800° C., 25 hr	6.65 ± 0.04	2

Fiber damage was observed after annealing at 800° C. for 24 hr, but the damage was not nearly as severe as for the fibers in the nickel matrix with no intervening CoW layer.

We claim:

1. A process for the production of yarns or tows of composite fibers, said process comprising:

(a) providing a continuous length of a plurality of semimetallic fibers,

(b) immersing at least a portion of the length of said fibers in a bath capable of electrolytically depositing on said fiber an alloy selected from the group consisting of CoW and NiW,

(c) applying an external voltage between the core fibers and the bath sufficient to deposit said alloy on said fibers and maintaining said voltage for a time sufficient to produce a firmly adherent layer of said alloy on said fibers,

(d) immersing at least a portion of the length of said fibers to which said alloy is adhered in a bath capable of electrolytically depositing a metal on said fibers and

(e) applying an external voltage between the fibers and the bath sufficient to deposit said metal on said fibers and maintaining said voltage for a time sufficient to produce an outer layer of said metal on said fibers.

2. The process of claim 1 wherein said fibers comprise carbon, graphite or a combination thereof.

3. The process of claim 2 wherein said fibers comprise carbon.

4. The process of 2 wherein said alloy is CoW.

5. The process of claim 1 wherein said metal is selected from the group consisting of copper, aluminum, lead, zinc, silver, gold, magnesium, tin, titanium, iron and nickel.

6. The process of claim 1 carried out continuously.

7. The process of claim 1 wherein the thickness of the alloy layer is less than or equal to about 0.3 microns.

8. The process of claim 7 wherein the thickness of the alloy layer is less than or equal to about 0.1 microns.

9. The process of claim 8 wherein the thickness o the alloy layer ranges is about 0 1 microns.

10. A process as defined in claim 2 wherein the thickness of said outer metal layer on said fibers ranges from about 0.1 to about 5.0 microns.

11. A process as defined in claim 10 wherein the thickness of said outer metal layer ranges from about 0.2 about 3.0 microns.

12. A process as defined in claim 11 wherein the thickness of said outer metal layer ranges from about to about 3.0 microns.

13. A process as defined in claim 1 including the step of weaving, braiding or knitting yarns produced by the process alone, or in combination with yarns of a different material, into a fabric.

14. A process as defined in claim 1 including the step of laying up the yarns produced by the process alone, or in combination with yarns or a different material into a non-woven sheet.

15. A process as defined in either of claim 13 or 14 including weaving, knitting or laying up the material into a three-dimensional article of manufacture.

16. A process as defined in claim 1 including the step of chopping the yarns produced by the process into shortened lengths.

* * * * *

COOPERATIVE RESEARCH AND DEVELOPMENT AGREEMENT

NATIONAL INSTITUTE OF STANDARDS AND TECHNOLOGY

UNITED STATES DEPARTMENT OF COMMERCE
Technology Administration

TECHNOLOGY DEVELOPMENT PROGRAM
OFFICE OF TECHNOLOGY COMMERCIALIZATION

Physics Building; Room B-256
Gaithersburg, Maryland 20899
Telephone: (301) 975-3084; Telecopy (301) 975-2183

Cooperative Research and Development Agreements (CRADAs)

What is a Cooperative Research and Development Agreement (CRADA)?

The Federal Technology Transfer Act (FTTA) of 1986 (P. L. 99-502) introduced the Cooperative Research and Development Agreement as a mechanism to increase Federal laboratories' interactions with industry.

The CRADA provides the Federal laboratories and their research partners greater flexibility in accommodating the needs of each organization and research situation. For collaborative R&D efforts, the Act provides flexibility in treating patent licenses, assignments, or options in these. Also, the Act provides flexibility in the types of contributions to be made by the research partners.

Prior to 1986, if a firm worked collaboratively with a Federal laboratory and patentable results were jointly developed, the firm and the Federal laboratory would jointly own the research. However, the firm would not own the results exclusively; and a competitor could license the technology from the Government. Through a CRADA, a Federal laboratory may grant, a priori, an exclusive license to research results.

NIST uses CRADAs for its collaborative relationships when intellectual property rights are important to the research partner. Please note that a CRADA is not a procurement, cooperative agreement, or grant.

What are the benefits of conducting cooperative research with NIST?

The specific benefits of a CRADA depend upon the circumstances of the firm. Some of the benefits a firm may derive are:

Breadth of technical expertise. NIST has experts in many technologies ranging from bioanalytic sensors to computer security to robot controller design to superconductors. Today, research efforts often require multi-disciplinary teams to achieve a solid technical solution. Many firms, particularly small firms, do not have the necessary in-house technical talent to address these problems. Working with NIST may provide access to excellent and diverse technical personnel that would otherwise be unaffordable.

Access to technical experts in new technologies or technologies new to the firm. Firms can avoid "reinventing the wheel" and quickly ramp-up on new technologies. A firm may enter an ongoing NIST research program to learn the technology.

Leverage its resources. NIST is often willing to invest some of its resources in cooperative research efforts of mutual interest. Consortium efforts reflecting broad industry interest offer the greatest leverage.

Exclusivity in Cooperative Research Results. Depending on the circumstances of the research effort, the non-Federal partner may obtain an exclusive license to the patentable research developed in the CRADA. Research results may also be protected from Freedom of Information Act Requests.

Who can enter into a CRADA with NIST?

Virtually any organization may enter into a CRADA with NIST. According to statute (P.L. 99-502), "units of State or local government; industrial organizations (including, but not limited to, corporations, partnerships, limited partnerships, and industrial development organizations); public and private foundations; nonprofit organizations (including universities); or persons (including licensees of inventions owned by the Federal agency)" may enter into CRADAs with NIST.

What types of resources may partners contribute to a CRADA?

Non-Federal partners may contribute funds, personnel, equipment, services, and property to a cooperative research and development effort. Federal laboratories may also contribute funds (but not to the non-Federal partner), personnel, equipment, services and property to the cooperative effort.

Are there constraints on the use of these resources?

NIST funds (or other federal funds contributed to the CRADA) can not flow to the non-Federal partner--directly or indirectly. For example, software or equipment contributions by the non-Federal partner that are part of the CRADA cannot have maintenance contracts that require payment by the Federal partner. Also, when purchasing supplies, equipment, or services with CRADA funds, NIST must follow Government procurement rules.

Does a CRADA protect a firm's proprietary information?

In some cases, the non-Federal partner may need to disclose proprietary information to NIST in order to have an effective cooperative research program. Under a CRADA, NIST must protect proprietary information disclosed to it. NIST can also protect proprietary information developed under the CRADA from disclosure for a period of five years.

In addition to the long-standing ability of NIST to protect from disclosure trade secrets and commercial or financial information that is privileged or confidential, an amendment to the FTTA added a specific statuary provision exempting certain CRADA information from disclosure under the Freedom of Information Act.

Specifically, those statutory exemptions are as follows:

"(7)(A) No trade secrets or commercial or financial information that is privileged or confidential under the meaning of section 552(b)(4) of title 5, United States Code, which is obtained in the conduct of research or as a result of research activities under this Act from a non-Federal party participating in a cooperative research and development agreement shall be disclosed.

(7)(B) The director, or in the case of a contractor-operated laboratory, the agency, for a period of up to 5 years after development of information that results from research and development activities conducted under this Act and that would be a trade secret of commercial or financial information that is privileged or confidential if the information had been obtained from a non-Federal party participating in a cooperative research and development agreement, may provide appropriate protections against the dissemination of such information, including exemption from subchapter II of chapter 5 of title 5, the United States Code."

How does NIST treat the research results of a cooperative research and development effort?

NIST believes that U.S. industry needs open access to its technical information, and accordingly, NIST emphasizes publication of its research results. Yet, NIST also recognizes that its research partner may desire to gain competitive advantage from its investment in its research efforts with NIST, and thus NIST provides some flexibility in its arrangements with its partners. Research partners should explicitly discuss with NIST their desires for an exclusive license to patentable results, brief publication delays, and protection of research results.

How does one initiate a CRADA with NIST?

To begin, review the NIST publication Research. Services. Facilities. to identify the appropriate technical contacts. Copies of the publication are available free by calling (301-975-2762).

Source: NIST Technology Development Program, Office of Technology Commercialization
Physics B-256; Gaithersburg, MD 20899
(301-975-3084) 1/92

The Technology Development Program implements several of NIST's technology transfer efforts. Specifically, the Program is responsible for NIST's patents, licenses, cooperative research interactions (CRDAs, consortia and domestic guest researchers), user facility arrangements, and NIST's Small Business Innovation Research Program.

CRADA: CN-___
Collaborator: _____

COOPERATIVE RESEARCH AND DEVELOPMENT AGREEMENT WITH THE NATIONAL INSTITUTE OF STANDARDS AND TECHNOLOGY

Article 1. INTRODUCTION

This Cooperative Research and Development Agreement (CRADA) between the National Institute of Standards and Technology (NIST) and the Collaborator will be effective when signed by all Parties. The research and development project(s) which will be undertaken by each of the Parties in the course of this CRADA are detailed in the Research Plan (RP) which is attached as part of Appendix A. Any exceptions or changes to the CRADA are set forth in Appendix B.

Article 2. DEFINITIONS

As used in this CRADA, the following terms shall have the indicated meanings:

2.1 **"Cooperative Research and Development Agreement"** or **"CRADA"** means this Agreement, entered into by NIST pursuant to 15 U.S.C. section 3710a.

2.2 The term **"made"** in relation to any invention means the conception or first actual reduction to practice of such invention.

2.3 **"Principal Investigator"** or **"PI"** means the person designated respectively by each Party to this CRADA who will be responsible for the scientific and technical conduct of the research plan.

2.4 **"Project Team"** means all personnel assigned by the Collaborator to work on the Research Plan designated in this agreement; "Project Team" includes but is not limited to Collaborator's employees and contractors.

2.5 **"Proprietary Information"** means confidential scientific, business, or financial information, which may embody trade secrets, developed exclusively at private expense, provided such information:

2.5.1 Is not generally known or available from other sources without obligations concerning its confidentiality;

2.5.2 Has not been made available by the owners to others without obligation concerning its confidentiality; and

2.5.3 Is not already available to the Government without obligation concerning its confidentiality.

2.6 **"Research Products "** means all tangible materials other than Subject Data first produced in the performance of this CRADA.

2.7 **"Subject Data"** means all recorded information first produced in the performance of this Agreement.

2.8 **"Subject Invention"** means any invention made in the performance of research under this CRADA. Invention means any discovery which is or may be patentable under Title 35 U.S.C.

Article 3. COOPERATIVE RESEARCH

3.1 **Research Plan and Changes.** The Research Plan (RP) of this CRADA, its duration, and its objectives are detailed in Appendix A. The nature of this cooperative research precludes a guarantee of its completion within the specified period of performance or limits of allocated financial or staffing support. Accordingly, research under this CRADA is performed on a best efforts basis. Extensions and changes in the Research Plan are to be by mutual written consent.

3.2 **Reviews and Reports.** Periodic conferences shall be held by NIST and the Collaborator to review work progress. Parties shall exchange formal written interim progress reports on a schedule agreed to by the PIs, but at least every six (6) months after this CRADA becomes effective. Such reports shall set forth the technical progress made, identify such problems as may have been encountered, identify any intellectual property development, and establish goals and objectives requiring further effort. The Parties shall exchange final reports of their results within four (4) months after completing the projects described in the RP or after termination of this CRADA.

3.3 **Principal Investigators.** NIST shall be the supervising federal agency, both administratively and scientifically, for this CRADA. The NIST PI is responsible for the scientific and technical conduct of this project on behalf of NIST. The designated Collaborator PI is responsible for the scientific and technical conduct of this project on behalf of the Collaborator. The Collaborator shall designate the Project Team in Appendix A of this agreement. While at NIST, the Project Team shall pursue their activities at NIST on the work schedule and under the Government security and conduct regulations that apply to NIST employees. The Project Team shall conform to the requirements of Department of Commerce Administrative Orders 202-735 and 202-735-A while at NIST, as amended, hereby made part of this Agreement, to the extent that these orders prohibit private business activity or interest incompatible with the best interests of the Department. While it shall be the privilege and responsibility of the Collaborator to select those members of the Project Team that work at NIST, these members must also be acceptable to NIST.

3.4 **Eligibility for Participation in this Agreement.** Collaborator certifies the correctness of the eligibility information contained in Appendix A. Collaborator agrees to notify NIST within thirty days should it become subject to the control of a foreign company or government at any time during this Agreement, or if any other change occurs relevant to Appendix A.

Article 4. FINANCIAL OBLIGATIONS

4.1 **NIST and Collaborator Contributions.** The NIST contribution to the CRADA, in the form of personnel, services, facilities, and/or equipment, is listed in Appendix A. The Collaborator contribution to the CRADA, in the form of personnel, services, property, support for staffing and/or funding is listed in Appendix A. The Collaborator shall provide directly for travel and related expenditures for its Project Team. Payment schedules, if applicable, are also indicated in Appendix A.

4.2 **Disposition of CRADA Funds.** The Collaborator shall, as of the effective date of this Agreement, establish a fund at NIST from which RP expenses may be drawn. NIST shall not be obligated to perform any of the research specified herein or to take any other action required by this CRADA if the funding is not provided as set forth in Appendix A. Use of this fund shall require the approval of both the Collaborator PI and the NIST PI. The Collaborator shall reimburse NIST for the cost of special supplies, special material, computation, technical assistance, and/or other special services provided to the Project

Team not identified in Appendix A but which have been approved by Collaborator. Upon termination, NIST shall return excess monies to the Collaborator when the final report pursuant to Article 3.2 is completed.

Article 5. TITLE TO EQUIPMENT

5.1 **Equipment.** Equipment purchased by NIST with funds provided under this CRADA by the Collaborator shall be the property of NIST. All capital equipment provided under this CRADA by a Party remains the property of that Party unless other disposition is mutually agreed upon in writing. Collaborator's equipment will be returned to the Collaborator at the Collaborator's expense and risk as soon as practicable after termination of this Agreement. The Collaborator agrees to assume full responsibility for maintenance of such equipment and instruments and agrees to hold NIST free from liability for any loss thereof or damage to such capital equipment.

Article 6 TREATMENT OF PROPRIETARY INFORMATION

6.1 **Protection.** Each Party agrees to limit its disclosure of Proprietary Information to the other to the amount necessary to carry out the RP of this CRADA. The Collaborator shall place a Proprietary Information notice on all information it delivers to NIST under this Agreement, which the Collaborator asserts is proprietary. NIST agrees that any information designated proprietary shall be used only for the purposes described in the attached RP. However, NIST may object to the designation of information as Proprietary Information and may decline to accept such information. To the extent permitted by law, including the Freedom of Information Act (5 U.S.C. 552), Proprietary Information, so designated, shall not be disclosed or otherwise made available in any form whatsoever to any other person, firm, corporation, partnership, association or other entity without the consent of the Collaborator. NIST agrees to use its best efforts to maintain the confidentiality of Proprietary Information. NIST will promptly notify the Collaborator of requests for its Proprietary Information. The Collaborator agrees that NIST is not liable for the disclosure of information designated as proprietary which, after notice to and consultation with the Collaborator, NIST determines may not lawfully be withheld or which a court of competent jurisdiction requires disclosed.

Article 7. INTELLECTUAL PROPERTY

7.1 **Reporting.** Each Party shall promptly report in writing to the other Party each Subject Invention disclosed to it by its employees or Project Team members. Pursuant to 35 U.S.C. 205, such reports shall be maintained as confidential by the receiving Party until such time as a patent or other intellectual property application claiming that Subject Invention has been filed.

7.2 **Assignment Obligations.** The Collaborator shall ensure that all Project Team members (a) promptly report any Subject Inventions they make to the Collaborator, and (b) sign any documents necessary or desirable for the filing and prosecution of patent applications. If any Project Team member is not the Collaborator's employee, the Collaborator shall require the member to agree in writing to assist the Collaborator in fulfilling all of its patent responsibilities under this CRADA.

7.3 **Treatment of Subject Data.**

7.3.1 **Ownership of Original Copies of Subject Data.** NIST and the Collaborator agree to exchange all Subject Data. Subject to these sharing requirements, the creating Party will retain ownership of and title to the original copy of all Subject Data created solely by it. NIST shall retain title to the original copy of all jointly created Subject Data; NIST shall supply Collaborator with a copy of the original copy of jointly created Subject Data, and Collaborator shall have access

to the original copy. NIST and Collaborator shall each have the right to use all Subject Data for their own purposes, consistent with their obligations under this Agreement.

7.3.2 Ownership of Copyrights of Subject Data. Collaborator may elect to copyright works, or those identifiable portions of a joint work, developed solely by a Project Team member. When Collaborator obtains a copyright, Collaborator shall affix the applicable copyright notice of 17 U.S.C. §§ 401, 402, and 403, and an acknowledgement of the scientific and technical contributions of the National Institute of Standards and Technology. The Collaborator grants to the U.S. Government, a paid-up, non-exclusive irrevocable world-wide license to reproduce or have reproduced, prepare or have prepared in derivative form, and distribute or have distributed copies of the Subject Data for government purposes. Subject Data prepared by NIST employees, and Subject Data prepared jointly by NIST employees and the Project Team, are not subject to copyright in the United States pursuant to section 105 of title 17 of the United States Code. NIST may, however, own copyright in such works outside of the United States.

7.4 Ownership of Research Products. Except as provided for in Articles 7.6, NIST and the Collaborator agree to exchange samples of all Research Products. Research Products will be shared equally by the Parties unless the Parties agree in writing to other disposition. Subject to these sharing requirements, the Research Products created under this CRADA are the jointly owned property of the Parties. The Parties agree to make mutually acceptable arrangements for the disposition of unique or hard-to-replace Research Products.

7.5 Publication. Except as provided in Sections 7.1 and 7.6, the Parties are encouraged to make publicly available the results of their research. Before either Party submits a paper or abstract for publication or otherwise intends to publicly disclose information about a Subject Invention, Subject Data, or Research Products, the other Party shall be provided thirty (30) days to review the proposed publication or disclosure to assure that Proprietary Information and Subject Inventions are protected. In no event, however, shall the name of either Party or any of their trademarks and tradenames be used in publications of the other Party without each Party's prior written consent.

7.6 Patenting Subject Inventions

7.6.1 Government's Minimum Rights. All assignments made by NIST under this Article 7.6 and all licenses granted under Article 8 are subject to the reservation of statutorily required licenses in favor of the United States Government as described in this section 7.6.1. Pursuant to the Federal Technology Transfer Act of 1986 (15 U.S.C. 3710 a(b)(3)) NIST retains a nonexclusive, irrevocable, paid-up license to practice all Collaborator Subject Inventions or have all Collaborator Subject Inventions practiced throughout the world on behalf of the Government. Also pursuant to the Federal Technology Transfer Act of 1986 (15 U.S.C. 3710a(b)(2)) NIST retains a nonexclusive, nontransferable, irrevocable, paid up license to practice all NIST and joint Subject Inventions or have the NIST and joint Subject Inventions practiced, throughout the world by or on behalf of the Government.

7.6.2 Collaborator Inventions. The Collaborator shall retain intellectual property rights to any Subject Invention made solely by a Project Team member. If the Collaborator decides not to retain its rights, the Collaborator shall offer to assign its rights to the Subject Invention to NIST. If NIST declines such assignment, the Collaborator may release its rights to its employee inventors, subject to the reservation of patent licenses in favor of the United States Government as required in section 7.6.1 above.

7.6.3 **NIST Employee Inventions.** NIST, on behalf of the U.S. Government, shall retain title to each Subject Invention made by its employees. If NIST decides not to retain its rights, NIST shall offer to assign its rights to the Subject Invention to the Collaborator, subject to the reservation of patent licenses in favor of the United States Government as required in section 7.6.1 above. If Collaborator declines such assignment, NIST may release its rights to its employee inventors.

7.6.4 **Joint Inventions.** Collaborator and NIST shall retain joint title to all Subject Inventions made by Collaborator's employees and NIST employees. If either party decides not to retain title to its rights to a joint Subject Invention, the Party will offer to assign its rights to the other Party. If the other Party declines such assignment, the offering Party may release its rights to its employee inventors.

7.6.5 **Filing of Patent Applications.** The Party retaining title to a Subject Invention shall file patent applications in a timely manner; NIST shall be responsible for filing patent applications for joint Subject Inventions in a timely manner. The filing Party may elect not to file a patent application in any particular country or countries provided it so advises the other Party ninety (90) days prior to the expiration of any applicable filing deadline, priority period, or statutory bar date, and agrees to assign its intellectual property right, title, and interest in such country or countries to the Subject Invention to the other Party and to cooperate in the preparation and filing of patent applications.

7.6.6 **Patent Expenses.** All of the expenses attendant to the filing of patent applications shall promptly be paid by the party filing such application. Any post filing and post patent fees shall also be borne by the same party. If Collaborator exercises its option for an exclusive license under Section 8.1 below, Collaborator shall reimburse NIST for all such patent filing, post filing and post patent expenses. If Collaborator exercises its option for a nonexclusive license, Collaborator shall reimburse NIST for one-half of all such filing and post filing and post patent expenses for joint Subject Inventions.

7.6.7 **Prosecution of Patent Applications.** Each Party shall promptly provide the other party with copies of the application it files on any Subject Invention along with the power to inspect and make copies of all documents retained in the patent application files. The Parties agree to consult and cooperate with each other in obtaining and maintaining protection for Subject Inventions.

Article 8. LICENSING

8.1 **Option for a Commercialization License.** NIST, on behalf of the Government, hereby agrees to grant to the Collaborator an option to negotiate in good faith, the terms of an exclusive or nonexclusive commercialization license to NIST Subject Inventions and NIST's interest in joint Subject Inventions. The license will specify the licensed fields of use, geographic territory, markets, term and royalties, and will contain a requirement that products manufactured under the license will be manufactured substantially in the United States. The royalty rates will be based on product sales and the rates conventionally granted in the field identified in the RP for inventions with reasonably similar commercial potential. The royalty rates will also reflect the relative contributions of the Parties to the invention. Licenses granted under this Article are subject to the reservation of patent licenses in favor of the United States Government required in section 7.6.1 above.

8.2 **Exercise of License Option.** The option of Article 8.1 must be exercised by written notice mailed within three (3) months after the patent or other intellectual property application is filed. Exercise of this

option by the Collaborator initiates a negotiation period that expires nine (9) months after the patent application filing date. If the last proposal by the Collaborator has not been responded to in writing by NIST within this nine (9) month period, the negotiation period shall by extended to expire one (1) month after NIST responds. If no agreement is concluded in this period or if Collaborator exercises its option for a nonexclusive license, NIST shall be free to license such Subject Inventions to others.

Article 9. TERMINATION

9.1 **Notices.** The Collaborator and NIST each have the right to terminate this Agreement upon 30 days notice in writing to the other party.

9.2 **Termination by Collaborator.** In the event of withdrawal of the Collaborator, payments previously received by NIST pursuant to Article 4 of this Agreement will be retained by NIST to be used in support of the project but no further payment by the participant to NIST will be made. Notwithstanding the provision of 12.11, benefits to the Collaborator as defined in Articles 7 and 8 shall be forfeited.

9.3 **Termination by NIST.** If NIST terminates this Agreement, NIST shall repay the Collaborator any portion of payments previously made to NIST pursuant to Article 4 in excess of actual costs incurred by NIST in pursuing this project. A report on results to date of termination will be prepared by NIST and the cost of preparing the report will be deducted from any amounts due to participants from NIST.

9.4 **Termination After Change of Control.** NIST may terminate this Agreement immediately if direct or indirect control of the Collaborator is transferred to a foreign company or government; or, if Collaborator is already controlled by a foreign company or government, if that control is transferred to another foreign company or government.

Article 10. DISPUTES

10.1 **Settlement.** Any dispute arising under this Agreement which is not disposed of by agreement of the Parties shall be submitted jointly to the signatories of this Agreement. A joint decision of the signatories or their designees shall be the disposition of such dispute. If the parties cannot reach a joint decision, either party may terminate this agreement immediately.

10.2 **Continuation of Work.** Pending the resolution of any dispute or claim pursuant to this Article, the Parties agree that performance of all obligations shall be pursued diligently in accordance with the direction of the NIST signatory.

Article 11. LIABILITY

11.1 **Property.** The U.S Government shall not be responsible for damages to any property of the Collaborator provided to NIST or acquired by NIST pursuant to this Agreement.

11.2 **Indemnification.**

11.2.1 **Collaborator's Employees.** Collaborator's Project Team assigned to this RP are not employees of NIST. The Collaborator shall indemnify and hold harmless the U.S. Government for any loss, claim, damage, or liability of any kind involving the Collaborator's Project Team arising in connection with this Agreement, except to the extent that such loss, claim, damage or liability arises from the negligence of NIST or its employees. NIST shall be solely responsible for the payment of all claims for the loss of property, personal injury or death, or otherwise arising out of any negligent act or omission of its employees in connection with the performance of work under this Agreement.

11.2.2 **Collaborator's Use of Research.** The Collaborator shall indemnify and hold harmless the U.S. Government for any loss, claim, damage, or liability of any kind arising out of the use by the Collaborator, or any party acting on its behalf or under its authorization, of NIST's research and technical developments or out of any use, sale or other disposition by the Collaborator or others acting on its behalf or with its authorization, of products made by the use of NIST's technical developments.

11.3 **Force Majeure.** Neither party shall be liable for any unforeseeable event beyond its reasonable control not caused by the fault or negligence of such party, which causes such party to be unable to perform its obligations under this Agreement (and which it has been unable to overcome by the exercise of due diligence), including, but not limited to, flood, drought, earthquake, storm, fire, pestilence, lightning and other natural catastrophes, epidemic, war, riot, civic disturbance or disobedience, strikes, labor dispute, or failure, threat of failure, or sabotage of the NIST facilities, or any order or injunction made by a court or public agency. In the event of the occurrence of such a force majeure event, the party unable to perform shall promptly notify the other party. It shall further use its best efforts to resume performance as quickly as possible and shall suspend performance only for such period of time as is necessary as a result of the force majeure event.

11.4 **NO WARRANTY.** THE PARTIES MAKE NO EXPRESSED OR IMPLIED WARRANTY AS TO ANY MATTER WHATSOEVER, INCLUDING THE CONDITIONS OF THE RESEARCH OR ANY INVENTION OR PRODUCT, WHETHER TANGIBLE OR INTANGIBLE, MADE OR DEVELOPED UNDER THIS AGREEMENT, OR THE OWNERSHIP, MERCHANTABILITY OR FITNESS FOR A PARTICULAR PURPOSE OF THE RESEARCH OR ANY INVENTION OR PRODUCT.

Article 12. MISCELLANEOUS

12.1 **No Benefits.** No member of, or delegate to the United States Congress, or resident commissioner, shall be admitted to any share or part of this Agreement, nor to any benefit that may arise therefrom; but this provision shall not be construed to extend to this Agreement if made with a corporation for its general benefit.

12.2 **Governing Law.** The construction validity, performance and effect of this Agreement for all purposes shall be governed by the laws of the United States.

12.3 **Entire Agreement.** This Agreement constitutes the entire agreement between the Parties concerning the subject matter hereof and supersedes any prior understanding or written or oral agreement relative to said matter.

12.4 **Headings.** Titles and headings of the Sections and Subsections of this Agreement are for the convenience of references only and do not form a part of this Agreement and shall in no way affect the interpretation thereof.

12.5 **Amendments.** If either party desires a modification in this Agreement, the Parties shall, upon reasonable notice of the proposed modification by the party desiring the change, confer in good faith to determine the desirability of such modification. Such modification shall not be effective until a written amendment is signed by all the Parties hereto by their representatives duly authorized to execute such amendment.

12.6 **Assignment.** Neither this Agreement nor any rights or obligations of any party hereunder shall be assigned or otherwise transferred by either party without the prior written consent of the other party

except that the Collaborator may assign this Agreement to the successors or assignees of a substantial portion of the Collaborator's business interest to which this Agreement directly pertains.

12.7 **Notices.** All notices pertaining to or required by this Agreement shall be in writing and shall be directed to the signator(s).

12.8 **Independent Contractors.** The relationship of the Parties to this Agreement is that of independent contractors and not as agents of each other or as joint venturers or partners. Each Party shall maintain sole and exclusive control over its personnel and operations.

12.9 **The Use of Name or Endorsements.** Collaborator shall not use the name of NIST or the Department of Commerce on any advertisement, product or service which is directly or indirectly related to either this Agreement or any patent license or assignment agreement which implements this Agreement without the prior approval of NIST. By entering into this Agreement NIST does not directly or indirectly endorse any product or service provided, or to be provided, by the Collaborator its successors, assignees, or licensees. The Collaborator shall not in any way imply that this Agreement is an endorsement of any such product or service.

12.10 **Duration of the Agreement.** It is mutually recognized that the duration of this project cannot be rigidly defined in advance, and that the contemplated time periods for various phases of the RP are only good faith guidelines subject to adjustment by mutual agreement to fit circumstances as the RP proceeds. In no case will the term of this CRADA extend beyond the term indicated in the RP unless it is revised in accordance with Article 12.5.

12.11 **Survivability.** Except as provided for in Article 9.2, the provisions of Articles 3.2, 4.2, Articles 6-8, 10.1, 11, and 12.9 shall survive the termination of this CRADA.

CRADA Identification Number:
Collaborator:
Collaboration Project Title:

Appendix A
The Research Plan

NIST requires the information listed below. The company name, address and the project title are needed for public disclosure. The Collaborator may consider the information in items 6, 7, 9 and 10 proprietary. If the Collaborator wishes any of the information in items 6, 7, 9, or 10 kept proprietary, the Collaborator should label the information "PROPRIETARY INFORMATION" and place the information on a separate page. NIST must be willing to accept this information as proprietary.

1. Collaboration Project Title (Please provide a brief project title that NIST may use for public disclosure and management reporting.): _____.

2. Collaborator Eligibility. In order to assure compliance with section 2 of the Federal Technology Transfer Act of 1986 (15 U.S.C. 3710a), the Collaborator must provide the following information to NIST (please check the appropriate box):

[ ] Collaborator certifies that it is not subject to the control of any foreign company or government, and agrees to notify NIST within thirty days should it become subject to the control of a foreign company or government at any time during this agreement; or

[ ] Collaborator acknowledges that it is subject to the control of the following foreign company or government (if a company, please specify nationality):

_____
Company Name, Country/Government

Collaborator certifies to NIST that it is incorporated under the laws of one of the states or territories of the United States; and that it has a manufacturing presence in the United States; and that the foreign government listed above permits United States agencies, organizations, or other persons to enter into cooperative agreements and licensing agreements.

3. Collaborator Participation in NIST's Advanced Technology Program. NIST will enter into CRADAs with recipients of awards from the Advanced Technology Program ("ATP"). However, as a general policy, NIST will not accept, under CRADAs, contributions of ATP funds from ATP recipients. Collaborator hereby states that: (Please check the appropriate box.)

[ ] Collaborator is not a recipient of ATP funds.

[ ] Collaborator is a recipient of ATP funds, and the research to be conducted under this CRADA is part of the ATP project.

[ ] Collaborator is a recipient of ATP funds, and the research to be conducted under this CRADA is not a part of the ATP project.

CRADA Identification Number:
Collaborator:
Collaboration Project Title:

4. NIST's Principal Investigator (include mailing address and telephone number):

_____
_____
_____
_____
_____

5. Collaborator's Principal Investigator (or Principal Contact, include telephone and mailing address):

_____
_____
_____
_____
_____

6. Proposed Duration and starting date for the CRADA: _____

7. Collaborator Equipment, Facility, and/or Funds Contributions:

8. NIST Personnel, Services, Facilities and/or Equipment Contributions:

9. Collaborator's Project Team (please list):

Name	Telephone

10. The Research Project:

(Please describe the research project. The description should: 1) state the project's objectives, and 2) detail the research approach sufficiently to permit your management chain to review the proposed collaboration. A brief description, usually one page, is usually sufficient.)

CRADA Identification Number:
Collaborator:
Collaboration Project Title:

Appendix B

Exceptions or Changes to the CRADA